Dynamics of phosphorus and sulphur in a mangrove forest in Bragança, North Brazil

DISSERTATION

zur Erlangung des Grades eines
Doktors der Naturwissenschaften
- Dr. rer.nat. -

Angefertig am
Zentrum für Marine Tropenökologie
dem Fachbereich Biologie/Chemie
der Universität Bremen
vorgelegt von:

Ursula Maria Neira Mendoza

Bremen
Juni, 2007

Universität Bremen

z m t
b r e m e n

Erster Gutachter	:	Dr. habil. Rubén Lara ZMT an der Universität Bremen
Zweiter Gutachter	:	Prof. Dr. Venugopalan Ittekkot ZMT an der Universität Bremen
Erster Prüfer	:	Dr. habil. Matthias Zabel MARUM an der Universität Bremen
Zweiter Prüfer	:	Prof. Dr. Ulrich Saint-Paul ZMT an der Universität Bremen
Erstes Mitglied	:	Antje Baum Cand.rer.nat. ZMT an der Universität Bremen
Zweites Mitglied	:	Wolfger Strauss Student der Biologie an der Universität Bremen

Tag des öffentlichen Kolloquiums: 26 Juni 2007

Abstract

Three forests along a 600-m transect within a tropical mangrove in North Brazil were studied in a series of 1-m cores at rainy season to determine the chemical and physicochemical change relative to hydrology and species-specific effects. In North Brazil, macrotides (spring range 4 m) are an important factor associated with the spatial variation of the mangrove species. The results indicated an inundation two times higher at low plain (LP) colonized by a monospecific forests *Rhizophora mangle* than in high plain (HP) at *Avicennia germinans* forests. The flooding gradient result in a slightly acidic to basic pH (6.3-7.5) and lower redox potential (Eh) (0-100 mV) levels in LP sediments compared to HP (200 mV).

At surface sediments (10 cm) (HP), the Eh and pH showed stable values during non-submergence, whereas during submergence the Eh dropped drastically ~ 4.5-fold from 78 to -253 mV, concomitantly with pH increase to basic values. During submergence the relation ~50 mV and ~60 mV per pH unit was maintained, in sediments and water, respectively. The ~3-fold sulphide drop in the early stage of submergence was restored in a sinusoidal increase over time. Clearly, the effect of submergence on these trends is irrefutable. Meanwhile, the presence of the electrode can amplify the intensity of the measurements. The speciation of phosphorous (P) suggested that iron/aluminium-bound P (P-Fe/Al) is the main chemical bound in sediments (0.35 ± 0.09 to 0.56 ± 0.26 $mg.g^{-1}$) compared to calcium-bound P (P-Ca) (0.03 ± 0.01 $mg.g^{-1}$). In the horizontal layer (30 cm), the variation of extractable P (extr.-P) with inundation frequency (IF) was confirmed by a significant positive correlation ($r=0.81$, $n=29$). At HP, the higher Ca : P-Ca ratio (9-12) in relation to LP (4-8), reflected the low Ca-phosphate minerals precipitation, probably associated to the short-time inundation (2-3.5 h). The significant negative correlation ($r= -0.74$, $n=23$) between extr.-P and Al : P-Fe/Al ratio, suggested that the aluminium phosphate fraction seems to be the most significant fraction in controlling the P concentration in sediments.

In the vertical (50 cm) profiles, two oxidation and two reduction horizons were recognised. Stands of *R. mangle* and *A. germinans* differs in their responses to low sediment Eh conditions. *R. mangle* showed a moderate but constant root-induced oxidation capacity (ΔEh=66-125 mV), whereas *A. germinans* varied from low (ΔEh=22 mV, MP) to greater (ΔEh=193 mV, LP) oxidation. Implications of these findings in relation to P availability showed two features. In the first, the intense root-induced oxidation increased P-Fe/Al, total P (tot.-P) and acidification immobilized the extr.-P. In the second, the diminution of the root-oxidation was accompanied by the depletion of dominant pools of tot.-P and P-Fe/Al reflected in an extreme increase of extr.-P.

The low sedimentary OM (4.0 ± 0.8 %) (LP), supported evidence with respect to tidal hydrology, but do not clearly behaves with respect to decomposition processes. The significant negative correlation ($r= -0.74$, $n=13$) between C:N molar ratio and Eh confirmed the association of higher C:N ratios with reducing sediments, supported by the increase of organic carbon (org.-C) related to total nitrogen (tot.-N). Differences

of sulphur speciation between both species, demonstrated that their root-oxidation capacity greatly influence sulphur cycling in sediments. The SO_4^{2-} reduction was a less importance diagenetic pathway or the reoxidation of hydrogen sulphide due to the high abundance of iron keeps accumulating pore water sulphide concentrations low. In sediments below *A. germinans*, sulphide was only detected at middle plain (MP) (34-47 μM), whereas at LP higher sulphate (50 mM) occurred. The presence of two oxic-anoxic interfaces (Eh = 0 mV) were favourable for pyrite formation via polysulphide pathway. The degree of pyritization (DOP) values obtained here are indicative for sulphide-limiting suboxic conditions. Pyrite morphologies occur as minute dispersed grains, octahedral crystals, framboids and framboidal cluster. The wide variation in pyrite texture suggests that caution is needed in using pyrite as redox proxy to identify depositional environments. Phosphorus, sulphur and iron dynamics are closely coupled to the activity of mangroves trees and sulphate-reducing bacteria, suggesting that a combined effect of flooding with the P dynamics and the plant-sediment-microbial feedback contributes to the zonation of the investigated mangroves.

.

Zusammenfassung

Drei Wälder entlang eines 600 Meter langen Abschnittes innerhalb eines tropischen Mangrovenwaldes in Nordbrasilien wurden in der Regenzeit untersucht um den physiochemischen Wandel relativ zur Hydrologie und zum artspezifischen Effekt zu erforschen. Hier sind starke Überflutungen (Frühling: Höhe 4 m) ein wichtiger Faktor, der mit der räumlichen Veränderung der Mangrovenarten verbunden ist. Die Resultate zeigten im Vergleich eine doppelt so starke Überschwemmung im niedriger gelegenen Terrain (LP), kolonisiert ausschließlich durch *Rhizophora mangle*, wie im höher gelegenen Terrain (HP), den *Avicennia germinans* Wäldern an. Das Resultat der stärkeren Überschwemmungen zeigt sich in einem etwas leicht säurehaltigem bis basischem pH-Wert (6.3-7.5) und ein geringeres Redox-Potential (Eh) (0-100mV) in den LP Sedimenten verglichen mit HP (200mV).

Bei den Oberflächensedimenten (10 Zentimeter) (HP), zeigten die Eh- und pH-Werte zur Zeit der Nichtüberflutung stabile Niveaus wohingegen während der Überflutung der Eh-Wert drastisch fällt (ca. 4.5fach von 78 auf -253 mV), begleitend mit pH Zunahme zu den basischen Werten. Während der Überflutung es zeigte sich eine Relation von ~50mV und ~60 mV pro pH-Einheit in den Sedimenten bzw. im Wasser. Die sulfite Konzentration, die im ersten Stadium der Überflutung um 1/3 sank stieg im Laufe der Zeit sinusförmig wieder auf den zu Beginn gemessenen Wert an. Offensichtlich ist die Auswirkung der Überflutung auf diese Veränderungen unwiderlegbar. Allerdings kann die Präsenz der Elektrode die Werte der Messdaten erhöhen. Die Fraktionierung von Phosphor (P) zeigt, dass das an P gebundene Eisen/Aluminium (P-Fe/Al) die häufigste Chemische Verbindung in den Sedimenten (0.35 ± 0.09 to 0.56 ± 0.26 $mg.g^{-1}$) im Vergleich zu Kalzium gebundenem P (P-Ca) (0.03 ± 0.01 $mg.g^{-1}$). In der horizontalen Schicht (30cm) wurde die Dynamik von verfügbarem Phosphor (extr.-P) durch einen signifikanten positiven Zusammenhang ($r=0.81$, $n=29$) mit der Überflutungsfrequenz bestätigt.. Die höhere Ca: P-Ca ratio (9-12) im höher gelegenden Terrain, im Vergleich zum niedriger gelegenden Terrain, spiegelt den niedrigen Ca-Phosphat Mineralenausfall, der sicherlich verbunden ist mit der kurzzeitigen Überflutung, (2-3,5h) wider. Der signifikante negative Zusammenhang ($r= -0.74$, $n=23$) zwischen extr.-P und verfügbarer Al : P-Fe/Al Wert deutet darauf hin, dass die Aluminiumphosphatfraktion die signifikanteste Fraktion für die Kontrolle der Phosphorkonzentration in der Sedimentlösung zu sein scheint.

In den vertikalen (50cm) Bodenproben wurden zwei Oxidations- und zwei Reduktionsschichten festgestellt. Diese Ergebnisse zeigten, dass *R. mangle* Wälder und *A. germinans* Wälder sich in ihrer Reaktion auf niedrige Eh- Bedingungen des Sediments unterscheiden. Über den Abschnitt zeigte *R. mangle* eine moderate aber konstante wurzelinduzierte Oxidationskapazität (ΔEh=66-125 mV), wohingegen die wurzelinduzierte Oxidationskapazität von *A. germinans* zwischen niedrigeren (ΔEh=22 mV, MP) und höheren Werten (ΔEh=193 mV, LP) variierte. Die Auswirkung dieser Ergebnisse im Verhältnis zur Verfügbarkeit von P zeigen zwei Dinge. Erstens die intensive Wurzelinduzierte Oxidation erhöht den P-Fe/Al, das gesamte P (tot.-P) und durch Säurebildung fixierte das extr.-P. Zweitens wurde die Verringerung der Wurzeloxidation begleitet von der Abnahme überwiegender

Mengen von tot.-P und P-Fe/Al was sich in einem extremen Anstieg von extr.-P widerspiegelte.

Die niedrige Konzentration von organischem Material im Sediment (4.0 ± 0.8 %) (LP), unterstützte Hinweise von Flutungshydrologie aber keine deutlichen Hinweise auf einen Zusammenhang mit Zersetzungsprozessen. Der signifikante negative Zusammenhang (r= -0.74, n=13) der molaren Menge C:N und Eh sichert die Verbindung von höheren Mengen C:N und reduzierten Sedimenten, unterstützt vom Anstieg des organischen Kohlenstoffs (org.-C) in Beziehung zum gesamten Stickstoff (tot.-N). Unterschiede in den Schwefelfraktionen zwischen beiden Mangrovenarten belegen, dass ihre wurzelinduzierte Oxidationskapazität großen Einfluss auf die Schwefelzirkulation in den Sedimenten hat. Die SO_4^{2-} Reduktion ist entweder ein untergeordneter diagenetischer Pfad, oder die Rückoxydation von Schwefelwasserstoff wegen des Eisen Überflusses führt zu häufig auftretenden niedrigen Sulfidkonzentrationen im Porenwasser. In den Sedimenten unterhalb *A. germinans*, wurde Sulfid (34-47 µM) nur im mittlerem gelegenen Terrain (MP) aufgefunden, wohingegen im Vergleich im LP höhere SO_4^{2-} Werte (50 mM) auftraten. Die Anwesenheit von zwei oxidierten und unoxidierten Grenzflächen (Eh = 0 mV) begünstigte die Bildung von Pyrit durch Polysulfid Wege. Der hier aufgefundene Grad der Pyritisierung Werte (DOP) lässt Anzeichen von Sulfid hemmenden suboxisch Konditionen erkennen. Pyrit kommt in Form von minuziös kleinen Kristallen, octaedrisch geformten Kristallen, Framboiden und Framboidhaufen vor. Die grosse Vielfalt an Pyritformationen suggeriert, dass Pyrit als Indikator zur Bestimmung von Ablagerungen nur mit Bedacht gewählt werden darf. Die Dynamik zwischen P, Schwefel und Eisen ist eng verbunden mit der Aktivität der Mangroven und der Sulfat reduzierenden Bakterien. Der kombinierte Effekt von Überflutung mit P-Dynamik und Reaktion von Pflanzen-Sedimenten-Mikroben trägt zur Einteilung der untersuchten Mangrove bei.

Ackowledgements

I thank the Center for Tropical Marine Ecology and Núcleo de Estudos Costeiros for their support. This study is part of the Brazilian-German Cooperation Project MADAM and was financed by the Brazilian National Research Council (CNPq) and the German Ministry for Education and Research (BMBF) under the code no. 03FO154A. The author thanks the Deutscher Akademischer Austauschdienst (DAAD) for the scholarship support.

The author thanks Dr. habil Rubén Lara for supervising this thesis and his assistance in scientific support. As well, the author thanks Prof. Dr. Ulrich Saint-Paul for solves documents requests and his patience in the final phase of this work, especially thanks for his secretary Gaby Boehme.

The author is grateful for the collaboration of the Madam staff, in specially to Dr. Thorsten Dittmar, Helenice Santos, Cleise Cordeiro, Alexandre Rossi and Simplicio for the successfully team work, as well as, Matthias Birkicht, Dieter Peterke and Andreas Hanning for the technical support.

Especially mentioned are Prof. Dr. Venugopalan Ittekkot, Prof. Dr. Michael Böttcher and Dr. habil. Matthias Zabel for their interest and improve this work.

Last but not least, I would like to mention my parents and brothers for their precious support.

Tables of Contents

List of Figures

List of Tables

List of Equations

List of Abbreviations and Symbols

ACP	Amorphous Calcium Phosphate
ATP	Adenosin-tri-phosphate
Al : P-Fe/Al	Reactive-Al : Iron/Aluminium-bound P
AVS	Acid Volatil Sulphide
avail.-P	Available Phosphorus
BP	Before Present
BS	Bare Sediment
β-TCP	β-Tricalcium Phosphate
C	Carbon
ca	Circa
Ca^{2+}	Calcium
Ca : P-Ca	Reactive-Ca : Calcium-bound P
Chl a	Chlorophyl a
C_{inorg}	Inorganic Carbon
Conc.	Concentrate
C : P	Organic Carbon : Total Phosphorus Ratio
C : N	Organic Carbon : Total Nitrogen Ratio
C : N : P	Carbon : Nitrogen : Phosphorus Ratio
CV	Coefficient of Variation
DW	Dry Weight
D 1	Depression 1
D 2	Depression 2
DBH	Diameter at Breast Height
DCPA	Anhydrous Dicalcium Phosphate - Monetite
DCPD	Dicalcium Phosphate Dehydrate - Brushite
DIN	Dissolved Inorganic Nitrogen
DIP	Dissolved Inorganic Phosphorus
DIW	De-Ionized Water
DOC	Dissolved Organic Carbon
DOM	Dissolved Organic Matter
DON	Dissolved Organic Nitrogen
DOP^{1}	Dissolved Organic Phosphorus
DOP	Degree of Pyritization
DOS	Degree of Sulfidation
extr.-P	Extractable Phosphorus
Fe	Iron
Fe^{2+}	Ferrous Iron
$Fe(OH)_3$	Ferric Hydr(oxide)
FeS_2	Pyrite
FeS_{aq}	FeS clusters
Fe : P-Fe/Al	Reactive Iron : Iron/Aluminium-bound Phosphorus Ratio
Fig.	Figure
GIS	Geographical Information System

H^+	Protons
HAp	Hydroxyapatite
IF	Inundation Frequency
inorg.-P	Inorganic Phosphorus
Q	Freshwater Discharge
LOZ	Lower Oxidation Zone
LRZ	Lower Reduction Zone
MADAM	Mangrove Dynamics and Management
m.a.s.l	Meters Above Sea Level
max.	Maximal
min.	Minutes
nm	Nautical Miles
Nm	Number of Microcrystals
Mg^{2+}	Magnesium
N	Nitrogen
NH_4^+	Ammonium
O_2	Oxygen
OCP	Octacalcium Phosphate
OM	Organic Matter
org.-C	Organic Carbon
org.-P	Organic Phosphorus
P	Phosphorus
P-Ca	Calcium-bound Phosphorus
P-Fe/Al	Iron/Aluminium-bound Phosphorus
pH	pH_{H2O}
react.-Al	Reactive Aluminium
react.-Ca	Reactive Calcium
react.-Fe	Reactive Iron
ROL	Radial Oxygen Loss
POM	Particulate Organic Matter
POP	Particulate Organic Phosphorus
POR	Root Porosity
pyr.-Fe	Pyrite Iron
S	South
SO_4^{2-}	Sulphate
Sta.	Station
SEM	Scanning Electron Microscopy
SRM	Standard Reference Material
Tab.	Table
TDN	Total Dissolved Nitrogen
TDP	Total Dissolved Phosphorus
TEAP`s	Terminal Electron Accepting Processes
TFS	Total Free Sulphide
TOC	Total Organic Carbon
tot.-C	Total Carbon
tot.-N	Total Nitrogen
tot.-P	Total Phosphorus
TRS	Total Reduced Sulphide

TSS	Total Suspended Solids
UOZ	Upper Oxidation Zone
URZ	Upper Reduction Zone
VC	Variation Coefficient
W	West
ZMT	Zentrum für Marine Tropenökologie

List of Units

ΔG^o	Free Energy Change
^oC	Degree Celsius
^{14}C	Stable Carbon Isotope
h	Hour
km	Kilometer
km^2	Square Kilometer
‰	ppt (parts per thousand = g/kg)
lt	Liter
m	Meter
$mg.g^{-1}$ DW	Milligram per Gram per Dry Weight
mg/l	Milligram per Liter
min	Minutes
mm	Millimeter
mM	Millimolar
m^3/s	Cubic Meter per Seconds
mV	Millivolts
ppm	Parts per Million
PSU	Practical Salinity Units
sec	Seconds
t C/ha/y	Tons of Carbon per Hectare per Year
v	Volts
VC	Variation Coefficient
%	Percentage
$\delta^{13}C$	Stable nitrogen isotope
wt%	weight % of dry weight
Δ	Variation
$\bar{x}$	Average
µm	micrometer

CHAPTER 1 - INTRODUCTION

Mangroves represent a taxonomically-diverse group of woody shrubs, which possess a common ability to survive along sheltered tropical coastline in saline environments under tidal influence (Snedaker, 1982). On a global scale, about 60-75 % of mangroves are found throughout tropical and subtropical coasts, with a world-wide extension of about 181,000 km^2 (Spalding *et al*., 1997). In South-America mangroves cover about 23,800 km^2, from which 10,713 km^2 are estimated to grow along the Brazilian North coast in the States of Amapa, Pará and Maranhão (Schaeffer-Novelli *et al*., 1990). These mangroves are still conserved but under increasing anthropogenic pressure (Krause and Glaser, 2003), constituting the study area for an integrated research project initiated in 1996 in the frame of a Brazilian-German cooperation project on mangrove dynamics and management (MADAM).

Mangroves are highly productive ecosystems, where trees can reach net primary production rates as high as 30 t C/ha/y (Clough, 1988). One third of this production is represented by plant litter, mainly leaves (Robertson *et al*., 1992). The leaves, flower parts and propagules can be flushed by the tides into mangroves waterways, where decomposition by the processes of leaching, saprophytic decay and fragmentation occur, resulting in particulate matter net transport (export) to the adjacent coastal waters. There is also evidence for a substantial net export of dissolved organic mater (DOM), reaching the same order of magnitude as litter export in some mangrove areas (Dittmar and Lara, 2001a; Twilley, 1985). Outwelling of DOM from the mangrove may be associated by leaching of dissolved components of leaf litter. However, no general consensus has hitherto been reached about the role mangroves play for the export and import of nutrients for the adjacent coastal waters (Dittmar *et al*., 2001).

The main goal of the present study was the evaluation of the nutritional status of Bragança mangrove forest and oxygen- (trough its control on the iron cycle) and sulphate-controlled phosphorus release from sediments of aquatic. The performed estimations were integrated to the available researches of mangroves, saltmarsh, fens and wetlands rice soils in order to understand the contribution of the availability of

phosphorus by flooding and plant-induced processes to the overall nutrient budget of this tidally-driven costal ecosystem

1.1. Phosphorus in coastal waters

Oceanic fertility is largely dependent on the availability of the limiting nutrient phosphorus (P) for sustaining primary productivity (Redfield, 1958). In surface waters of oligotrophic region, dissolved organic phosphorus (DOP[1]) often comprises a significant fraction of the dissolved pool (Orrett and Karl, 1987; Karl and Yanagi, 1997); thus regeneration of P from DOM is a potentially important source of bioavailable-P (avail.-P) (Kolowith *et al*., 2001). Within pools of marine dissolved and particulate P, turnover rates of DOP and particulate organic phosphorus (POP) are faster than dissolved inorganic phosphorus (DIP), and seasonal, enabling low inorganic-P (inorg.-P) concentrations to support relatively high primary production (Benitez-Nelson and Buesseler, 1999). The behaviour of dissolved components in the mixture of fresh- and sea-water, can be analysed in a classic, linear, estuarine "mixing diagram" relationship with the salinity, where a conservative behaviour reflects only a physical mixing (i.e. no growth or decay) and the non-conservative reflect physico-chemical and/or biological processes. The non-conservative behaviour suggests the addition of matter gained by degradation of organic matter or desorption of mud, and the loss of matter within the estuary by adsorption on mud and phytoplankton uptake (Artemeyev, 1996). The fate of nutrients varies from estuary to river as a function of water flow, turbidity and biota, as a result of these influences, phosphate usually behaves non-conservatively in turbid estuaries (Morris *et al*., 1981).

Elemental ratios of carbon (C), nitrogen (N) and phosphorus (P) are used to evaluate marine organic matter (OM) production and diagenesis, as well as nutrient regeneration. Redfield ratios estimate the elemental properties in phytoplankton, with the atomic C:N:P ratio of marine particulate organic matter (POM). These elements are essential in the composition of basic functional and structural compounds of algae (Billen *et al*., 1991). The two major sources of OM to marine sediments are terrestrial and marine plants with distinctive C:N:P ratios. Marine phytoplankton has an average ratio of 106:16:1 (Redfield, 1958). In contrast, terrestrial plants are characterized by

organic C:P ratios ranging from 300 to 1300 and C:N ratios ranging from 10 to 100 for soft tissue, and C:P ratios greater than 1300 and C:N ratios ranging from 100 to 1000 for woody tissue (Hedges *et al*., 1986; Goñi and Hedges, 1995; Ruttemberg and Goñi, 1997). In river-dominated coastal areas a two end-members mixture of terrestrial and marine phytodetritus occurs. Elemental ratios should trend from high (above Redfield ratios) C:N:P ratios, in sediments closest to the riverine input, to progressively lower ratios approaching the Redfield ratios, with distance away from the mouth (Ruttemberg and Goñi, 1997). This pattern would result in a gradient, from near-shore sediments enriched in riverborne DOM, to more distal in which marine derived organic material becomes progressively a more important component between organic material pools. Given the predominant contribution of DOM and the rapid settling of particulate matter from rivers plumes, presume that much of the cycling of C, N, P in river plumes involve DOM. Large rivers also discharge significant amounts of particulate materials (Dagg *et al*., 2004). Thus, a large fraction of the river-borne POM is initially deposited near the mouth. The release of nutrients from fluvial particles into the seawater, occurs through remineralization or desorption from suspended particles and resuspended bottom sediment (Mayer *et al*., 1998). In oligotrophic waters, such as the Brazilian region, the Redfield ratios are most related to the ratio of total dissolved nitrogen (TDN) and total dissolved phosphorus (TDP), than the dissolved inorganic nitrogen (DIN) and dissolved inorganic phosphorus (DIP) alone, implying that dissolved organic nitrogen (DON) and DOP[1] are important nutrient sources (Karl *et al*., 1993; Kolowith *et al*., 2001). An understanding of the chemical factors that regulate the production of coastal marine ecosystem, requires also a detailed assessment of the controls on the availability of the essential nutrients at the adjacent wetland sediments.

1.2. Phosphorus in mangroves

Mangroves are very efficient mud traps, essential as physical substrate and nutrient source for forest development. Biogeochemical processes within the mangrove forest, mainly within the upper sediment horizon, are relatively well understood (i.e. reduction of oxides, interaction soil/plant). However the role of flushing time, inundation frequency, degree of water-logging and stagnancy dynamics for nutrient

trapping and mobilization are major questions in mangrove geochemistry. All of these interrelated variables can deeply influence the system, from which the inundation frequency acts as a controller on the nutrient availability, because it strongly influences salinity and anoxia (Boto and Wellington, 1984).

Mangrove sediments are usually anaerobic, with a good supply on OM and sulphate ions, where iron sulphides (FeS_2) are common. As in other tropical marine deposits, dissolved inorganic nutrients concentrations (except ammonium NH_4^+) are low in mangrove sediments, due their rapid turnover, lower redox potential condition and recalcitrant character of OM (Boto *et al*., 1989). Additionally, they have very small pools of labile OM, but very rapid DOM turnover, linked to the standing amounts of root materials (Nedwell *et al.,* 1994; Alongi *et al.,* 2000). Dissolved and particulate P concentrations in mangrove sediment are generally low (Alongi *et al*., 1992). Although organic P (org.-P) is the major fraction, the inorg.-P probably represents the largest potential pool of plant-available, soluble reactive P (Boto and Wellington, 1988). In the domain of pH that is relevant to most soils, $H_2PO_4^-$ and HPO_4^{2-}, are the dominant orthophosphate ions (Lindsay, 1979). To the exchange with the estuarine waters, the pore- and groundwater P can be leached by rainfall, tidal inundation or drainage (Dittmar and Lara, 2001b). Mean concentrations of extractable phosphorus (extr.-P) across a mangrove forest gradient decrease with tidal height, it can become limiting in elevated areas (Boto and Wellington, 1983; Silva and Sampaio, 1998). This supports that the differential flood tolerance is one of the possible cause determining a spatial pattern of distribution (i.e. zonation) of the mangrove species (Snedaker, 1982).

In this section are described 1) the nutrient uptake and changes in rhizosphere pH in terms of the P chemistry, 2) activity of roots due the redox conditions developing in sediments following submergence, and 3) precipitation and dissolution of phosphate minerals.

Phosphorus is present in plants as a constituent of compounds as nucleic acids, phospholipids and ATP (Marschner, 1995). The primary source of P for plants is

inorg.-P, depending on the methodology also termed extractable, exchangeable, labile, available or bioavailable P (Salcedo and Medeiros, 1995). In most natural ecosystems plant growth is limited by the availability of inorg.-P (Smith *et al*., 2003). The major processes responsible for the maintenance of cation-anion balance in plants and changes in rhizosphere pH are: 1) extrusion of H^+ or OH^- and 2) accumulation and degradation of organic acids (Haynes, 1990). The generation of rhizosphere acidity or alkalinity is directly influenced by plant roots since unequal amounts of nutritive cations and anions are typically absorbed. In order to maintain the electroneutrality at the soil-root interface, the uptake of the anion P (PO_4^{2-}, $H_2PO_4^-$, HPO_4^{2-}), can be stoichiometrically balanced by the active excretion of OH^-, similarly than the uptake of a cation (e.g. NH_4^+, Ca^{2+}, Mg^{2+}, K^+, Na^+) is balanced by H^+ excretion (Haynes, 1990). The biochemical pH maintenance within the cells, or pH-stat, can be modified by strong or weak organic acids via carboxylation/decarboxylation mechanisms (Davies, 1986). The amount of organic acids excreted solubilize P by chelating metals ions that would immobilize it or forming soluble complexes with P via metal ions, or both (Saleque and Kirk, 1995; Kirk, 1999; Neumann *et al*., 2000). Such changes in rhizosphere pH can occur in response to adverse nutritional conditions, such as P deficiency (Haynes, 1990).

A morphological adaptation of mangrove species to flooding is the formation of various forms of aerial and adventitious roots (Scholander *et al*., 1955; Blom *et al*., 1994). In *Rhizophora* the aerial components are divided in horizontal arches and vertical columns known as stilt roots. The columns supply oxygen to the underground roots. Air passes into the column roots through lenticels and roots entering the sediment are composed by aerenchyma tissue. In *Avicennia*, shallow, horizontal roots radiate outwards, often for a distance of many meters. At intervals of 15 to 30 cm vertical structures known as pneumatophores emerge up to 30 cm above the mud interface. A single *Avicennia* tree of 2 to 3 m height may have more than 10 000 pneumatophores. The pneumatophores, like the column roots in *Rhizophora*, have lenticels and aerenchyma. Simple physical diffusion trough the lenticels and along the aerenchyma is probably the main mode of gas movement in mangrove roots (Hogarth, 1999). Gas transport by mangrove root systems is so effective that it even aerates

surrounding sediment in a radial direction the so-called radial oxygen loss (ROL) (De Simone *et al*., 2002; Haase *et al*., 2003; Begg *et al*., 1994). The radial extension of the oxidized zone (higher redox potentials then the bulk sediment) around the root tips extended for < 3cm to 0.5 m (McKee, 1993).

The leakage of O_2 supports the oxidation of ammonia to nitrate and sulphide to sulphate, and consequently the suppression of phytotoxins such as soluble sulphide species (i.e. H_2S, HS^-, S^{2-}) (Thibodeau and Nickerson, 1986; McKee *et al*., 1988). However, oxidation of sulphides to non-toxic sulphur compounds may occur in the oxidized rhizosphere or in the root prior to assimilation (Mendelssohn and McKee, 1988). Previous studies of flood-tolerant plants such as rice, demonstrated roots uptake sulphur as sulphate (i.e. SO_4^{2-}) (Pezeshki *et al*., 1988). Sulphate uptake was a major factor causing foliage damage and yield reduction in rice plants (Vamos and Koves, 1972).

Additionally, the produced oxygen can immobilize iron through the oxidation of Fe(II) which is precipitated as Fe(III) (hydr)oxides, resulting in a zone of Fe(III) accumulation near the roots (i.e. iron plaques), generation of protons (H^+) and consequently pH decrease (Begg *et al*., 1994) (**Equation 1**, Begg *et al*., 1994).

$$4Fe^{2+} + O_2 + 10H_2O \rightarrow 4Fe(OH)_3 + 8H^+ \qquad \textbf{Eq. 1}$$

This process may have some effects on the trapping of P as $FePO_4$ (**Equation 2**, Silva and Sampaio, 1998). The supply of P to roots would therefore depend on the balance between sorption on Fe (III) (hydr)oxides and release from acid-soluble forms, such as calcium-bound P (P-Ca) (Saleque and Kirk, 1995; Silva, 1992).

$$Fe(OH)_3 + H_2PO_4^- \rightarrow FePO_4 + OH^- + H_2O \qquad \textbf{Eq. 2}$$

The reduction of a submerged sediments proceeds roughly in the sequence predicted by thermodynamics (O_2, NO_3^-, Mn(IV), Fe(III), SO_4^{2-}), when one oxidant (electron acceptor) is depleted, the next more energetic redox reaction (i.e. higher free energy

change - ΔG^o) will occur in a specific redox potential (Stumm and Morgan, 1981; Libes, 1992). In fact, in a real system these reactions can overlap as the theoretical considerations. Concomitantly, organic matter is oxidized, dissolved CO_2 accumulates, and the pH of acid sediments tends to increase and that of alkaline sediments to decrease, stabilizing in the range 6.5-7.0 (Kirk, 2003). The initial Eh drop is apparently due to the release of reducing substances accompanying O_2 depletion, such as Fe(II), Mn(II), NH_4^+ and S^{2-}, before Mn (IV) and Fe(III) (hydr)oxides can mobilize their buffer capacity (Ponnamperuma, 1972). The most relevant consequence of reduction for the plants is the increase in concentration of plant-available P. Since most flooded acids soils have a supply of Fe (III) (hydr)oxides than any other oxidant, the increase in pH of acids soils is largely due to the reduction of Fe (Ponnamperuma, 1972) (**Equation 3**, Ponnamperuma, 1972).

$$Fe(OH)_3 + 3H^+ + e \rightarrow Fe^{2+} + H_2O \qquad \textbf{Eq. 3}$$

In intermittently flooded sediments, as the mangrove, anoxic conditions affect the equilibrium of $Fe(OH)_3$-Fe^{2+} system (Ponnamperuma, 1972). An example of this change is illustrated for $FePO_4.2H_2O$ (strengite) and $Fe_3(PO_4)_2.8H_2O$ (vivianite). Iron in strengite is present as Fe(III), whereas in vivianite it is present as Fe(II). When acid sediments are flooded and reduction occurs, Fe(II) increases and depresses the solubility of vivianite, making it the most stable phosphate mineral. When the submerged sediments are again drained, oxidizing conditions return, causing vivianite to dissolve. The P is released in some other form, most likely Fe and/or Al phosphate. In this way tightly bound Fe and Al can be solubilised under reducing conditions. In acid sediments, $AlPO_4.2H_2O$ (varicite) is shown as the most stable mineral, followed by strengite in equilibrium with sediment-Fe (Lindsay *et al*., 1989).

In alkaline sediments Ca phosphates are the most stable minerals. They decrease in solubility in the order $Ca_9(PO_4)_6.nH_2O$ (amorphous calcium phosphate-ACP) $CaH(PO_4).2H_2O$ (brushite or dicalcium phosphate dehydrate-DCPD) > $CaH(PO_4)$ (Monetite or anhydrous dicalcium phosphate-DCPA) > $Ca_4H(PO_4)_3.2.5\ H_2O$ (octacalcium phosphate-OCP) > β-$Ca_3(PO_4)_2$ (β-tricalcium phosphate- β-TCP) >

$Ca_5OH(PO_4)_3$ (hydroxyapatite - HAp) > $Ca_5F(PO_4)_3$ (fluorapatite) (Lindsay *et al*., 1989). Apatite written in this work as P-Ca, is the main source of inorg.-P in nature (Dorozhkin, 2002). Autighenic apatite is precipitated in estuarine pore-water and in the water-sediment interface of marine sediments during early diagenesis (Cappellen and Berner, 1991). The precipitation of apatite from aqueous solutions involves multiple steps, such as nucleation of a precursor calcium phosphate phase, cluster aggregation, crystal growth and transformation to apatite. The net precipitation reaction depends of several factors, including pH, ionic strength, Ca:P ratios, and the presence of other ions such as Mg^{2+}, CO_3^{2-} and F^- (Sahai, 2003). From these ions, H^+ catalyze the precipitation and Mg^{2+} can block the adsorption sites on calcite inhibiting the precipitation (Brown, 1981; Yadav *et al*., 1984; Wang *et al*., 1995). In experimental studies the precipitation did not start at a low Ca:Mg ratio (0.2), Mg^{2+} ions can impede the nucleation and growth of apatite for one week in carbonate-free synthetic seawater (Cappellen and Berner, 1991) and for 700 days in brackish seawater, at 23-25^oC and pH 6.75-7.3 (Gunnars *et al*., 2004). At a given degree of saturation, the formation of apatite is significantly faster at a high Ca:Mg ratio (4.5-9) (Gunnars *et al*., 2004). Moreover, a high Mg/Ca ratio benefits Mg^{2+} only in the first step, but because the overall ΔG^o for $CaPO_4$ is faster, Ca^{2+} ultimately prevails (Sahai, 2002). The precipitation is performed in neutral to alkaline environments as follows (**Equation 4**, Nriagu, 1976).

$$5CaCO_3 + 3HPO_4^{2-} + H_2O + H^+ \rightarrow Ca_5(PO_4)_3OH + 5HCO_3^- \qquad \textbf{Eq. 4}$$

Protons catalyse apatite precipitation by neutralization of its surface charge, point of zero surface charge at pH 7 to 8, and reduction of the surface tension between nuclei and solutions, thus promoting nucleation and growth (Christoffersen *et al*., 1989). At pH = 7 the growth rate of fluorapatite is nearly twice than at pH = 8 at 25^oC, for identical degrees of supersaturation (Cappellen and Berner, 1991). It has been suggested that protonation of PO_4^{3-} groups on the apatite crystal catalyzes the exchange of PO_4^{3-} between the bulk solution and crystal surface, and, hence, accelerates both precipitation and dissolution (Christoffersen and Christoffersen, 1982; Cappellen and Berner, 1991). This explains why the rate of dissolution at

constant pH in non-stoichiometric solutions far from equilibrium, is not uniquely given by the ionic product, but depends on the actual values of both the calcium and the phosphate concentrations (Christoffersen and Christoffersen, 1982).

For the mechanisms of apatite dissolution, eight models have been already proposed to simulate the processes involved. Each model was found to have limitations and draw-backs, none of them was able to describe apatite dissolution in general. Most of them were elaborated for apatite dissolution in slightly acidic or nearly neutral conditions (4< pH < 8) and temperatures of 25 to 37^{o}C (Dorozhkin, 2002). The chemical approach describes the transformation of apatite into acidic calcium phosphates, considering as a hydrogen catalytic mechanism (**Equations 5a**, Nriagu, 1976; **5b**, Dorozhkin, 2002):

$$Ca_5(PO_4)_3OH + 4H^+ \rightarrow 5Ca^{2+} + 3H_2PO_4^- + H_2O \qquad \textbf{Eq. 5a}$$

$$Ca_5(PO_4)_3(OH, F) + 7H^+ \rightarrow 5Ca^{2+} + 3H_2PO_4^- + HF, H_2O \qquad \textbf{Eq. 5b}$$

Pore waters of sediments deposited on the continental margins are often more acidic than the overlying seawater as a result of the microbial degradation of OM (Ben-Yaakov, 1973). The values of pore-water pH in organic-rich mangrove sediments are in the range 5.5-8, with a mean value around 6-7 (Middelburg *et al*., 1996, Clark *et al*., 1998; Marchand *et al*., 2004; Alongi *et al*., 2004). The lower pH values found in these sediments are unfavorable to apatite precipitation since the solubility of apatite increases with decreasing pH. This effect, however, is partially offset by the kinetic effect of the flooding water pH which acts in the opposite direction. The residence time of the flooding water can act as a factor controlling the dissolution kinetics of apatite. In manure, the longer the residence time (< 16 weeks), the closer the solution P levels would approach the chemical equilibrium (Wang *et al*., 1995). In wetlands, P flux in soil drained for 6 weeks was 10-fold higher than in soils drained for 3 weeks (Olila *et al*., 1997). The prediction of long-term P retention in daily-flooded surface horizons of mangroves, caused probably due the basic flooding water that increase the porewater pH, requires a better knowledge of the stability of phases with which P is associated. To date, it is uncertain to what extent the inundation degree and creek

water pH may be relevant for the stability of P compounds in mangrove sediments on the short scale of a tidal cycle (Cohen *et al*., 2004).

The dynamic of mangrove roots growing in flooded soil in relation to nutrient uptake is poorly understood. More detailed investigations are needed on the interaction between sediment characteristics, flooding, bacteria induced reduction of sediment environment and the root-induced oxidation and/or acidification controlling the nutrient status of the whole ecosystem.

CHAPTER 2 – STATE OF THE ART

2.1. Phosphorus in coastal waters

Despite the important role that mangroves play in the biogeochemical cycles of coastal and even off-shore environments, only a few quantitative long-term export/import balances exist. These are Hinchinbrook Island (Australia) (Boto and Bunt, 1981; Boto and Wellington, 1988; Alongi *et al*., 1998; Ayukai *et al*., 1998), Rookery Bay (FL, USA) (Twilley, 1985), Klong Ngao (Thailand) (Wattayakorn *et al*., 1990) and Bragança Peninsula (North Brazil) (Dittmar, 1999; Dittmar and Lara, 2001a). In Hinchinbrook Island the mangrove functions as source and also effective sink for dissolved nutrients and organic carbon (org.-C); in Rookery Bay was determined a net export of dissolved nutrients and suspended org.-C; and in Klong Ngao was reported export of inorganic nutrients. All mangrove flux investigations were carried out in micro- and mesotidal regions with exception of Bragança Peninsula, where macrotides enable a net export. Many discrepancies between the studied mangroves may have the resulted from methodological differences and difficulties in accurately determining temporal and annual material fluxes (Boto and Wellington, 1988), and different tidal range, topography, sediment chemistry or community structure of the ecosystems (Ayukai *et al*., 1998).

In the Bragança Peninsula, Dittmar et al. (2001b) based on the "Eulerian" approach and time-series of nutrients, identified a net export of dissolved inorganic nutrients (e.g. N, P and silicate) from a creek catchment area (2.2 km^2) to the Caeté Estuary. A significant export of phosphate with average 0.05 $mmol/m^2/d$, occurred principally during the dry season. Previous studies suggested the immobilization of Ca-species during mangrove inundation (Cohen *et al*., 2001), leading to asymmetries in the tidal concentration oscillations (Dittmar *et al*., 2001a). Tidal range and flooding therefore determined direction and quantity of nutrient and OM exchange between mangroves and the ocean.

2.2. Phosphorus in mangroves

Various factors can contribute to mangrove zonation, such as, an expression of plant sucession, a response to geomorphic change, a physiological response to tide gradients and differential propagule dispersal (Snedaker, 1982). In mangrove systems, most available information on inundation regime and nutrient dynamics focused two main topics:

1) the impact of physicochemical properties on mangrove zonation (Snedaker, 1982; Boto and Wellington, 1984; Matthijs *et al*., 1999).
2) the study of various redox processes in relation to organic matter (Hesse, 1961; Clark *et al*., 1998; Alongi *et al*., 1998a; Alongi *et al*., 1999; Marchand *et al*., 2004) and nutrients (Boto and Wellington, 1983; Silva *et al*., 1998).

In these literatures, some discrepancies exist about the differential abilities of *R. mangle* and *A. germinans* to make the sediments less hypoxic. Nickerson and Thibodeau (1985) described on a mangrove in Bahamas a strong correlation between the distribution of these species and the amount of hydrogen sulphide in the sediment, and proposed that only *A. germinans* has a capacity to reduce pore-water sulphide. In another, similar studies, the opposite associated to the Belizean mangroves (McKee, 1988) and Gazy Bay (Kenya) (Matthijs *et al*., 1999) was found. The apparent differential effect reported by these authors, did not consider previous studies (Scholander *et al*., 1955; Gill and Tomlinson, 1977) which demonstrate physiological adaptations to flood tolerance for both species (e.g. aerenchyma and lenticels). All these studies, utilized electrochemical measurements with electrodes for the determination of sulphide and redox potential, inserted in extracted pore-water or directly on sediments. Strictly, only the latter methodology is physical-chemically meaningful, but is also subjected to various error sources.

A redox stratification model was proposed by Clark et al. (1998) for an *Avicennia*-dominated Australian mangrove sediment profile (<70 cm depth), where the concentration and chemical speciation of metals are influenced by the distribution of geochemically distinct horizons. In the reduction horizons with a pH > 7 and an Eh < -150mV, metals are largely present as sulphide-bound species (e.g. FeS_2), whereas in

the oxidation horizons with pH < 7 and an Eh > +100 mV, most metals are present as exchangeable or (hydr)oxide-bound species (e.g. $Fe(OH)_3$, Fe_2O_3). The upper oxidation zone was related to the periodically drying and re-oxidation of sediments and also the bioturbation. The lower oxidation zone was related to oxygen intrusion in the sediment via adventitious roots of plants and via diffusion of air through pores, drained during low tides. As a result of rapid changes in redox potential in the upper horizons of mangrove sediments, sulphate reducing bacteria (e.g. *Desulphiovibro desulphuricans*) utilise the organic molecules and obtain energy by reducing sulphate to potentially metal-biding sulphides, from ferric compounds (e.g. Hematite Fe_2O_3 or Fe(III) (hydr)oxide) to iron sulphides (e.g. Mackinawite $FeS_{(1-x)}$, Greigite Fe_3S_4, Pyrite FeS_2) (**Equations 6a,** Kirk, 2004; **6b,** Clark *et al*., 1998). In equation 6b M^{2+} represents any divalent metal, usually Ca^{2+} and Mg^{2+}. The dissolution of iron sulphides occurs when it reacts with oxygen, this oxidation generates H^+ and large amount of sulphuric acid, lowering pore-water pH in the oxidation zones (**Equations 7a** and **7b**, Kirk, 2004).

$$2Fe_2O_3 + 8SO_4^{2-} + 16CH_2O + O_2 \rightarrow 4FeS_2 + 16\ HCO_3^- + 8\ H_2O \qquad \textbf{Eq. 6a}$$

$$9CH_2O + 4SO_4^{2-} + 4Fe(OH)_3 + 4M^{2+} \rightarrow 4FeS + 4MCO_3 + 15H_2O + 5CO_2 \qquad \textbf{Eq. 6b}$$

$$4FeS_2 + 15O_2 + 14H_2O \rightarrow 4Fe(OH)_3 + 8SO_4^{2-} + 16H^+ \qquad \textbf{Eq. 7a}$$

$$FeS + 3/2\ O_2 + H_2O \rightarrow Fe^{2+} + SO_4^{2-} + 2H^+ + 2e^- \qquad \textbf{Eq. 7b}$$

The formation of pyrite is an indicator of the oxic-anoxic transition (Wilkin *et al*., 1996) or the iron oxide barrier (Clark *et al*., 1998). Pyrite formed in mangrove sediments has the dominant textural forms of euhedral cristals and framboids (Gleason *et al.*, 2003). Studies of sulphur, iron (Fe) and P dynamics in other wetlands, indicates that a strong sulphide/reactive Fe dependency controls P solubility under reduced conditions (Boto *et al.*, 1984; Caraco *et al*., 1989). The latter hypothesis suggests that formation of iron sulphides can prevent the re-supply of iron oxides to surface sediments, enhancing the formation of extr.-P available for the vegetation.

The effect of oxidation and acidification mediated by plants on mobilization and remobilization of nutrients, has been seldom studied in mangrove species. Worldwide, several studies on this effect were done mainly in wetland rice sediments. Saleque and Kirk (1995) suggested that the bulk of P taken up by the plants was from the acid-soluble pools included calcium-bound P, amorphous ferrous hydroxides and carbonates. Since the zones of acid-soluble P depletion coincided with the acidification zones, they concluded that the acidification caused P solubilization. Another studies investigated the P uptake by rice from alternately flooded and drained soils (Huguenin-Elie *et al*., 2003). They concluded that in the continuously flooded soil, the P solubilization was consistent with acidification as a result of oxidation of Fe^{2+} by oxygen (O_2) released from roots (**Equation 1**), contrary to the moist sediment alternately flooded where the P solubilization was coincident with organic anion excretion from roots.

In Brazil, pioneer studies showed that P-Ca (Silva, 1992) and iron/aluminium-bound P (P-Fe/Al) (Silva and Sampaio, 1998) were the main inorg.-P species. In both studies the tidal inundation appears to influence these chemical reactions involving P retention and release. The hypothesis that differential flood tolerance is one of the possible causes determining a pattern of mangroves distribution has been studied in Bragança Peninsula, where macrotides constitute the main hydrodynamical features of the coastal ecosystem. The available information was based on chemical methods (Reise, 2003), GIS tools (Cohen *et al*., 2004) and empirical models (Berger *et al*., in submission). The variation in structure, biomass and productivity studied by Reise (2003) showed an interdependency between inundation frequency, bulk density, sediment salinity and P concentration. In the empirical models, the structural pattern was characterized by a disproportionate change in growth rates beteween *L. racemosa* and *A. germinans* during early forest succession, which might be explained by species-specific differences in nutrient-uptake efficiency (Berger *et al*., in submission).

Our study considered for the plant availability of P the topography, the inundation frequency and the physiological plant response (i.e. oxidation/acidification) to tide-

maintained gradients, in agreement with the most relevant mangrove zonation factors considered by Snedaker (1982). Physiologically, the effect of the substrate conditions is ultimately reflected in the distribution and accumulation of nutrients in roots and leaves.

CHAPTER 3 – OBJETIVES

3.1. Physicochemical patterns and phosphorus status of mangroves

The major aims of this chapter, was to explore the general hypothesis that differences in sediment chemistry in relation to phosphorus uptake by mangrove forests colonized by *R. mangle* and *A. germinans*, are a function of physical environment (e.g. low- vs. high-intertidal position) and the species-specific capacity to alter sediment conditions. Along a topographic gradient in North Brazil, the comparisons of physicochemical (Eh, pH) and chemical (i.e. phosphorous fractionation) parameters in paired stations at equivalent topographic elevations were aim to a) identify the species-specific effects relative to the effects of the hydrology (i.e. inundation frequency), and b) assess the intensity and importance of each parameter (e.g. species-specific effects and hydrology) as factors influencing the phosphorus availability and mangrove zonation.

This chapter was attempts to gain information upon the following specific points:

a) Evaluation of the variation for physicochemical parameters (e.g. Eh, pH, sulphide) in surface (10 cm) sediments subjected to submergence and non-submergence of macro-tides, to examine the impact of short-time inundation on the precipitation and dissolution of phosphate minerals (e.g. P-Fe/Al, P-Ca).

b) Determination whether the sediment physical-chemical parameters (e.g. Eh, pH, sulphide) were affected by proximity to mangrove aerating structures (i.e. prop roots for *R mangle* and pneumatophores for *A. germinans*), to compare the relative effect of the presence of one and two species aerating structures on sediment physicochemical parameters (e.g. Eh, pH, sulphide).

3.2. Dynamics of sulphur in mangrove sediment

In this study, *R. mangle* and *A. germinans* forests inhabiting different tidal elevations settings in the Bragança Peninsula (North Brazil) were addressed to determine the spatial pattern of iron sulphur speciation in sediments of both forests. The distribution of mangrove forest allowed us to test the hypothesis that difference in the sulphur and iron pools are a function of physical settings (e.g. low- vs. high-intertidal position and regional differences in sediment composition) rather than the capacity of different species to alter sediment conditions.

This chapter was aim to provide additional information on the following specific points:

a) Examination of the differences in organic matter diagenesis among the present plant species precursors, assessing the origin and degree of organic matter preservation by C:N ratios. The data on carbon and nitrogen pools allow the estimation of their efficiency of mineralization at some of the habitats.

b) Formation of iron sulphides, the importance of reactive iron and limiting factors for pyrite formation. Further, the stability of pyrite used as a redox proxy to identify depositional environments.

CHAPTER 4 - DESCRIPTION OF THE STUDY AREA

4.1. Location

The research region is the mangrove ecosystem located Southeast of the Amazon delta in the State of Pará, Northeast Brazil. The sector between Belém (Pará) and São Luis (Maranhão) represent 83% of the total mangrove area of the Amazonian States Amapá, Belém and Maranhão (**Fig. 1**). This sector is considering the world's largest unitary mangrove system, estimated to cover a total area of about 8,900 km^2 of coastline (Kjerfve and Lacerda, 1993; Kjerfve and Macintosh, 1997; Kjerfve *et al*. 1997).

4.1.1. Mangrove forest

The study area is situated on a higher part of the central sector to the East side of the mangrove peninsula of Bragança, which is part of the mangrove belt along about 350 km southeast of the Amazon estuary (46°42'16''W - 46°42'02''W to 0°55'40''S - 0°55'58''S, 2.4 m.a.s.l.) (Cohen *et al*., 1999). The MADAM project area is located between the mouth of the Rivers Maiaú and Caeté **(Fig. 2)**.

4.2. Hidrology

4.2.1. Amazon region

The mouth of the Amazon estuary, which is the dominant freshwater source influence in Northern Brazil, is composed by two major systems: The Amazon and the Pará Rivers, whose discharge greatly varies with season. The Amazon has large enough flow year-round to prevent the intrusion of salt water into the river mouth (Gibbs, 1970), allowing unimpeded transport of sediment to the continental shelf. The suspended load from the Amazon River varies from 23 to 123 mg/l during dry and rainy season, respectively (Gibbs, 1967). The coastal sediments adjacent to these rivers contains organic carbon to nitrogen ratios (Corg:N) which exceed 10, reflecting the terrigenous or freshwater POM, these ratios decrease seaward remaining higher than 5 (Milliman, 1975). Superficial sediments on the middle and inner shelf South of the Pará River are composed with greater than 90% sand (Shepard, 1932).

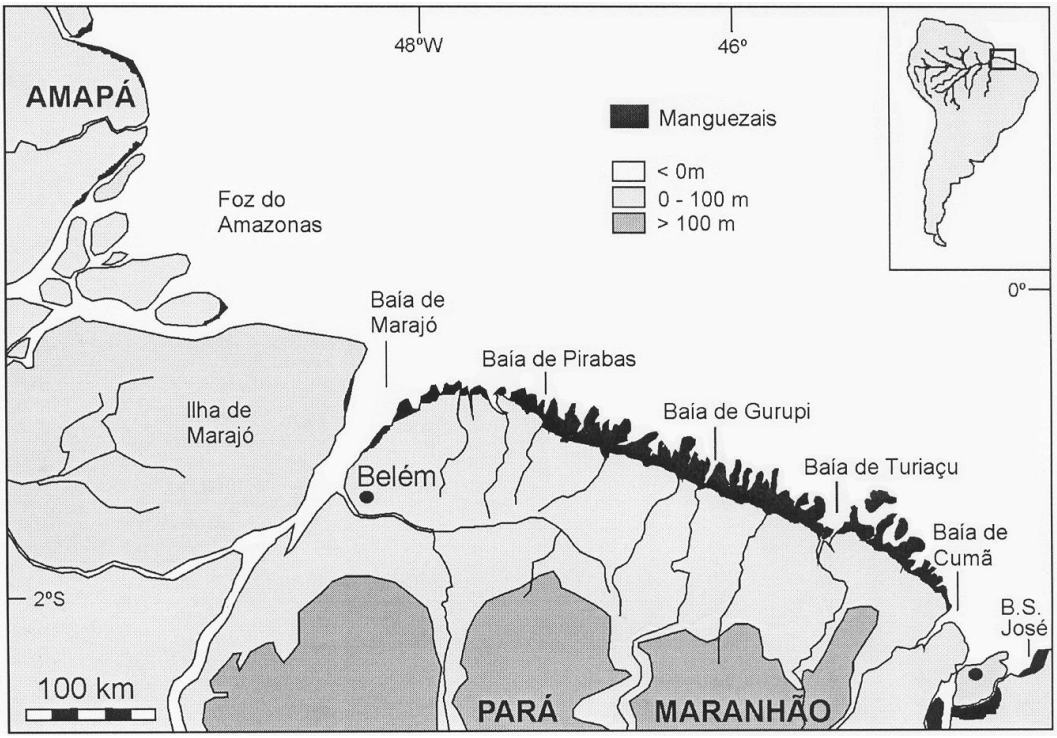

Figure 1: Distribution of mangrove in the Northeast coast of the States of Pará and Maranhão. Source: Souza-Filho, P.W.M and Lara, R. Reprinted with permission. *Journal of Coastal Research* (In submission).

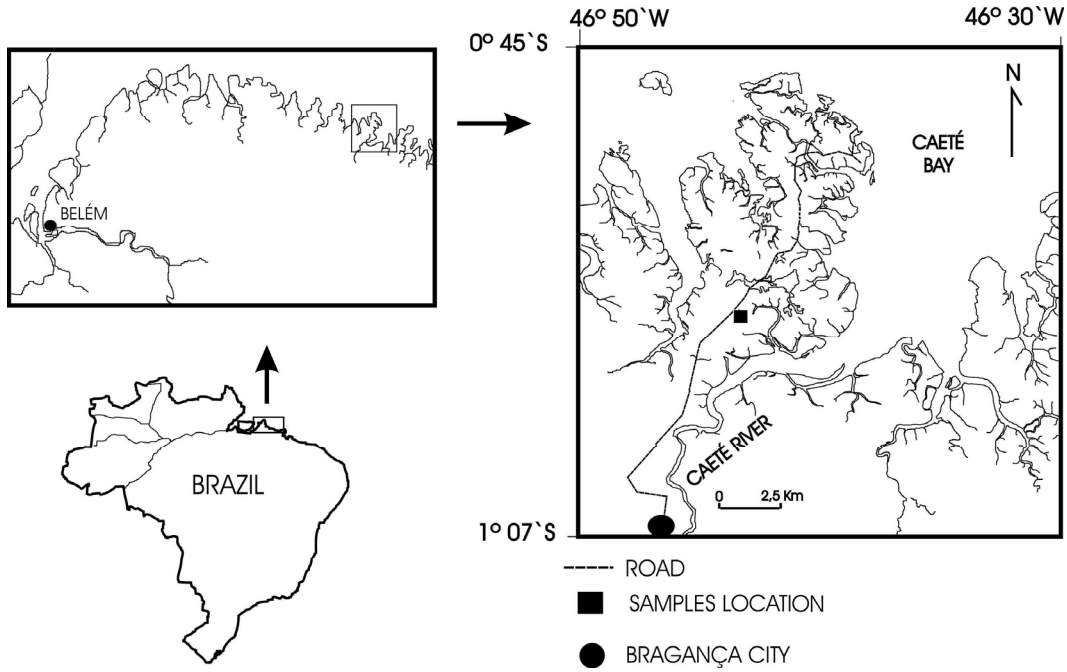

Figure 2: Study area on the central sector of the Bragança Peninsula.

4.2.2. Coastal waters

A large number of rivers drain the coastal area Southeast of the Amazon-Pará system. Foremost amongst these rivers are the Caeté, Gurupi, Maraçumé and Turiaçu, which flow throughout the year. The plumes of these rivers are advected to the northwards-flowing western boundary current-the North Brazil-Guyana System flowing onto a broad (200 km) shelf, which led to transport the suspended load to the Northwest along the coast. Its inner edge reaches within 20 to 40 km of the coast and the strength of the current depends greatly on the local wind stress (Milliman *et al*., 1975; Edmond *et al.*, 1981). The Amazon-Pará system can also receive sediments of the Amazon basin, especially at the rainy season due the more erosional regimen and coastal circulation.

4.2.3. Mangrove forest

The mangrove system of Bragança Peninsula can be described as a riverine /fringe mangrove according to the criteria of Lugo and Snedaker (1974), which the tide dominated with strong bidirectional flux (Woodroffe, 1992). The Caeté Estuary is characterised as macrotidal, with tidal amplitudes of about 4 m range, where a major part of the mangrove is inundated only during spring tides (Schwendenmann, 1998; Cohen *et al.* 1999). The Caeté River is about 100 km long and drains upstream from the mangroves about 3000 km^2 of the basin (Schwendenmann, 1998).

The circulation in the mangrove creeks of the Bragança Peninsula is across several tidal channels which link the forest flooding system with the estuary of the Caeté River and the Maiaú Bay (Cohen *et al*., 1999). The construction of a embankment 35 km road at the middle of the peninsula, from 1986 to 1974 impides the transversal flow of the water tide at several locations (Cohen *et al*., 1999) **(Fig. 2)**. As suggested in others mangroves (Wolanski *et al*., 1992), the pronounced asymmetry between the ebb and flood tides, results in larger ebb currents exporting sediments and maintaining deep the tidal channels. This tidal motion was considered as a possible vehicle of nutrients from different sources (Lara and Dittmar, 1999). Tides are semidiurnal with strong tidal currents (1.5 m/s) (Cohen *et al*., 1999), resulting in no vertical salinity

gradient and large areas of active erosion and deposition in the external part of the estuary, with strong shifting of sand banks.

4.3. Mangrove vegetation

The mangrove areas quantification with remote sensing along the Northeast of Pará and Northwest of Maranhão, sector considering as the world`s largest unitary mangrove system, estimated an area of 7500 km^2 (Kjerfve and Lacerda, 1993) **(Fig. 1)**. This area represents 57% of the total Brazilian mangroves for still conserved mangroves, but under increasing anthropogenic pressure.

In the Bragança Peninsula several vegetational units are found, such as salt marshes, different mangrove types, restinga and coastal grassland in stable and mobile dune vegetation. The salt marsh areas localized in the central peninsula region occur at slightly higher elevations than mangroves (Cohen *et al*., 2004). The mangroves are the dominant vegetation type covering about 90% of the 180 km^2 Bragança Peninsula (Krause *et al*., 2001). Three typical mangrove species dominate this region: *Rhizophora mangle* (Rhizophoraceae), *Avicennia germinans* (Avicenniaceae) and *Laguncularia racemosa* (Combretaceae) and comprise a well-developed forest with tree of 10-25 m height (Menezes *et al*., 2003). These species are representative for others coastal regions of the State of Pará (Almeida, 1996). Concerning the pattern of mangrove distribution, *Avicennia* dominates in high elevated areas, *Rhizophora* and *Avicennia* co-occur in intermediate areas, while on lower areas, including borders of tidal creeks and channels, *Rhizophora* dominates (Menezes *et al*., 2003). *Laguncularia* occurs in a wide distribution, but dominates in disturbed sites (e.g. channel borders) (Thüllen and Berger, 2000). In the transition zones to the higher elevated salt marsh area, scrub or dwarf *Avicennia* stands of 2-3 m tall occur (Menezes *et al*., 2003).

4.4. Geology

A large proportion of the Amazonia consists of Cretaceous or Tertiary sedimentary deposits (Sombroek, 1984). The Bragança region, occurs along the Bragança-Viseu coastal basin, with Quaternary deposits controlled by the paleotopography of the basin (Souza Filho, 2000). The Holocene sedimentary evolution of this coastal plain began at aprox. 5,100 ^{14}C years BP, when the relative sea level reached a maximum. From 5,100 ^{14}C years BP the sedimentary evolution is a result of coastline progradation with development of the mangrove system (Souza Filho and El-Robrini, 1998; Behling *et al*.,
2001).

The Amazon Basin is widely covered by lateritic rocks, especially ferruginous and bauxites (Costa, 1991). Laterites are defined as products of intense sub-aerial rock weathering whose Fe and/or Al content is higher and silica content is lower than the bedrock (Schellmann, 1983; 2003). They consist predominantly of mineral assemblages of goethite, hematite, aluminium hydroxides, kaolinite minerals and quartz. The relative positions of the fields of kaolinisation, weak or immature lateritisation, moderate lateritisation and strong or mature lateritisation vary, depending on the parent rock material (Bourman and Ollier, 2002). In the Proterozoic Gurupi Group (Pará-Maranhão) exists a wide diversity of lateritic rocks, prevailing the phosphoric. This material is localized in plateaus as Serra do Pirocaua between the Gurupi and Maraçumé Rivers (Costa and Araújo, 1996), in islands as Trauira near the Turiaçú River (Brandt, 1932) and as Itacupim near the Gurupi River (Costa *et al*., 2004a). These laterites are derived from basic-ultrabasic and meta-sediment bedrocks (Costa, 1991). The mature phosphoric laterites found in plateaus and islands are characterized by 1) a ferruginous crust generally at the top of the profile (1-7 m thickness), 2) an Al-phosphate horizon lying below (maximum 2-6 m thickness), and 3) a saprolitic clay horizon (30-50 m thickness) above the bedrock. Contrary, the immatures laterites occur only in low-land and are characterized by 1) a sand/clay covering (0.3-2 thickness), 2) a ferruginous horizon (0-3 m thickness), and 3) a saprolitic clay horizon (< 15 m thickness) above the bedrock. The immatures laterites

were identified by Costa (1991) as part of the sediment sources from the Barreiras sediments.

The Bragança coastal area can be subdivided in alluvial, estuarine and coastal plain. The basement of these plains, which forms the coastal plateau, is formed by the Pirabas Formation of Miocene age, occupied by Tertiary sediments of the Barreiras Formation and post-Barreiras Formation (Bigarella, 1975; Goés *et al.,* 1990; Arai *et al.,* 1994; Souza Filho *et al*., 1997). The chemical composition of the Barreiras Formation display two signatures 1) a terrigenous one with material interpreted as weathered products (laterites) of the source area (most made of SiO_2, Al_2O_3 and Fe_2O_3) and 2) a robust marine influence, as indicate the strong salinisation and diatoms presence, reinforced by the presence of Na and Cl as halite, K as feldspars and Mg as complex clay mineral (Rossetti *et al.,* 1989, Souza Filho *et al*., 1997; Costa *et al*., 2004b, Behling and Costa, 2004; Berrêdo, 2006). Additionally, higher-plant, algal- and animal-derived organic matter promotes diagenesis and the new formation (autigenic mineral) of minerals (mainly pyrite) (Marchand *et al*., 2003; Behling and Costa, 2004). It was also proposed that the source of phosphorus is accumulated in the higher-plant and can be available after de degradation of the organic matter (Costa *personal communication*).

4.5. Climate

The coastal region of Northeastern Pará is characterised by a tropical warm and humid climate. The average temperature of 25 ^{o}C has a narrow annual thermal amplitude (22-32 ^{o}C) characteristic of intertropical regions. The average rainfall is 2500 mm (period 1973-1997) with 75 % of the precipitations between January and May (INMET, 1992). During the rainy season, increased freshwater runoff by the Caeté River reduces salinity in the mouth of the estuary (17 $^{o}/_{oo}$), while during dry season salinity 38 $^{o}/_{oo}$ prevail (Dittmar, 1999).

CHAPTER 5 – METHODOLOGY

5.1. Experimental design

5.1.1. Elevation surface of the mangrove

In order to evaluate the inundation dynamic in the transect, a topographic survey of the mangrove floodplain was undertaken during a spring tide at September 2001. The water level relative to the sediment surface was determined through water-measurements devices installed at 32 stations along the transect (**Fig. 3**). The measurements of the maximal high-tide were taken and these values were adjusted to tidal level after Cohen et al. (2001). Afterwards, inundation frequency (IF), is expressed as the number of times that the tides reached each topographical quota on this transect in one year calculated from the tide table.

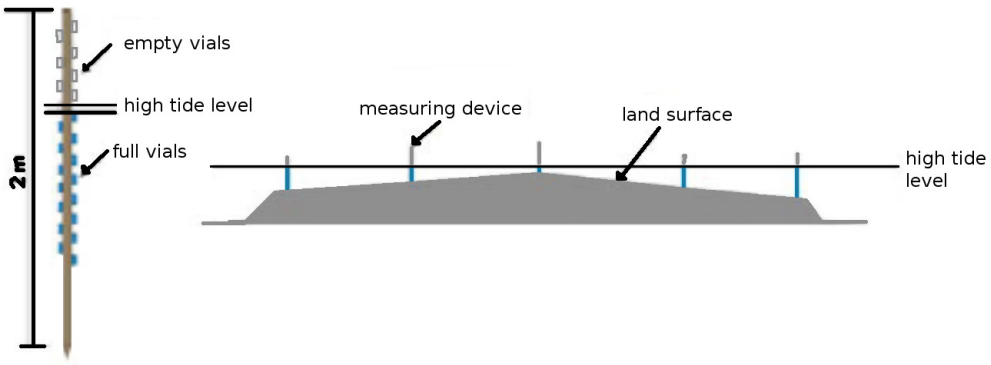

Figure 3: Devices utilized to measure the height of inundation during spring high tide. Modified from Cohen et al. (2001).

5.1.2. Physicochemical pattern and nutrient status of mangroves

The field work was carried out in order to determine the differential flood tolerance as a factor influencing zonation of mangroves during September 2001 to April 2002. Three forest zones were chosen in the same transect of the elevation surface, each of these extending approximately 200 m. At a total of 11 sampling stations, approximately 200 sediment samples were collected for physicochemical and chemical analysis. The first zone began at the edge of the central road (**Fig. 2**) through an *A. germinans* monospecific forest, the second zone was a mixed stand of *A. germinans* and *R. mangle*, and the third zone was a *R. mangle* monospecific forest ending at the Caeté Estuary **(Fig. 4)**. To encompass the nutrient status with a comprehensive description of the spatial forest structure, a standard Point Centered Quarter (PCQ) method was used (Cottam and Curtis, 1956). At each sampling station, the species less abundant (i.e. principal) was identified and considered as the center of a 10 to 10 m quadrant. Three to five trees of the species more abundant in the quarter with the canopy around the principal tree (i.e. neighbors) were also considered. In this approach the structural attributes for the neighbor group of trees was assessed (Staupendahl, 2001). In the mixed stand alternate species positioned as central tree were regarded.

5.1.3. Effect of water logging and rhizosphere on physicochemical parameters

5.1.3.1. Field experiment I: water logging

A fixed station was established at the high plain in *A. germinans* monospecific forest to examine the instrumental variation (i.e. electrodes) with time of measures and to determine the physicochemical changes in response to flooding dynamics during two spring tides of April 2002 **(Fig. 4)**. Station A was localized at 50 cm distance from the principal trunk of an *R. mangle* tree to examine the possible roots influence during the inundation (00°55’40.5’’ S, 46°42’16.4’’ W). Sensors of pH, redox potential (Eh), sulfide (S^{2-}) and temperature fixed at 10 cm depth on the sediment took measures every 10 minutes, with higher resolution during submergence (3-5 min.), during 12 and 24 hours. The level of flooding water was recorded each 5 min. during both inundation periods. Mobile sensors recorded the physicochemical parameters of the

floodwater at approximately 2 cm above the sediment layer (surface) and 2 cm below the water surface (bottom).

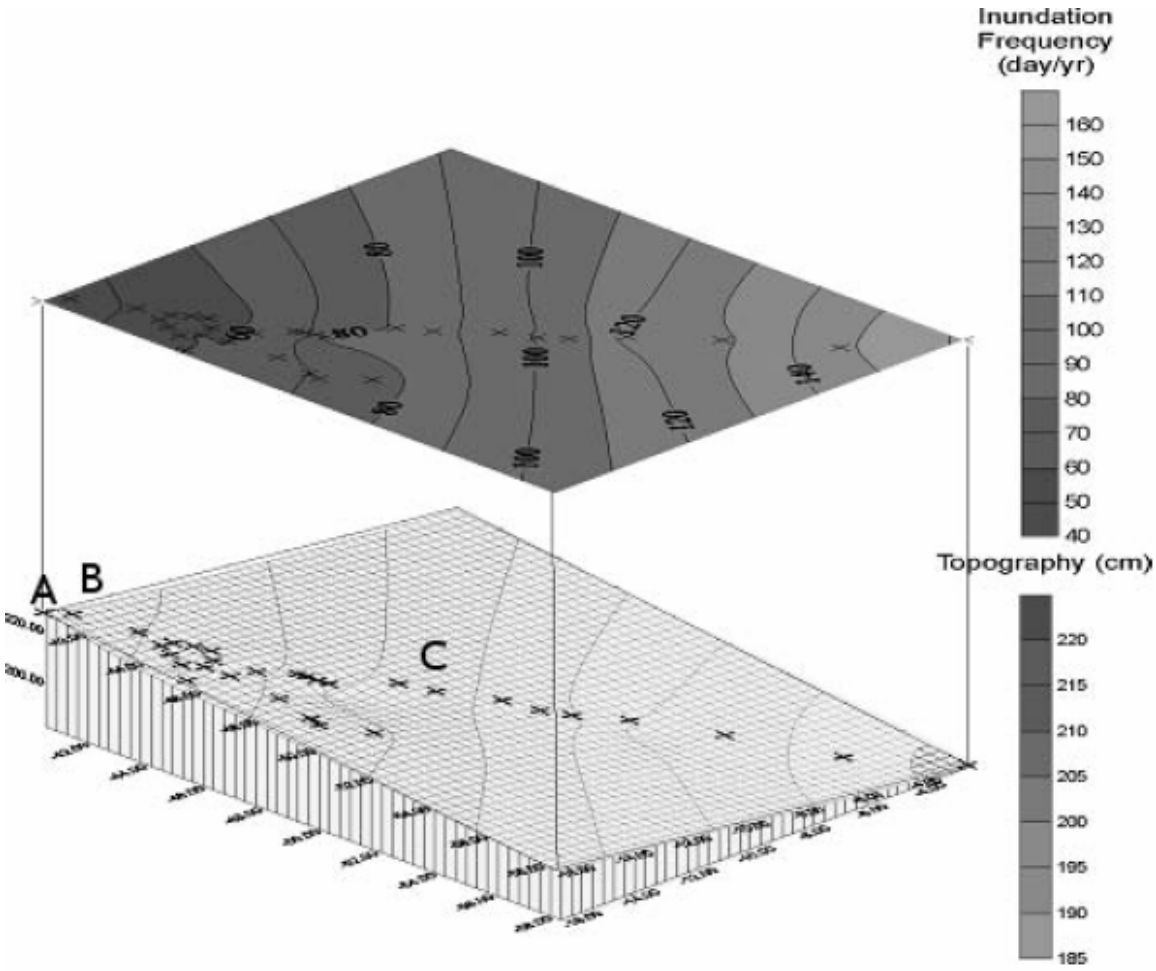

Figure 4: Combination of site topography with contour levels (cm) and inundation frequency (days/year) of the total area flooded. Distribution of the transect along the topography and position of the measurements with sensors. Station. A = fixed station, Station. B and. C = horizontal profiles.

5.1.3.2. Field experiment II: rhizosphere

In order to determine the baseline of the physicochemical modifications in sediments by the presence of roots, two areas with different inundation frequency were selected. At each area with different length, horizontals profiles of pH, redox potential (Eh), sulfide (S^{2-}) and temperature for the evaluation of the effect of root superposition were done. The high plain area (Sta. B) was localized in the *A. germinans* monospecific forest at 50 m from the road (00°55'40.9'' S, 46°42'15.8'' W) **(Fig. 4)**. Here, the measurements (n=14) were taken at 10 cm depth along a 22 m transect perpendicular to the road, following one of the network of pneumatophores branches for two opposite *Avicennia* trees separated by bare sediment **(Fig. 5)**.

The middle plain area (Sta. C) was located in a mixed stand of *A. germinans* and *R. mangle* at 280 m of distance from Sta. B (00°55'50.8'' S, 46°42'09.5'') **(Fig. 4)**. The measurements (n=12) were taken at 10 cm depth along an 11 m transect following the same scheme as for Sta. B. The transect followed one aerial root from a *R. mangle* tree, crossed a bare sediment until reaching one pneumatophore branch of a central *A. germinans* tree, continuing to the opposite side site until reaching another *R. mangle* (**Fig. 5**).

5.2. Field work

5.2.1. Sediments

A stainless steel sediment corer, 1 m long by 8 cm diameter, was used at each station to sample near (<1 m) the trunk of the central tree and one of the neighbor trees. These paired stations are subjected to the same inundation frequency, allowing separately comparing the biological effect of each species on the sediment. The core was covered with a plastic foil immediately after extraction to avoid oxidation. *In situ* 5 cm thick sub samples were taken centred at the depths of 5, 10, 15, 20, 30, 40, 50 cm and thereafter at 25 cm intervals down to 1 m depth. The samples were put into dark airtight polyethylene bags, returned to the laboratory on ice and stored at 4°C. Before analysis, the 5 cm sections of the sediment cores were homogenized, oven dried at 60°C until constant weight and powdered in a porcelain mortar to pass a 1 mm mesh.

Station B

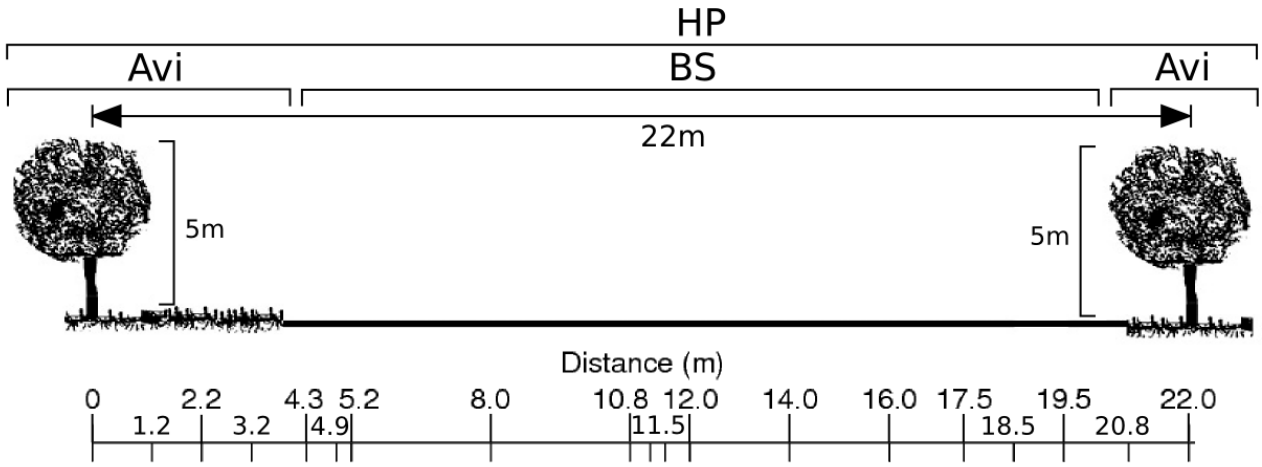

Station C

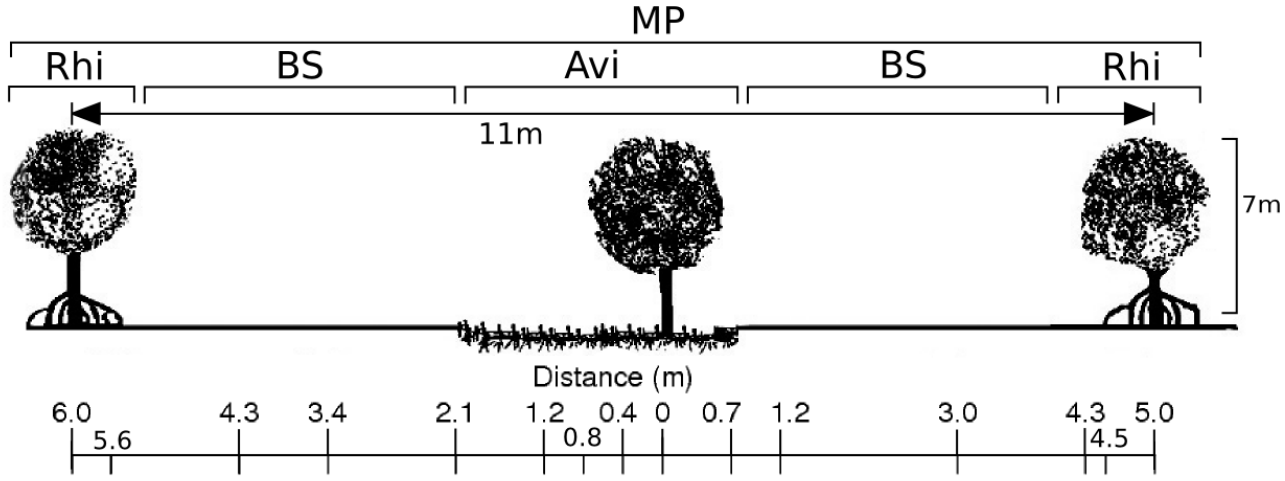

Figure 5: Diagram of sampling with electrodes showing the distribution of *A. germinans* stands and bare substrate (**Station B**), and *A. germinans* and *R. mangle* stands (**Station C**). Abbreviations: HP, high plain; Avi, *A. germinans*; BS, bare sediment; MP, middle plain; Rhi, *R. mangle*.

5.2.1.1. Sensor measurements

To compare the effect of roots (i.e. oxidation) on the sediments, paired measurements were made in the proximity (50-100 cm) to the adventitious roots (i.e. pneumatophores) or aerial structures for the respective species. Vertical profiles were done across the transect by insertion of steel needle electrodes (Microscale Measurements) in 11 stations during low tide. Each profile was measured *in situ* down to 0.5 m depth with resolution of 5 cm. The electrodes were inserted for several minutes into the mud until stable values were reached, in the same range of the stabilization time needed in the calibration. After each insertion, they were thoroughly washed and subsequently dried with tissue paper in order to prevent poisoning by sulphide. The instruments employed were a 50 cm length combined Eh / sulphide electrode and a pH electrode, both connected to a separate reference electrode (Ag/AgCl) filled with a 3M KCl solution. Each sensor was linked to one of the sockets of a digital millivolt meter and fixed in a depth gauge with a fine-scale resolution until 50 cm depth. All the sensors were checked and calibrated before, during and after the field work.

5.2.2. Vegetation

Height and breast height diameter of *A. germinans* and *R. mangle* from the principal tree and the canopy neighbor's trees were recorded.

5.3. Colorimetry and laboratory analysis

The colorimetric method for the determination of phosphate, is based on the reaction of these ions with an acidified molybdate reagent to yield a phosphomolybdate complex, which is then reduced by ascorbic acid to a blue color proportional to P concentration present in the sample. For the analysis of orthophosphate, aliquots of 10 ml sample were reacted with 0.2 ml of the reductant (acidified ascorbic acid solution) and 0.2 ml of mixed reagent (Grasshoff *et al*., 1983). The P concentration in sediment samples was determined utilizing absorption quartz cells of 1 cm, using a Hitachi U-2000 Spectrophotometer at a wavelength of 880 nm.

A phosphate standard stock solution (Titrisol) of 1000 mg PO_4/L was utilized to prepare two stock standards (526 and 52.6 μM PO_4), used for different calibration standards. The calibration curve prepared at the same day of the analysis considered two blanks and five to eight working solutions of increasing concentrations. Each batch of samples (n = 10) included two blanks. Most of the chemical analyses were conducted on duplicate and triplicate, its experimental error was expressed as an average for variation coefficient (% VC) (**Tab. 1**). The chemical and physical-chemical analyses without replicate were not considered in this table.

Table 1: Total variability calculated in the measurement of various physicochemical parameters and concentration of elements by different methods. Average values for variation coefficient (VC) and number of replicates (n).

Methodology	VC (%)	n	Authors
Porewater			
pH	2.5	37	Grasshoff *et al*., 1983
Potential Redox (Eh)	13	37	Küster & Thiel, 1982
Sulphide	10	107	Cline, 1969; DIN 38405-D26
Sediment			
Total Phosphorus	2.8	2	Leeg & Black, 1955
Inorganic Phosphorus	2.6	2	Leeg & Black, 1956
Iron/Aluminium-bound P	8.0	2	Kurmies, 1972
Calcium-bound P	9.0	2	Kurmies, 1973
Extractable Phosphorus	4.5	2	Hesse, 1957; 1961
Total Carbon	3.2	2	Hedges & Stern, 1984
Organic Carbon	3.6	2	Verardo *et al*., 1990
Nitrogen	3.7	2	Hedges & Stern, 1984
Sulphate	1.6	2	Hesse, 1957
Reactive Iron, Aluminum and Calcium	1.0	2	Lord, 1982
Pyrite Iron	1.2	2	Lord, 1983

All lab ware used in the determinations was washed with HCl solution (10%) and thoroughly rinsed with de-ionized water (DIW). Glassware used for the colorimetry of P and sulphate/sulphide was washed separately. Traces of organic matter from the teflon bottles were completely removed by submitting them to a preliminary digestion with acid persulphate similar as for sample analysis. The control of bottle air tightness during the oxidation, was checked by weighing the teflon bottle with screw caps before and after the autoclaving. In all samples the colour interference of suspended particles was corrected by filtration of the extract before the addition of the chromogenic reagent. Only in the fractionation analysis of sediments, the brown colour interference of the unfiltered sediments extracts, was corrected with a "colour blank" obtained by the measure of the samples a second time with all reagents except the chromogenic reagent.

5.3.1. Sensor calibration, checking and calculation

5.3.1.1. pH

The pH electrode was calibrated in 50 ml of five standard phosphate buffers (200 mM). The acid-base buffers were prepared with potassium hydrogen phosphate (K_2HPO_4) and potassium dihydrogen phosphate (KH_2PO_4), using the Henderson-Hasselbach equation to compute the ratio of the base form to acid form and a pH-meter to guide to the correct pH. The regression analysis (pH as independent, mV signal as dependent variable) calculated the slope as a response to the ion being detected and this was compared with the linear theoretical Nernstian slope 59.16 mV/pH at 25^{o}C (i.e. for each pH unit the potential change 59.16 mV) (Cheng and Da-Ming, 2005). The electrode was regenerated considering 1) the slope correction, when the slope dropped to values <50 mV (85 % of the effective output) and 2) the asymmetric potential correction, when the deviation of the isopotential point (0 mV = pH 7) ± 30 mV increased. Additionally, the temperature compensation was controlled by measurements using a steel temperature electrode of 50 cm length (HI 8757, Hanna). The temperature error, resulting in a drifting signal as response of the sensor to different environments temperature, can be reduced by the correction coefficient of 0.0114 pH units per each grad Celsius proposed for Grasshoff et al. (1983). For this study the temperature correction was applied, considering that the buffers and *in situ*

measurements performed in different media resulted in an average temperature difference of approximately 3°C, which corresponds to a correction coefficient from 0.0342 pH units.

5.3.1.2. Redox Potential (Eh)

The redox potential (Eh) electrode was calibrated using seven separate phosphate buffers (200 mM) in 50 ml DIW saturated with chinhydrone (~1 crystal/5 ml phosphate buffer). For all campaigns, the seven pH-equidistant buffers were prepared taken in account the field pH range (6-8). The potential of this saturated redox buffers depends only on pH and temperature, thus after regression analysis, the mV values of the chinhydrone solution at each pH were compared to the respective standard solutions at 25°C and calculated from the expression as follows (Näser, 1976; WTW, 1997):

Standard solutions at 25°C:

pH 1.68 = 383 mV

pH 4.01 = 255 mV

pH 4.60 = 220 mV

pH 7.00 = 78 mV

Calculation:

U (mV) = Uo (mV) – slope (mV) x pH – U ref (mV)

Uo (chin) (mV) = 0.7175 – 0.00074 x t (°C) x 1000 (mV)

$$Slope(mV) = \frac{\ln 10 \cdot R \cdot T \cdot 1000mV}{F} \approx 59 \text{ at } 25^{o}C$$

Uo = measured electrode potential

Uo chin = Temperature compensation of the potential of chinhydrone solution (0-37 °C) ≈ 0.0699 V

U ref = potential of reference

F = the Faraday Constant (96,485 coulombs per mole)

R = the Gas Constant (8.3145 joules/degree/mole)

T (K) = the Absolute Temperature (273.15 + t (°C))

2.303 = the conversion factor from natural to base 10 logarithm

The rH-value (hydrogen-redox exponent by Clark) is used to characterize the redox strength for a redox system, setting the redox potential and the respective pH-value related to the system.

rH- value = Uo / 0.029 V + 2pH

The reported redox data are relative to the standard hydrogen electrode, by adding 207.7 mV to the original millivolt reading obtained with an Ag/AgCl 3M KCl reference electrode at 25°C (Küster and Thiel, 1982).

U_H (mV) = Uo (mV) + U ref (mV)

U_H = redox potential (Eh)

5.3.1.3. Sulphide

The sensing tip of the ion-specific sulphide electrode is a crystal of silver sulphide (Ag/Ag_2S), mounted on top of a conducting wire. The potential between the sulphide electrode and a reference electrode is related to the concentration of fully dissociated sulphide (S^{2-}) ions in aqueous solutions, but not to the concentration of undissociated sulphide (H_2S) or partly dissociated sulphide (HS^-) (**Equations 8 a, b**). In natural systems is that reduced systems may change from oxidized to reduced merely by changing pH, from H_2S-dominant (oxidizing) at pH <7, through HS^--dominant in neutral at pH=7, to S^{2-}-dominant (reducing) at pH >7 (Rickard and Luther, 1997). Due the fact that the S^{2-} fraction of the total free sulphide (TFS) concentration ($\Sigma H_2S + HS^- + S^{2-}$) depends on pH, the value of the latter is highly important focusing two options:

1) convert all forms of free sulphide to S^{2-} by raising the pH to e.g. 12, applying the so-called sulphide anti-oxidant-buffer (SAOB), or
2) calibrate the electrodes at the ambient pH value

The first option is recommended for water samples and the second option for *in situ* measurements, the latter applied in this work.

The calibration of the S^{2-} electrode was performed under anaerobic conditions removing the oxygen by autoclaving. A sulphide stock solution of ±100 mM was prepared washing crystals of sodium sulphide, wiped dry with a cellulose tissue and weighed (± 2.4 g $Na_2S.7\text{-}9H_2O$). The crystals were added to 100 ml hot DIW and subsamples were dispensed in 5 or 10 ml aliquots. After allowed to room temperature the concentration of TFS with an iodometric titration was assayed (Jander and Jahr, 1963) and colorimetrically performed with the methylene-blue method (Cline, 1969) after German standard methods (DIN 38405-D26).

For the calibration of the S^{2-} electrode, five pH-adjusted (4.5 - 8.5) phosphate buffers of 200 mM strength in triplicates equilibrated at the same temperature (± 1°C) were prepared. To a clean, dry 100 ml beaker, 50 ml of phosphate buffer was added. The beaker was placed on a magnetic stir plate, added a magnetic stir bar and stirred at slow speed (no visible vortex). After rinsing the reference, sulphide and pH electrodes with DIW and blot dry, the electrodes tips were immersed in the buffer solution. To each pH-adjusted buffer concentrate seven stepwise 100 µl of the sulphide stock solution were added, resulting in a TFS increase from 162.3 to 1077.8 µM (log TFS 2.2-3.0 µM). By each of these serial additions, after stabilization readings (3-5 min), the mV directly from the meter display was read. This procedure was repeated for all the buffers.

One calibration curves per pH-adjusted buffer were constructed by plotting an average of the measured potential (mV) as dependent variable as a function of the sulphide ions activities (or effective concentration) in an increasing series (log TFS 2.2-3.0 µM) as independent variable. The measured potential, corresponding to the level of S^{2-} ion in solution, is described by the Nernst equation:

$$Uo = Uref + Slope \log (A)$$

Uo = measured potential

U ref = potential of reference

A = level of sulphide in solution

$$Slope(mV) = \frac{2.3 \cdot R \cdot T}{nF} \approx -29 \text{ at } 25\ ^{o}\text{C}$$

n = ionic charge

The ionic level (A) refers to the activity or effective concentration of an ion in solution. The sulphide ion activity is related to free-ion concentration in a specific ionic strength. In fact, is a measure of the number of ions taking part in any given reaction, in this case those interacting with the ion selected by the electrode (Orion, 2003).

To check the performance of the electrodes the slope value was calculated using linear regression. Log-linear calibration curves with a theoretical slope of -29.5 mV per concentration decade at room temperature were obtained (Boudreau and Jørgensen, 2001). The slope in the range of -25 to -30 mV between 25 to 30 ^{o}C was acceptable (Orion, 2003) (**Fig. 6**). If more as two calibration points not provided a slope within the appropriate range the calibration was not considered. For this case the electrode membrane was cleaned with cotton paper, afterward with polishing paper for a few seconds and rinsed with DIW for about five minutes.

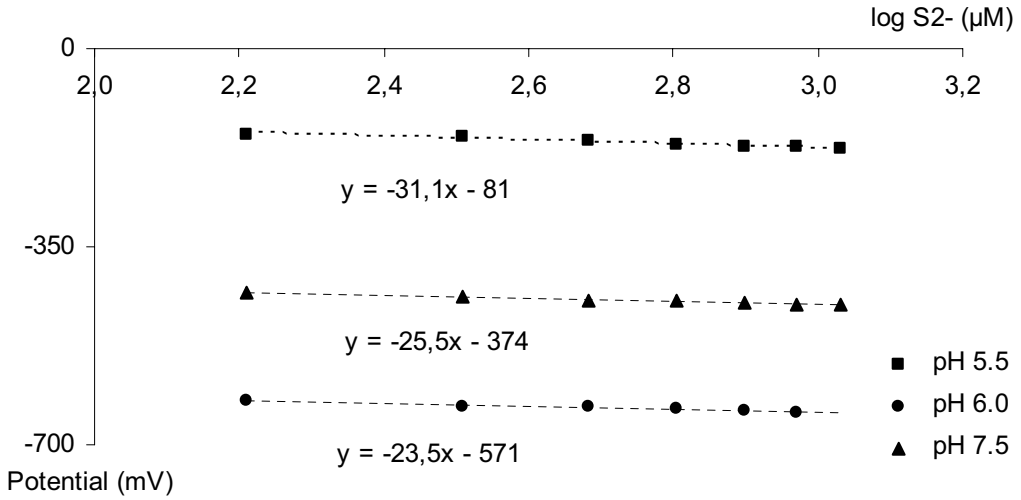

Figure 6: Log-linear calibration curves for checking the S^{2-} electrode performance.

In the electrodes manual, an illustration of S^{2-} calibration shows for concentrations lower than 162.3 µM (log TFS < 2.2 µM) an evident higher slope as the theoretical value (data non-showed). To encompass the lower field S^{2-} signal (i.e. < -200 mV) with the standard calibration method, the sulphide stock solution was diluted 10 to 100 times with the respective pH-adjusted phosphate buffer. Calibration curves per pH-value were constructed by plotting the measured potential (mV) as a function of the log TFS from the dilution factors 10 (log TFS 1.2-2.0 µM) and 100 (log TFS 0.2-1.0 µM) in an increasing series. In fact, the slopes obtained by log-linear calibrations with the dilution factors of 10 (-134 to -82 mV/decade) and 100 (-80 to -44 mV/decade) were higher as the theoretical.

Table 2: Coefficients utilized for the calculation of low concentrations of sulphide. DF, dilution factor.

log Sulfide (µM)	Buffer (mV)	log Sulfide (µM)	Buffer (mV)	Coefficient
pH 4.5 DF 10		pH 4.5		pH4.5 / pH 4.5 DF 10
1.21	-228	2.21	-286	1.25
1.51	-237	2.51	-289	1.22
1.68	-242	2.68	-300	1.24
1.80	-242	2.80	-303	1.25
1.90	-242	2.90	-307	1.27
1.97	-245	2.97	-311	1.27
2.03	-243	3.03	-316	1.30
pH 6.5		pH 7.5		pH 7.7 /pH 6.5
2.21	-432	2.21	-427	0.99
2.51	-482	2.51	-449	0.93
2.68	-502	2.68	-514	1.02
2.80	-512	2.80	-532	1.04
2.90	-522	2.90	-544	1.04
2.97	-525	2.97	-551	1.05
3.03	-533	3.03	-561	1.05

Moreover the potential (mV) difference between diluted and non diluted consecutive pH-buffers results in a constant coefficient of 1.12 ± 0.07 **(Tab. 2)**. Four average coefficients between pH-values 4.5 to 7.5 were calculated. The field potentials lower than -200 mV were multiplied by these coefficients until attaining the respective pH-value of the field sample before the standard sulphide calculation.

The use of well-functioning Ag/Ag_2S electrodes can, however, be problematic due to the large uncertainty in the determination of the second dissociation constant of H_2S (Meyer *et al*., 1983, Millero *et al*., 1988) calculated for the conversion of S^{2-} activity to total sulphide concentrations (**Equation 8 a, b** Kühl *et al*., 1998). The very high pK_2 of the sulphide system also precludes the application of Ag/AgS_2 electrodes in acidic environments, where S^{2-} is practically non-existent (Kühl *et al*., 1998).

$$H_2S + H_2O \leftrightarrow HS^- + H_3O^+ \qquad \textbf{Eq. 8a}$$

$$K_1 = [HS^-][H_3O^+] / [H_2S]$$

and

$$HS^- + H_2O \leftrightarrow S^{2-} + H_3O^+ \qquad \textbf{Eq. 8b}$$

$$K_2 = [S^{2-}][H_3O^+] / [HS^-]$$

with

$$[S_{tot}^{2-}] = [H_2S] + [HS^-] + [S^{2-}]$$

leads to

$$[H_2S] = [S_{tot}^{2-}] / \left(1 + K_1 / [H_3O^+] + K_1K_2 / [H_3O^+]^2 \right)$$

Considering these limitations, in a test performed in cooperation with Julian Oxmann and Ing. Matthias Birkicht (ZMT), the sulphide ion activity derived from our S^{2-} voltametric macroelectrode (tip 1mm) was compared with an H_2S amperometric microelectrode (tip <30µm), designed by AMT (Analysenmesstechnik GmbH, Rostock) (Jeroschewski *et al*., 1996) and hired from UFT (Zentrum für Umweltforschung und Umwelttechnologie, Bremen). The comparison was performed in a defined phosphate buffer solution of 200 mM strength at pH 6.7 and temperature of 23°C. Both sensors were inserted in this buffer solution and the concentrate ions (S^{2-}, H_2S) were simultaneously measured by 17 stepwise additions (7x25µl, 4x125µl,

6x50µl) of sulphide stock solution, resulting in an increasing concentration range (3.6 to 518.2 µM). This curve considered a wide concentration range, with the aim to check the previous separately calibrations (i.e. non- dilution, dilution factors 10 and 100).

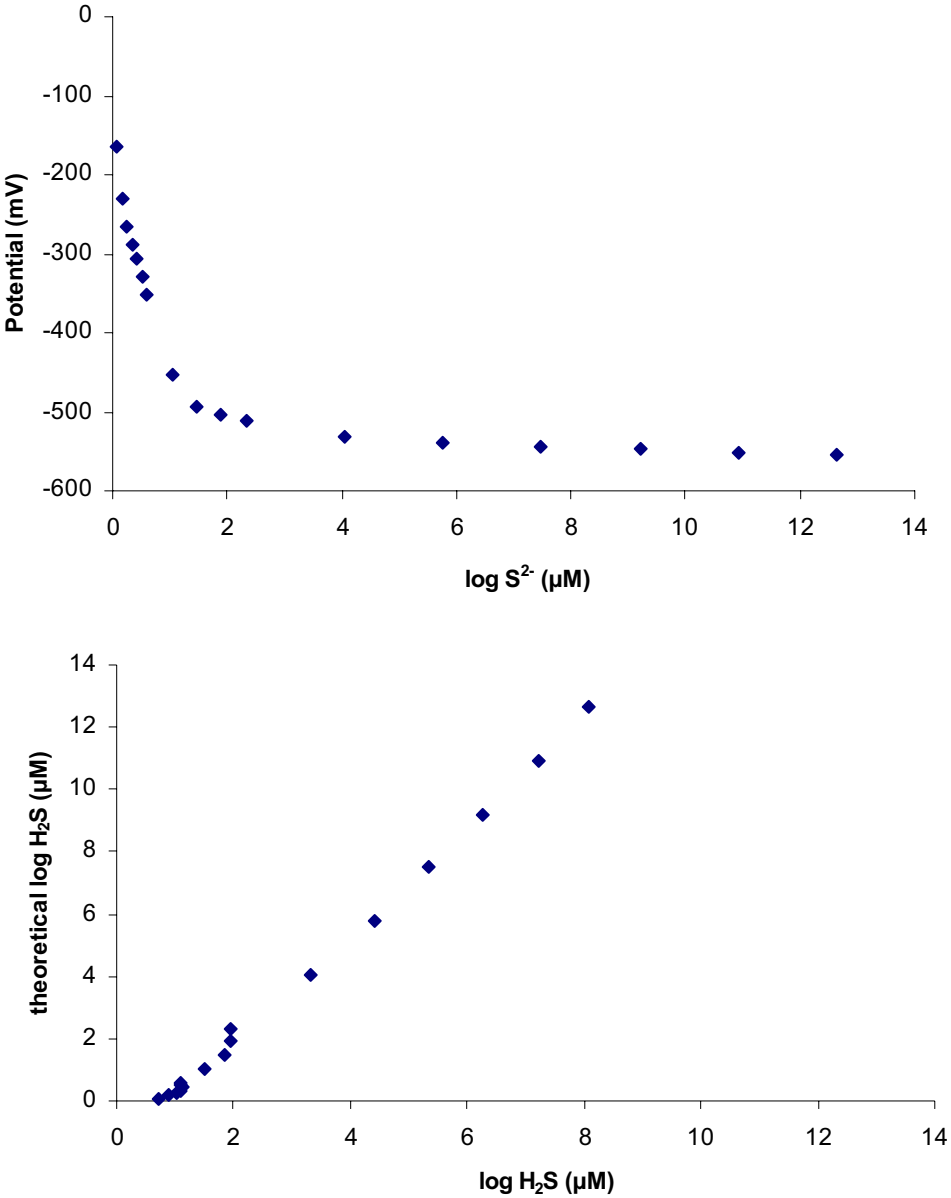

Figure 7: Performance comparison of S^{2-} and H_2S electrodes.

In this test, it was compared the procedure to recognize the concentrations data by each electrode. The results gave evidences for its good measurements performances **(Fig. 7)**. Attention was given to the H_2S glass electrode with wider curve linearity than the S^{2-} needle electrode. Therefore, the limit of determination and detection for both electrodes are different. Moreover, both electrodes lost the linearity at concentrations less as 64 μM (log TFS 1.8 μM). It is important to note, that the H_2S amperometric microelectrode is suitable for a liquid medium and the water-sediment interface. Newer development designed electrodes, are able to measure in soft sediments, when the electrode can be inserted into the sediment with a micro device. The use of needle (stainless steel) electrode can be a possibility, especially for *in situ* sediments depth profiles, also when it is necessary to find several linear areas, but the pH should be theoretically >12, what make their use under field conditions un-practicable.

5.3.2. Water content and organic matter

The determination of water content is often used for dry weight correction of other analytical data (e.g. salinity), where soil moisture is usually determined by thermal drying. For this study, a fresh sediment sample (3 g) was dried in an oven at 105ºC until constant weight. The loss in weight (i.e. water) was expressed as percentage of dry matter.

The total organic matter (OM) content of the sediments was determined from the loss in weight when OM was destroyed. It was estimated in the same dried sample after ignition or 'loss-on-ignition' at 550ºC for 4 hours. The weight loss was expressed as per cent OM. Both methods were run according to the German standard methods DIN38414-S2 and -S3, respectively.

5.3.3. Salinity

Total soluble salts of a 1:5 soil-water extract were homogenized with a glass stirrer and allowed to stand 12 hours. Conductivity was determined in the clear supernatant

(WTW-LF 197). The results of the specific soil conductance were expressed as salt content of the sediment sample (Ensminger, 1996) by equation:

$$Ks = \frac{Ke \cdot ((W \cdot M/100) + Vm)}{(W \cdot M/100)}$$

Ks ($^{o}/_{oo}$) = calculated salt concentration of the sediment sample
Ke ($^{o}/_{oo}$) = salt concentration in extract
W (g) = weight of sediment sample
M ($^{o}/_{oo}$) = sediment moisture content
Vm (ml) = volume of water used to prepare the 1:5 sediment-water extract

5.3.4. Granulometry

The method of Folk (1974) was used to determine the particle size-distribution of sand and silt/clay fractions of the core samples for 5 cm intervals. 15 g DW sediment was dispersed with 250 ml of 0.5 g/l sodium hexametaphosphate (calgon solution), overnight under stirring and sieved through a 64 μm sieve. The proportion remaining in the sieve, considered as sand fraction, was oven-dried and the DW was recorded as a percentage of initial sample weight. The proportion of the silt/clay fraction was calculated by difference and expressed as percentage.

5.3.5. Total phosphorus in sediments

It was used Leeg and Black´s ignition method (1955), on the experimental basis obtained by these authors with different ignition temperatures. They verified the accuracy of an ignition procedure focussing two critical points 1) that the solubility of the original inorg.-P does not change as a result of ignition, and 2) that the entire amount of org.-P present in the non-ignited sample appears in the extract of the ignited sample in the form of inorg.-P. At 240 ^{o}C they found an equal (10 %) of positive and negative errors related to the increase in solubility of P_i and incomplete decomposition of org.-P, respectively. Additionally, this method was selected for a suitable standard of comparison with the P status reported for other Brazilian mangroves (Silva, 1992; Silva *et al*., 1998; Silva and Sampaio, 1998; Oliveira, 1999). In this procedure 0.5 g DW of sediment sample was placed in a muffle furnace (240

^{o}C, 1 hr). To the ignited samples were added 4 ml of concentrated hydrochloric acid (HCl), heated in a steam plate (60 ^{o}C, 20 min) and allowed to stand at room temperature. An additional quantity of 5 ml HCl was added, allowed to stand room temperature, after which was agitated for 30 minutes. The suspension was centrifuged (3000 rpm, 10 min) and after dilution (1:100) of the supernatant, the P concentration was measured by colorimetry. A same sample was extracted and analyzed by the same procedure but without ignition. The increase in extracted inorg.-P resulting from ignition was taking as the content of org.-P in the non-ignited sample.

5.3.6. Phosphorus fractionation

To investigate the fractions of inorg.-P that react with Ca, Fe and Al, it was used the fractionation procedure based on the differential solubility's of the various inorganic forms in the extracts. The basic assumption of specificity of this procedure is that the reagents used are able to selectively extract one phase without any solubilisation of the others. The limitations underlined by several authors (Etcheber *et al*., 1983; Martin *et al*., 1987) are basically matrix effects and re-adsorptions. The first occurred when unsatisfactory recovery of an element in the first fractions is largely reproduced in the other extraction phases, resulting in correlative errors in the last fractions, and the second occurred by complexation, precipitation, adsorption and loss on the vial walls during the extraction.

The original fractionation procedure (Chang and Jackson, 1957) was improved by several authors (Williams *et al*., 1967; Kurmies, 1972; Hieltjes and Lijklema, 1980; Ruttemberg, 1993). The inorg.-P fractionation in this study was performed according to the Kurmies (1972) scheme (**Fig. 8**). This method was utilized in some Brazilian estuaries and specifically in the Amazon estuary by Silva and Sampaio (1998). In this method 0.5 g DW sediment was washed three times with 7.5 ml of an alcoholic-KCl 1N solution to eliminate calcium ions. This solution was prepared by the dilution of 74.55 g of dry KCl (110 ^{o}C, 2 h) in 100 ml DIW, completed with etilic alcohol to 1 lt (Morita and Viegas, 1981). The residual sediment from the KCl extraction was used "as is" for the extraction of iron/aluminium-bound P (P-Fe/Al) in two sequential phases. These phases consisted of the extraction with 7.5 ml NaOH 1N and 7.5 ml

Na_2SO_4 1N, followed by a heating period for 2 hrs at 95°C (only second phase) and the addition of 2.5 ml H_2SO_4 1N favouring the flocculation during one hour. The residual sediment for the second phase was washed with 7.5 ml Na_2SO_4 4% to remove NaOH excess before the third phase started. In this next phase the extraction of calcium-bound P (Ca-P) utilized 7.5 ml H_2SO_4 1N in a heating period for 2 hrs at 95°C. After the analytical procedure of colorimetry for each phase, the phosphate concentration was determined. The P-Fe/Al concentrations of the first and second phases were added.

5.3.7. Extractable phosphorus

The amount of tot.-P in the sample that might be readily available for biological use, termed in this work as extractable P (extr.-P), is the inorganic form occurring in soils solution and which is almost exclusively orthophosphate (Hesse, 1971). The underlying principle for determination of extr.-P, is to shake the soil with a solution to dissolve the fraction available for plant roots, afterwards the extract is analyzed for soluble phosphorus. In our study, the choice of an adequate extraction method considered the significant correlation between the extr-P and the Australian mangrove growth (Boto and Wellington, 1983). This method (Hesse, 1957; Hesse 1961), performed in cooperation with Cleise Cordeiro, extracted 10 g DW of sediments with 100 ml of a weakly acid (pH 4.8) 10% w/v sodium acetate in 3% v/v acetic acid the buffer solution known as Morgan's extractant (Allen, 1989). The use of an acid extract soil P does make sense in weakly acid soils, especially in agriculture for which this method was widely used. After shaking for 30 minutes the solution was filtrated and analyzed by colorimetry.

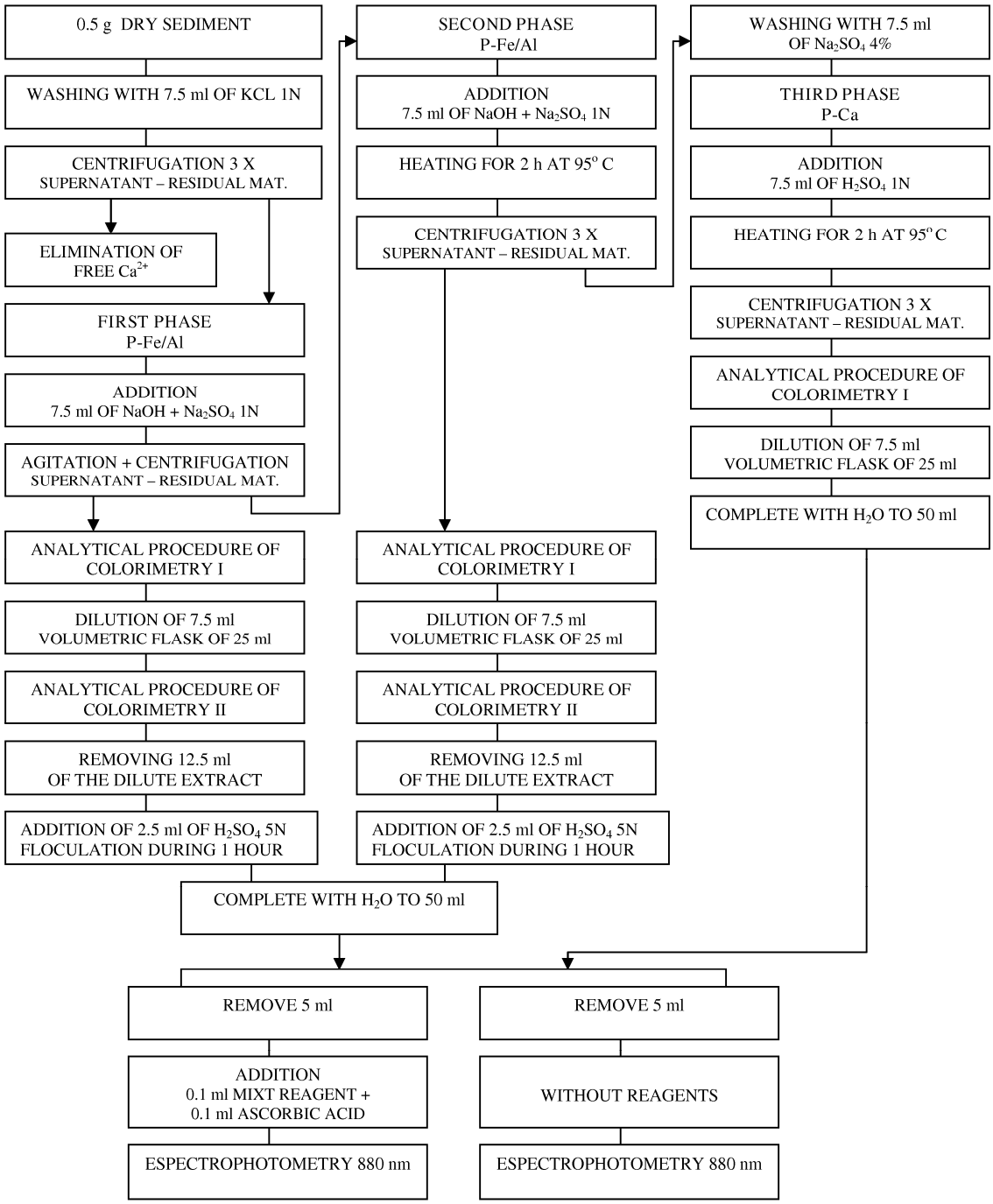

Figure 8: Sequential extraction scheme for quantification of two sedimentary phosphorus reservoirs: iron/aluminium-bound P (P-Fe/Al) and calcium-bound P (P-Ca).

In the molybdenum blue method by the colorimetry, the reduction stage by ascorbic acid is crucial. The overall acidity is one important parameter which must be controlled, due the color suppression caused in strong acid solutions (Grimshaw *et al*., 1989). In spite of this precaution, a sediment extract was spiked to test the possible interference of the acid, Morgan's extractant with the molybdenum blue method. The spiking solution was prepared by adding 5 ml of a P working solution (50 ppm P) to 10 ml sediment extracts sub-samples (30.2 ppm P). The added concentrations were confirmed by determining P concentrations before and after spiking. The result expressed as concentration (ppm) was calculated as follows:

Concentration (ppm) = (C1- (C2 –C3))

C1 = concentration of non spiked sample

C2 = concentration of spiked sample

C3 = concentration of standard

The difference found between the spike and unspiked values results in -0.47 ppm P (-1.55 %). This evaluation exhibited similar error acceptance of concentration as tested for P references material by Aminot and Kérouel (1997).

5.3.8. Elemental analyses

Carbon (C) and Nitrogen (N) content were quantified with an elemental analyser (Fisons, NA 2100) after Hedges and Stern (1984).

Analysis for total carbon (tot.-C) and nitrogen (tot.-N) not required pre-treatment. In the procedure, a pair of sediment sub-samples (10-15 mg DW) was weighed into tin cups and sealed. For the analysis of organic carbon (org.-C) a second pair of sub-samples was prepared by weighing into silver cups, which are more resistant to acid attack than tin. The samples in the open silver cups were acidified with 200 µl HCl 1N and heated in an oven for 24 h at 40 ^{o}C to loss the acid-soluble carbon during carbonate dissolution (Verardo *et al*., 1990). After allowed to room temperature the cups were crimped closed.

The untreated and acidified samples were handled separately, because residual acids vapour in the HCl treated samples could react with carbonates in untreated counterparts. Inorganic (carbonate) carbon (inorg.-C) was derived from the difference between tot.-C and org.-C and calculated as [8.33 x (tot.-C – org.-C)] (Verardo *et al*., 1990).

The samples, encapsulated in sample vials, were introduced into a combustion column reactor by means of an auto sampler. The samples were oxidized in oxygen flow by high temperature flash combustion (1050 ^{o}C). In a helium flow the oxidation products were transported to a chromatographic column, in which C and N oxides were reduced over copper quantitatively to CO_2 and N_2, respectively. Detection was carried out with a thermal-conductivity cell. The instrument response was calibrated for each sample batch (n=10) using 10 standards (Acetanilide) and 1-2 empty vials (blanks) to obtain a linear calibration curve. The quality of the standard was tested after every fifth sample using a certified soil standard (LECO 1009).

5.3.9. Sulphate

Sulphate (SO_4^{2-}) was measured by Hesse's (1957) modification of the turbidimetric method of Chesnin and Yien (1950). This turbidimetric determination of SO_4^{2-} involves the precipitation under controlled conditions of barium sulphate. A 10 g DW sample was extracted with 100 ml acid (pH 4.5) sodium acetate buffer solution or Morgan solution (Allen, 1989). After shaking for 30 min. the suspension was centrifuged (2500 rpm, 5 min) and filtered through Whatmann No. 41 filter paper into a volumetric flask. An aliquot of 10 ml of the extract was transferred into a 25 ml graduate flask, and 1 ml ferric chloride (5%) and 1 ml sodium hydroxide (40%) were added. During the addition the flask was gently mix several times. The extract was filtered through Whatmann No. 41 filter paper to remove of not only the colloidal organic matter, but of Fe (III) and soil color as well, as suggested the modification of Hesse (1957; 1971). The original flask, precipitate and paper were washed with 7 ml DIW, and to the combined filtrate and washings, 1 ml of concentrate glacial acetic acid was added. An aliquot of 10 ml of clear extract was transferred into a 25 ml graduate flask and 1 g of graded barium chloride crystals was added. The flask was

gently mixed during 1 minute and 1 ml of gum acacia solution 0.25% w/v was added. The solution was diluted to 25 ml and again gently mixed. The turbidity was finally measured by the decrease in intensity of light that goes through the suspension of the barium sulphate with a spectrophotometer at 670 nm using a 1 cm cell. SO_4^{2-} concentration in the samples was estimated by comparing the turbidity readings with a calibration curve prepared by seven SO_4^{2-} standards (10, 25, 50, 75, 100, 250, 500 mg/l SO_4^{2-}).

5.3.10. Percentage of expected concentration

In order to discriminate the influence of the pure mixing of brackish and marine waters from other effect on the variability of SO_4^{2-}, salinity was considered as a conservative parameter (biologically and chemically non-reactive) and used as a tracer to determine whether decrease in SO_4^{2-} concentrations were due to either hydrological or biogeochemical processes. Considering seawater as the only source of SO_4^{2-} in mangrove sediment, the SO_4^{2-} concentration of 2712 ppm and the standard salinity 35 $^{o}/_{oo}$ of seawater were used as reference (Libes, 1992). Thus, equation will provide the percentage of the expected concentration (PEC) at a given salinity under a conservative condition as the ratio of measured/expected concentration (Cohen *et al*., 1999).

$$PEC\ (\%) = \frac{(\text{Salinity standard} \times [SO_4^{2-}]\ \text{sample})}{([SO_4^{2-}]\ \text{standard} \times \text{salinity sample})} \times 100$$

5.3.11. Iron

The term “reactive” fraction was utilized to describe that fraction of metals in sediment that are likely to be readily available for participation in chemical reactions under normal early diagenetic conditions (Huerta-Diaz, 1989). Iron (Fe), which has been widely studied in this sense can illustrate this concept.

Different definitions for “reactive” iron (react.-Fe) exist in the literature (Canfield, 1989; Kostka and Luther, 1994), an as such, different techniques for its extraction have been applied in the past. We consider react.-Fe as the fraction of iron, mainly non-silicate-bound iron, that readily reacts with dissolved sulphide to produce iron

monosulfides and eventually pyrite (Roychoudhury *et al*., 2003). The emphasis of several studies has been of which Fe(III) minerals are reactive for reduction to Fe(II) and subsequent iron sulfide precipitation (Berner, 1970; Jorgensen, 1977; Raiswell and Berner, 1985). Generally, the most "reactive" Fe(III) is described as amorphous Fe (ferrihydrite or $Fe(OH)_3$) and less crystalline Fe (lepidocrocite). Less "reactive" Fe is defined as the more crystalline Fe(III) phases (e.g. goethite and hematite) (Canfield and Berner, 1987; Canfield, 1989; Luther *et al*., 1992), in addition to Fe which has been transformed to pyrite (pyr-Fe) (Poulton and Canfield, 2005).

The determination of Fe was performed, in cooperation with Helenice Santos, by a sequential extraction following Huerta-Diaz (1989), a modification method of Lord (1982). Two operationally defined sediment Fe fractions are characterized: react.-Fe and pyr-Fe. Both Fe fractions were cold sequentially acid extracted under oxic conditions from 0.5 g DW of sediment sample. The react.-Fe was leached with 4 ml HCl 1M and the pyr-Fe was subjected to a series of leaching procedures with 6 ml HF 10 M, 1 g H_3BO_3 and 2 ml HNO_3 conc. (**Fig. 9**). In the same solution of react.-Fe was determined the reactive aluminium (react.-Al) and calcium (react.-Ca), also named as available or extractable. After dilution (1:500) the extracts for each phase were analyzed separately by atomic absorption spectrometry (AAS).

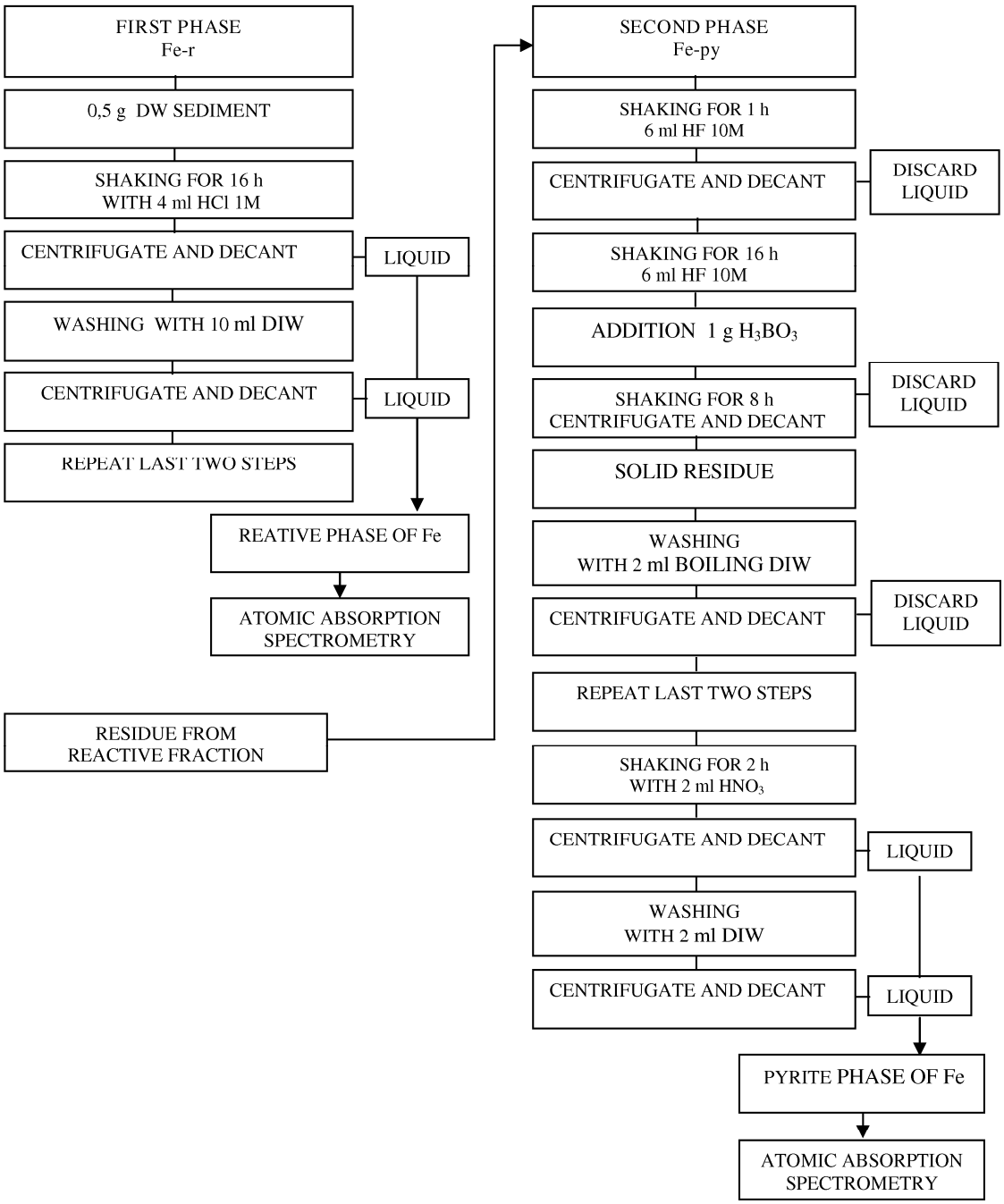

Figure 9: Flow diagram of the sequential extraction scheme for the reactive- (react.-Fe) and pyrite-iron (pyr.-Fe).

5.3.12. Degree of pyritization

The initial redox proxy based on Fe speciation was the degree of pyritization (DOP) (Berner, 1970), named in this work as DOP and defined as:

$$DOP\ (\%) = \frac{\text{Pyrite-Fe}}{\text{Pyrite-Fe + Reactive-Fe}} \times 100$$

Where Pyrite-Fe was defined by Berner as:

Pyrite-Fe = 1/2 (TRS-AVS)

TRS = Total Reduced Sulphide
AVS = Acid Volatil Sulphide

Afterwards, in sediments where the AVS was present as a significant fraction of TRS and the DOP approach not provide a good accounting of Fe availability during early diagenesis, the degree of sulfidation (DOS) was proposed (Boesen and Postman, 1988). The redox-proxy in this study, was performed according to Berner (1970). This method was in some Brazilian estuaries of the Sepetiba Bay by Bastos (2002) utilized.

The DOP is a measure of the completeness of the reaction of the react.-Fe with aqueous sulfide (Leventhal and Taylor, 1990). Normal marine well-oxygenated bottom water give a DOP value generally less than 0.4 on the sediments covered by this water, whereas suboxic sediments (also called dysaerobic or dysoxic – very low O_2 to no O_2, but no H_2S) implied DOP values around 0.5 to 0.7, and euxinic sediments (containing H_2S in place to O_2 - term derived from the Black Sea whose ancient Latin name was *Pontus Euxinius*) refers to DOP values greater than 0.7 suggesting anaerobic depositional conditions (Raiswell *et al*., 1988). Under euxinic conditions the reaction of H_2S with iron-minerals can occur both before and after burial, even during sedimentation itself (Leventhal, 1983).

5.3.13. Pyrite

For the microscopy work, three disaggregated sediment samples from 6 cores (1 m depth), sampled for both tree species in each forest type, were mounted in aluminum stubs and gold coated. These impregnated samples were examined using a standard method of Scanning Electron Microscopy - SEM (LEO 1450VP) in the Goeldi Museum, State of Pará (Goldstein *et al.,* 2003). The diameter size and number of microcrystals of pyrite and framboidal morphology observed in the sample were measured using an optical microscope. The grains were measured to ± 0.25 μm with a standard ocular calibrated with a stage micrometer.

Framboids are densely-packed, raspberry-like, spherical to sub-spherical aggregates of equal micro-sized pyrite crystals (Love and Amstutz, 1966; Rickard, 1970). They range from a few to several tens of microns in diameter (Wilkin *et al*., 1996), with rare "polyframboids" (Love, 1971) or "framboidal clusters or aggregates" (Sawłowicz, 1987) occasionally reaching several microns to millimeters. The processes causing pyrite to have framboidal morphology, are generally thought to occur during the replacement of progressively more S-rich phases: disordered mackinawite ($FeS_{(1-x)}$) → ordered mackinawite (Fe_9S_8) → greigite (Fe_3S_4) → pyrite (FeS_2). Within individual framboids, microcrystals are remarkably uniform in size and shape, therefore the diameter is independent of orientation (Wilkin *et al*., 1996). The number of microcrystals (Nm) in spherical and oblate (dumbbell) framboids composed of uniformly sized spherical microcrystals in a cubic closest-packed (ccp) arrangement was calculated. This equation considered the framboid diameter (D), microcrystal diameter (d) and packing coefficient of the microcrystals (ø = 0.74) (Wilkin *et al*., 1996) as follows:

$$Nm = ø\,(D/d)^3$$

The notion of pyrite stability has resulted in the wide use of pyrite formation as a redox proxy for identifying depositional environments and a cyclic transition (Raiswell and Berner, 1985; Raiswell *et al*., 1988, Wilkin *et al.,* 1997).

In fact, very slow deposition under euxinic conditions increase the amount of pyrite formed, because slowly reacting Fe compounds are given more time for reaction with H_2S (Berner, 1984). An important distinction has been made by Raiswell and Berner (1985) between *syngenetic* pyrite formed in the water columns of euxinic environments that settles to the sediments-water interface prior to burial and *diagenetic* pyrite formed *in situ* within the pore-waters of anoxic marine sediments underlying oxic water columns. This distinction between *syngenetic* and *diagenetic* sedimentary pyrite affects the interpretation of the DOP observed in ancient sediments (Raiswell *et al*., 1988).

5.3.14. Molar ratios

The parameters org.-C, tot.-N, react.-Fe, react.-Al, react.-Ca, P-Fe/Al and P-Ca were expressed in weight % and their ratios were calculated on w/w basis. The latter can be obtained multiplying these parameters (w/w) values by their moles (mol/mol) values. This calculation was applied for the following molar ratios:

- C : N = organic carbon versus total nitrogen
- Fe : P-Fe/Al = reactive-Fe versus iron/aluminium-bound Phosphorus
- Al : P-Fe/Al = reactive-Al versus iron/aluminium-bound Phosphorus
- Ca : P-Ca = reactive-Ca versus calcium-bound Phosphorus

CHAPTER 6
PHYSICOCHEMICAL PATTERN AND PHOSPHORUS STATUS OF MANGROVES

6.1. Results

6.1.1. Topography and forest structure

At the elevation surface, three main topographic features could be identified: high (HP), intermediate (MP) and low plain (LP), where the hidro-edaphic conditions of topography and flooding showed a clear gradient (**Fig. 4**). The HP was defined into the boundary of 41-67 days/year and was inundated only during spring tide. The MP had a boundary of 80-101 days/year, whereas LP 124-162 days/year. At the boundaries of HP and LP with MP, slight depressions of 5-8 cm depth occurred, appearing to be remains of a paleochannel identified as depression one (D1) and two (D2), respectively **(Tab. 3)**. IF values from the depressions do not correspond to higher frequencies, they indicate higher permanency time of the flood water, moreover they were into the trend.

At the study area, situated at a higher part of the central sector of the Bragança Peninsula, the forest structure is characterized by a tree-height gradient including monospecific stands of *A. germinans* and *R. mangle* divided by a transition zone of both species. At the drier and more saline zone *A. germinans* dominated, belonged to the smallest stem diameter at breast height (DBH) (1-16 cm) and height size (4.5-10.5 cm) classes. Conversely, in the most frequently inundated area *R. mangle* trees with highest DBH (9-19 cm) and height size (7-13 cm) classes occurred (Menezes, 2006). Such pattern of species zonation and forest structure along three main topographic features can been attributed as a response to geomorphic changes and physiological response to tide-maintained gradients (Snedaker, 1982).

Table 3: Phosphate fractions in sediments at 10 to 40 cm depth along a gradient of inundation frequency (IF). Mean values ($\bar{x}$), standard deviation (SD) and range in mg P.g-1. In parenthesis percentage contribution of the sum of the fractions.

Station	N	n	IF	tot-P	org.-P	inorg.-P	P-Fe/Al	P-Ca	extr.-P
				mg.g^{-1} DW					
HP	2	17	41 - 62	0.59 ± 0.15	0.03 ± 0.02 (7)	0.45 ± 0.09 (93)	0.35 ± 0.09 (77)	0.05 ± 0.01(12)	0.05 ± 0.02 (11)
				0.28 - 0.84	0.01 - 0.08	0.21 - 0.59	0.11 - 0.46	0.03 - 0.08	0.02 - 0.08
D1	1	9	67	0.68 ± 0.24	0.07 ± 0.03 (12)	0.58 ± 0.23 (88)	0.42 ± 0.21 (70)	0.06 ± 0.01 (12)	0.10 ± 0.05 (18)
				0.31 - 0.96	0.04 - 0.09	0.27 - 0.86	0.12 - 0.68	0.04 - 0.07	0.04 - 0.20
MP	2	33	80 - 101	0.39 ± 0.13	0.05 ± 0.03 (13)	0.39 ± 0.13 (87)	x	x	0.06 ± 0.02
				0.17 - 0.72	0.01 - 0.09	0.16 - 0.54			0.05 - 0.10
D2	1	12	124	0.61 ± 0.28	0.10 ± 0.02 (17)	0.53 ± 0.21 (83)	0.37 ± 0.20 (67)	0.03 ± 0.01 (6)	0.13 ± 0.05 (27)
				0.32 - 1.12	0.03 - 0.12	0.29 - 0.88	0.17 - 0.73	0.01 - 0.04	0.06 - 0.19
LP	2	18	128 - 162	0.74 ± 0.36	0.06 ± 0.03 (9)	0.68 ± 0.29 (91)	0.56 ± 0.26 (81)	0.07 ± 0.05 (11)	0.05 ± 0.01 (8)
				0.40 - 1.58	0.02 - 0.08	0.31 - 1.28	0.23 - 1.12	0.02 - 0.12	0.03 - 0.08

Abbreviations: N, number of stations; n, number of samples; IF, Inundation Frequency (days/year); HP, high plain; MP, middle plain; D, topographic depressions; LP, low plain; tot.-P, total P; org.-P, organic P; inorg.-P, inorganic P; P-Fe/Al, iron/aluminium-bound P; P-Ca, calcium-bound P; extr.-P, extractable P.

6.1.2. Eh, sulphide and pH: Changes with flooding time

During tide stability conditions the values of fixed electrodes in sediments (10 cm) along a time period (24 h- and 12 h-expeditions) were taking as an indicator of the measurements variation. This instrumental variability, expressed as variation coefficient (VC), results for sulphide 10 % (0.80 ± 0.08 µM), pH 2.5 % (7.4 ± 0.19) and Eh 13 % (70 ± 9 mV) (**Tab. 1**, **Fig. 10** (I)**, Fig. 11**). The VC of sulphide did not consider the initial measure period (14:45-17:25 h) due adaptation of the electrode signal to lower sediment sulphide concentrations (**Fig. 10** (I) A). The mean values of the fixed stations were calibrated with the downcore electrode dates performed in the sediment (10 cm) at the same station (HP) one month latter (**Fig. 17**). The comparison with sulphide (1 µM, data not show), pH (7.7) and Eh (81 mV) resulted in similar values suggesting reliable measurements in the profiles of the entire transect.

The overall effects of submergence and non submergence on physicochemical parameters of sediment and water for the 24 h-expedition are shown in Figures 10 and 11. During flood, but before the submergence of sediments, a smooth sulphide increase was seen, which kept stable for 12 min (**Fig. 10** (I) A, C). At the same sectors, during the course time of submergence (20:15-20:45 and 8:30-8:50 hrs), a largest sulphide decrease occurred. This ~3-fold sulphide depletion was sharper at higher (C, 23 cm) than at lower (A, 8 cm) water height, and was characterized by an initial drop of 0.87-0.59 µM (A) and 0.97-0.44 µM (C) followed by a gradual depletion of 0.59-0.31 µM (A) and 0.44-0.28 µM (C). During ebb a gradual sinusoidal sulphide increase was seen returning to steady state (B, C).

At the 12 h-expedition, the Eh and pH were characterized by stable values during non submergence (9 hrs) (**Fig. 11** B, C). The submergence of sediments (20:00-21:00 hrs**)** reaching 34 cm water height caused an intense opposite change of these parameters (C). The Eh depletion (194 mV) was concomitant with the pH increase (4 units), showing a relation of ~50 mV per pH unit, maintained also during ebb conditions (**Fig. 11** D, **Fig. 12**). During the 2.5 hours of submergence (20:00-22:30), the Eh dropped drastically ~4.5-fold from 78 mV to -253 mV, concomitant with the pH increased from 6.8 to 13.3 units. In the water height of 2 cm, the returning trend to stable values occurred.

The pH and Eh of floodwater was controlled to check the possible influence of the electrode tip causing fissures in the sediments and the percolation of floodwater during submergence (**Fig. 10** (II)). The water parameters showed a smooth opposite feature maintained a relation of ~60 mV per pH change of ~0.4 unit and stable values during ebb begin (9:02-9:16 hrs) (C, D). During inundation the presence of slightly basic pH (7.7-8.6) and oxic (195-71 mV) floodwater affecting the sediment pattern was not evident (**Fig. 12**). At the end of submergence the pH and Eh values of floodwater showed a tendency to reach the sediment stable values (**Fig. 12** (I)(II)). The relation of 0.5 volts per 1 pH unit in sediment was maintained during submergence (**Fig. 12** (III)) supporting the experimental data of Gotoh and Patrick (1974) and Gomez et al. (1999).

6.1.3. Eh, sulphide and pH: Changes relative to mangrove roots

In the comparison of two areas with different inundation frequencies, a higher sediment Eh and lower sulphide concentrations occurred in the surface sediments (10 cm) of the monospecific *A. germinans* forest (HP) (**Fig. 13**, **Fig. 4** B, C). Eh ranged 12 to 349 and 260 to 298 mV, whereas S^{2-}concentrations ranged 0.4-1.0 and 0.4-3.7 μM, both for HP and MP respectively. Topographic elevation and inundation frequency between stations locations B and C differ 20 cm and 60 days/year, respectively (**Fig. 4**). At MP, in the bare substrate at 0.5-1.5 m distance of the vegetated zone, sulphide values (2.1-3.7 μM) were highest. The sediment pH ranged 6.6-7.0 and 6.2-6.5 in HP and MP, respectively. Non significant differences in Eh and pH were found between bare sediment (BS) and vegetated area.

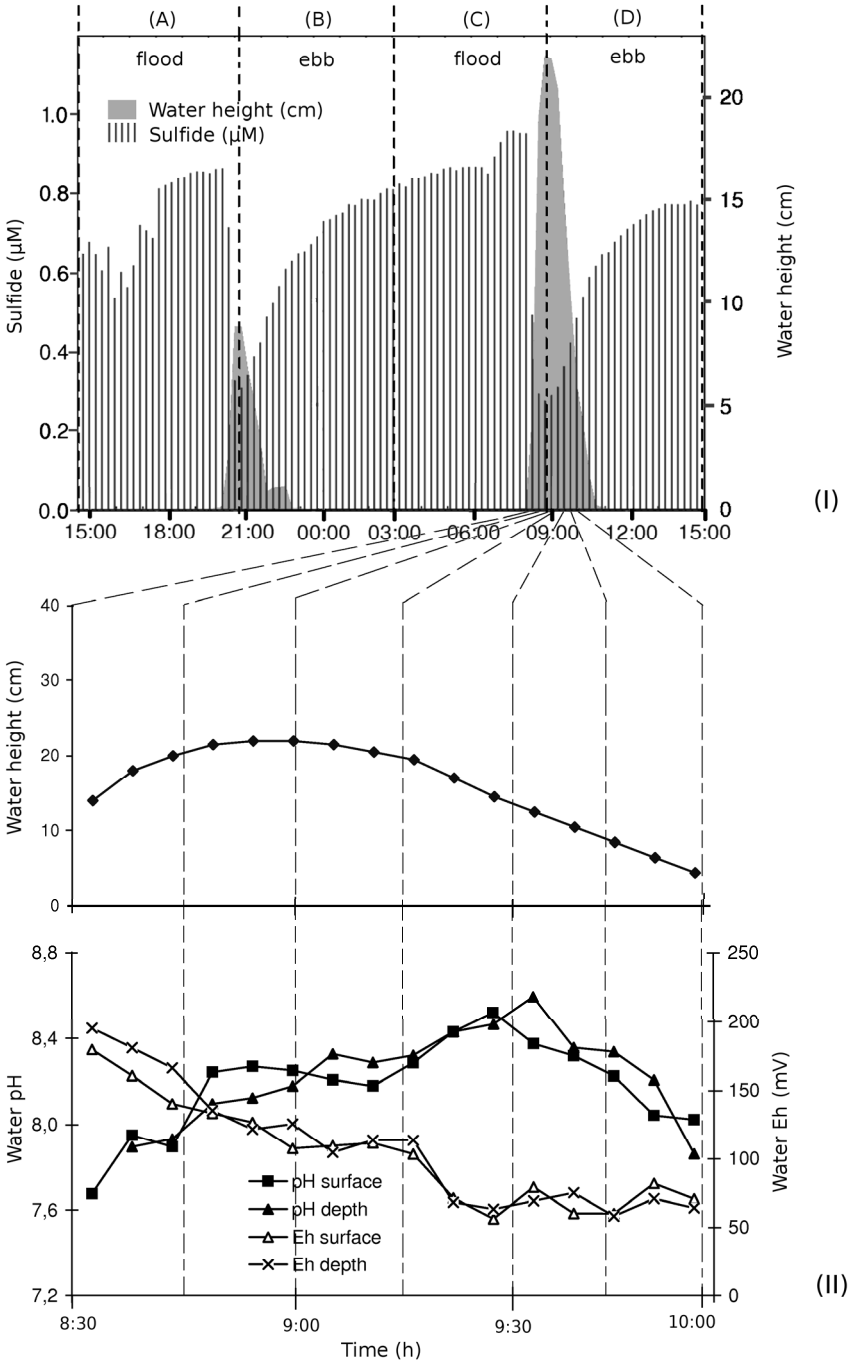

Figure 10: **(I)** Changes for sulphide in sediments at 10 cm depth (27.6 ^{o}C) and water height (cm) variation during flood and ebb. **(II)** Changes in pH and redox potential (Eh) of flood water surface and depth (25.5 ^{o}C) during spring tide.

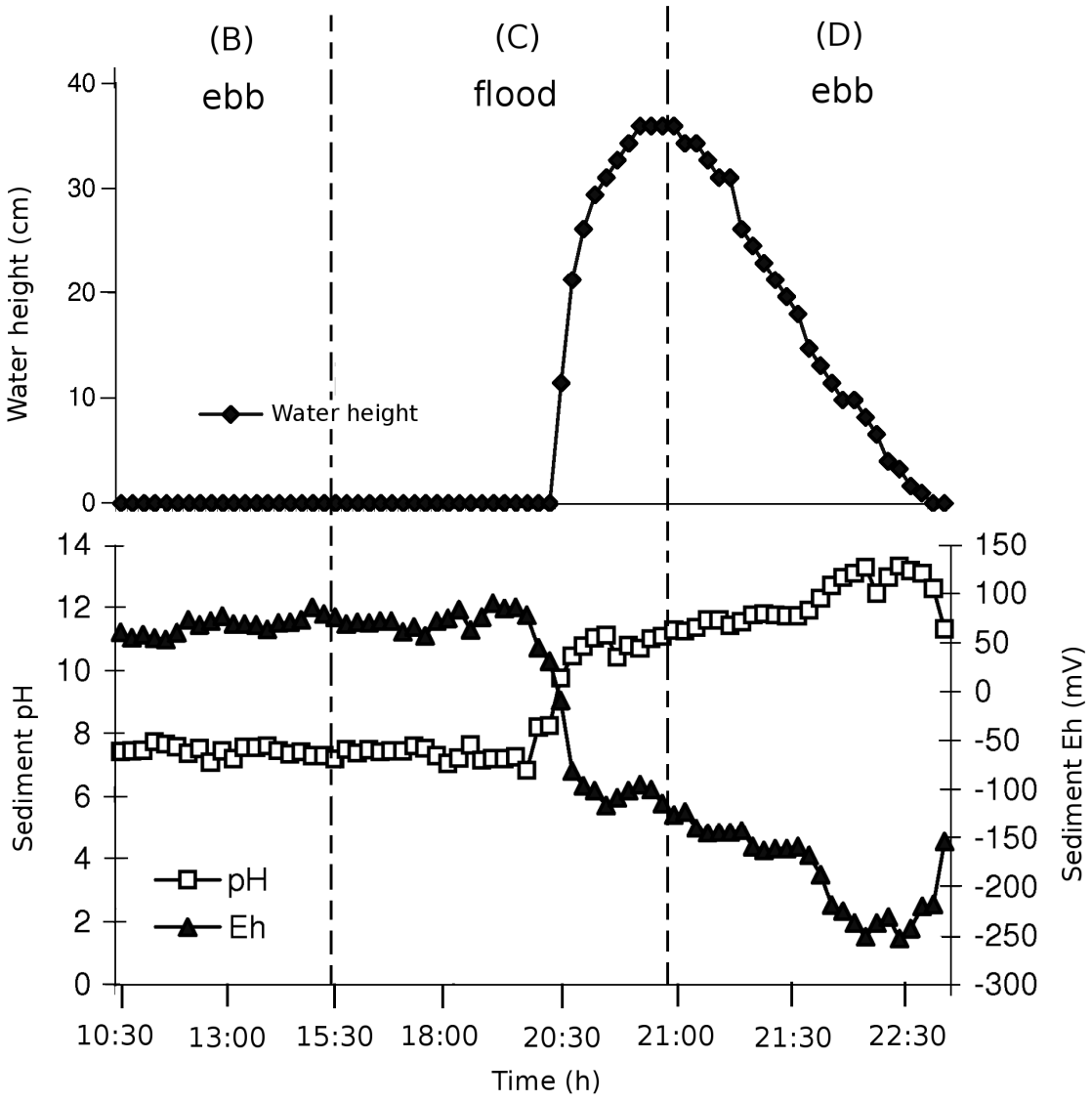

Figure 11: Variation in water height (cm), pH and redox potential (Eh) in sediments at 10 cm depth (26.5 ^{o}C) during spring tide.

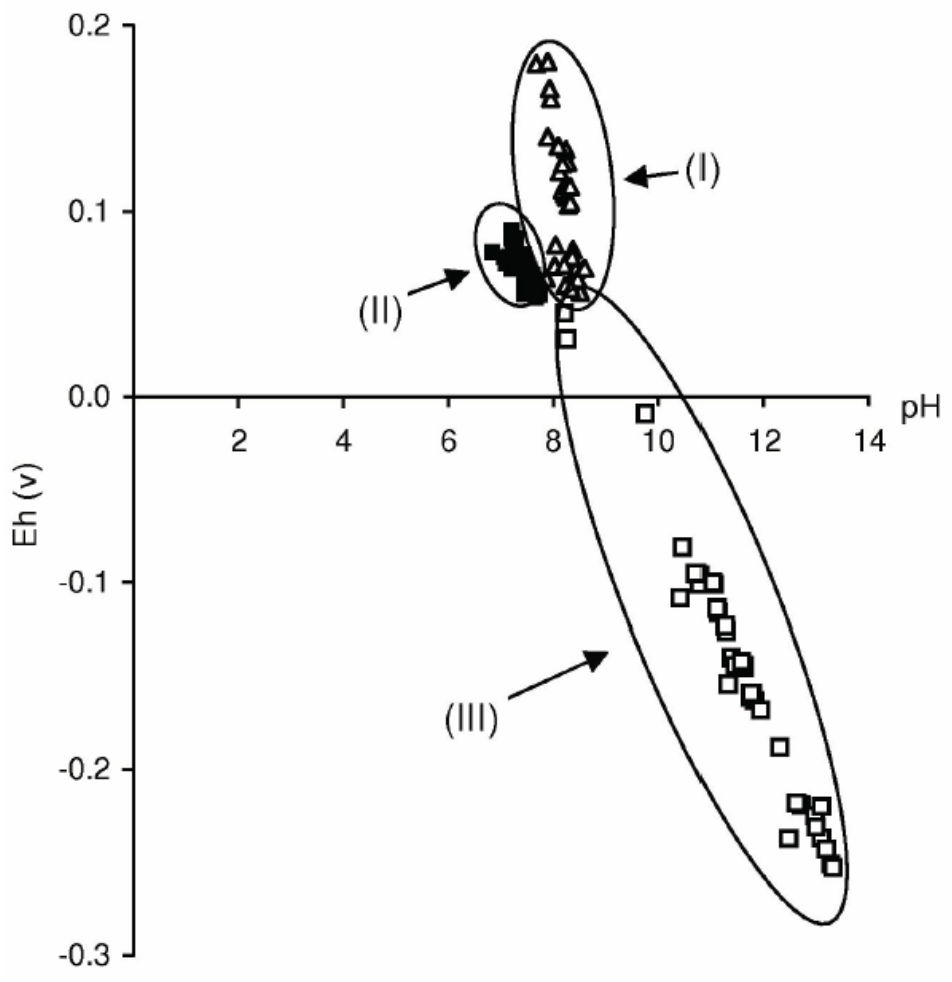

Figure 12: Feature of Eh versus pH values for flood water **(I)** (24 h-expedition) and sediment during flood **(II)** and submergence **(III)** (12 h-expedition).

Station B

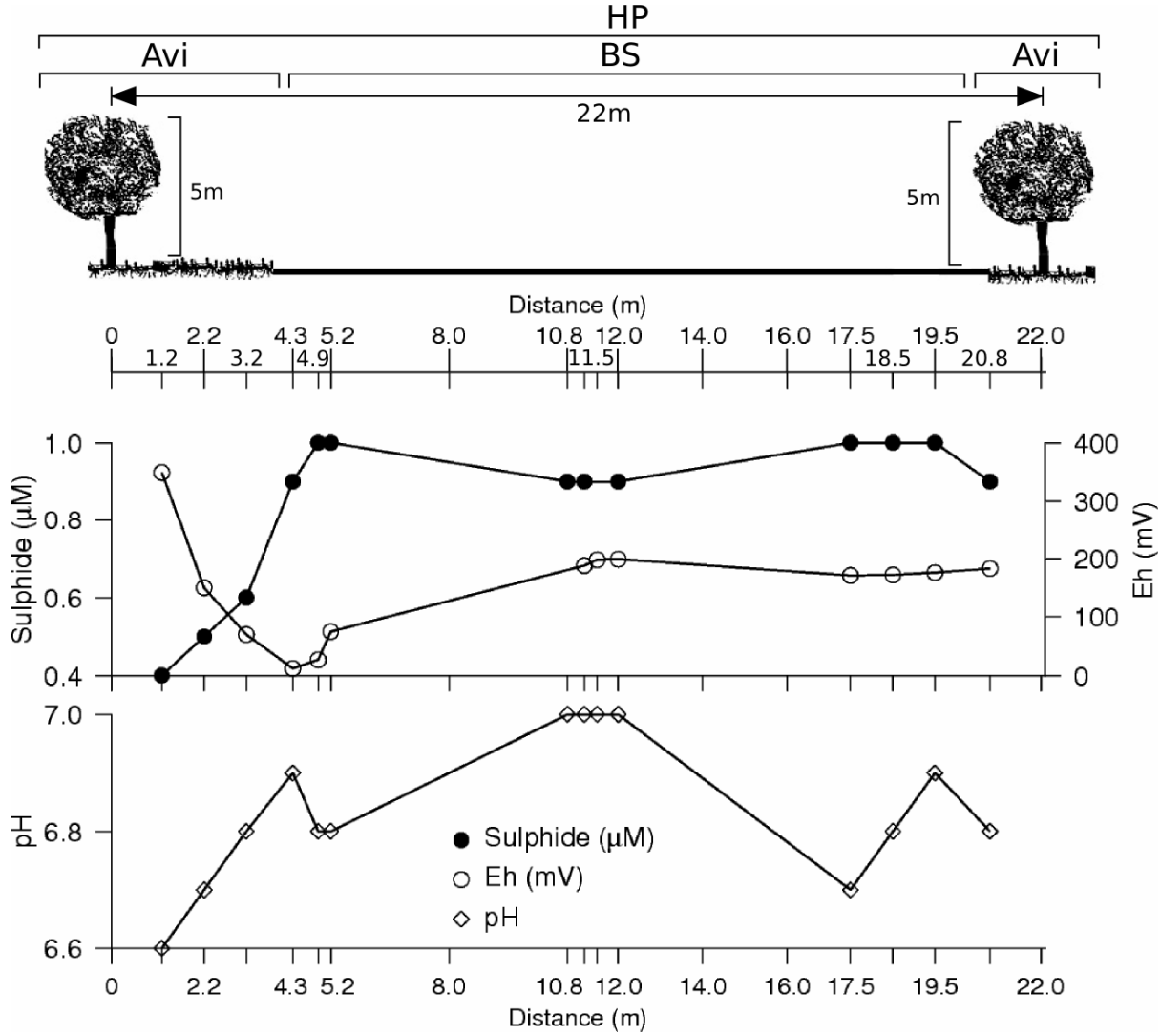

Figure 13: Variation of surface (10 cm) sediment sulphide, pH and redox potential (Eh) along a horizontal profile in: **Station B,** mangrove forest dominated by *A. germinans* and bare sediment (BS) at high plain (HP), and **Station C,** mixed forest of *A. germinans* and *R. mangle* at middle plain (MP).

Station C

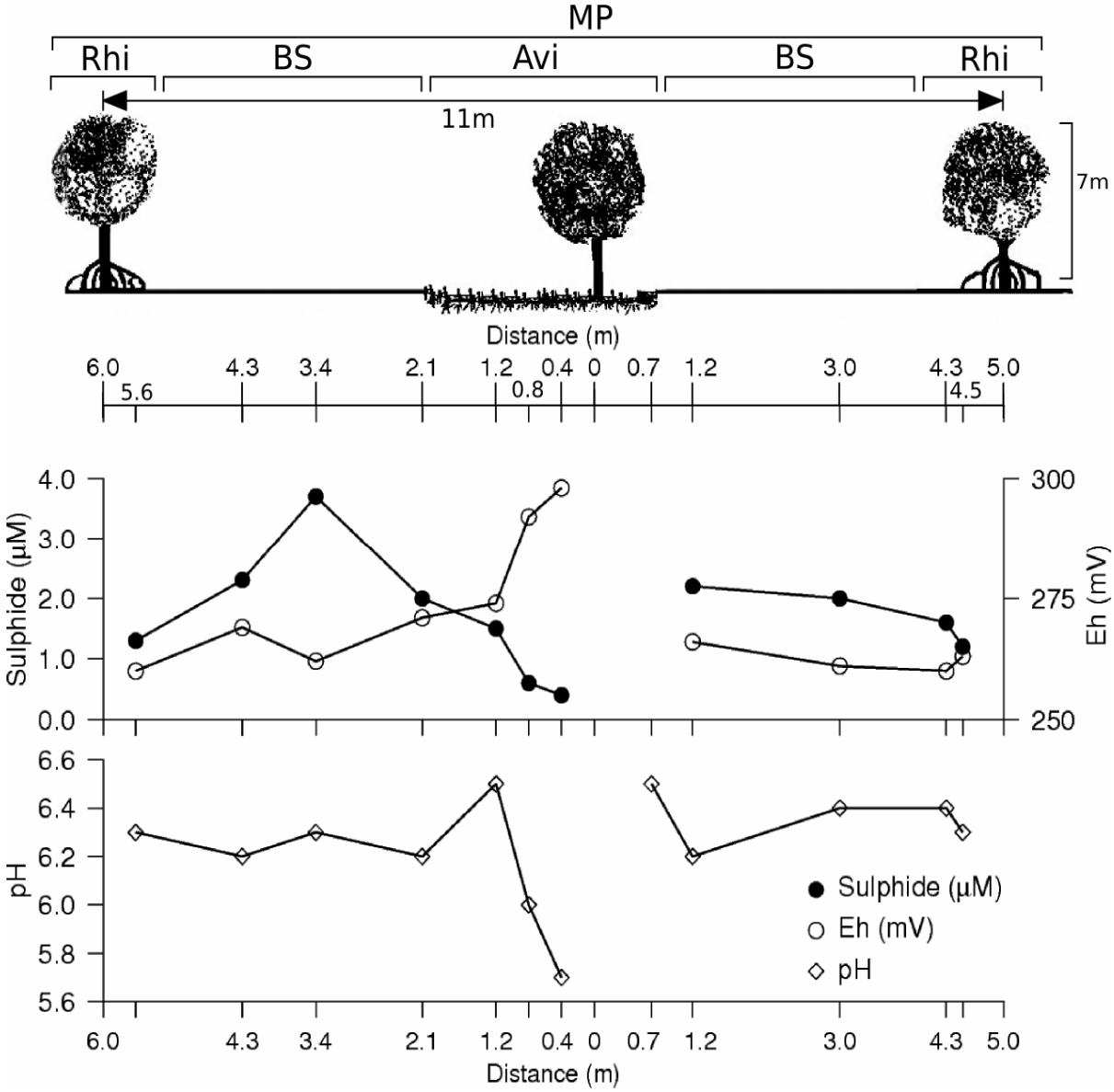

Continuation Figure 13

6.1.4. Eh and pH changes with depth (50 cm) in sediments

Along the transect, changes in sediment Eh (-121 to 296 mV) and pH (6.4 to 8.0) exhibited a wide range in the profile (50 cm). This vertical variation in Eh and pH was strongly associated with the different IF, vegetation zonation and depth. In several stations, the Eh zonation was similar to the redox stratification model proposed by Clark et al. (1998) for an *Avicennia*-dominated mangrove forest. In this model two oxidation and two reduction horizons were proposed, each accompanied by acidic and basic pore-water pH, respectively (**Fig. 14**).

In HP, the upper horizon of sediments (5 cm) named by Clark et al. (1998) as "upper oxidation zone - UOZ", was characterized by oxic conditions in *R. mangle* (262 mV) and *A. germinans* (106 mV). Beneath the oxidized surface layer (10 cm), the "upper reduction zone - URZ" was characterized by lower Eh conditions in *R. mangle* (207 mV) and *A. germinans* (82 mV) in relation to the UOZ. At the "lower oxidation zone - LOZ" (10-35 cm) an Eh increase in *R. mangle* (ΔEh_1=89 mV) and *A. germinans* (ΔEh_2= 139 mV) was recorded. Beneath the roots zone (40-50 cm) merge the "lower reduction zone - LRZ" characterized by Eh depletion and/or stabilization. Additionally, there may be appreciable two different pH features. The first pH feature observed at *A. germinans* was consistent with the redox stratification model. At URZ and LOZ, this trend ranged from basic (7.8) to neutral (7.0) values, at LRZ the slightly basic (7.3) conditions were re-established. The second pH feature occurred below *R. mangle* by pH depletion (6.9-6.4).

At the intermediate plain (MP), Eh kept positive (57-184 mV) in both species with a maximum localized under *R. mangle* trees. Below *R. mangle*, a moderate intensity of the redox stratification was maintained with Eh increasing at LOZ (ΔEh_5=50 mV, ΔEh_7=125 mV). Beneath *A. germinans* non specific Eh pattern was appreciable characterized by low Eh variation at LOZ (ΔEh_6=22 mV, ΔEh_8=38 mV). Concerning pH profiles, in both species a marked decrease (7.8-6.4) was evidenced, similar to the second pH pattern described in HP.

At the depressions (D1, D2) an intense redox zoning was established, except by *A. germinans* in D1. These depressions were characterized by extreme lower Eh beneath *R. mangle* (-110 mV) and *A. germinans* (-79 mV), in D1 and D2, respectively. Here, at LOZ, the Eh increase accounted moderate variation for *R. mangle* (ΔEh_3= 76 mV, ΔEh_9= 59 mV) and *A. germinans* (ΔEh_4= 25 mV, ΔEh_{10}= 65 mV). The redox profiles below *A. germinans* (D1) and *R. mangle* (D2), showed a peculiar stable Eh values at 7-25 and 15-30 cm depth, respectively. The pH was recorded only at D1, showing a decrease feature (second pH pattern) ranged 7.3-6.7 for *R. mangle* and 7.7-7.1 for *A. germinans*.

At the low plain (LP), *R. mangle* was localized in more oxidized sediments than *A. germinans* similar as in D2. Below *R. mangle*, a peculiar stable Eh for 7-13 cm depth followed by a shorter Eh increase (ΔEh_{11}=66 mV) was observed. This trend was associated to smooth acidic (6.6-6.8) values. In contrast, beneath *A. germinans*, a clear redox stratification was exhibited, accounted by the minimum Eh value (-121 mV) and the highest Eh increase at LOZ (ΔEh_{12}=193 mV) of the transect. This feature was characterized by pH of 7.4-6.9.

Differences among species are of interest since they provide information with respect to their relative tolerance to flooding stress. Below *A. germinans* (LOZ), an intense root-induced oxidation was observed from oxic (HP) (ΔEh_2= 139 mV) to anoxic sediments (LP) (ΔEh_{12}=193 mV). Opposite to *A. germinans*, beneath *R. mangle* (LOZ), the root-induced oxidation was attenuated from oxic (HP) (ΔEh_1=89 mV) to anoxic conditions (LP) (ΔEh_{11}=66 mV). At medium plain (MP) *A. germinans* did not showed any oxidizing power. These data suggest that low and high flooding would lead to a higher root-induced oxidation in *A. germinans* than in *R. mangle*.

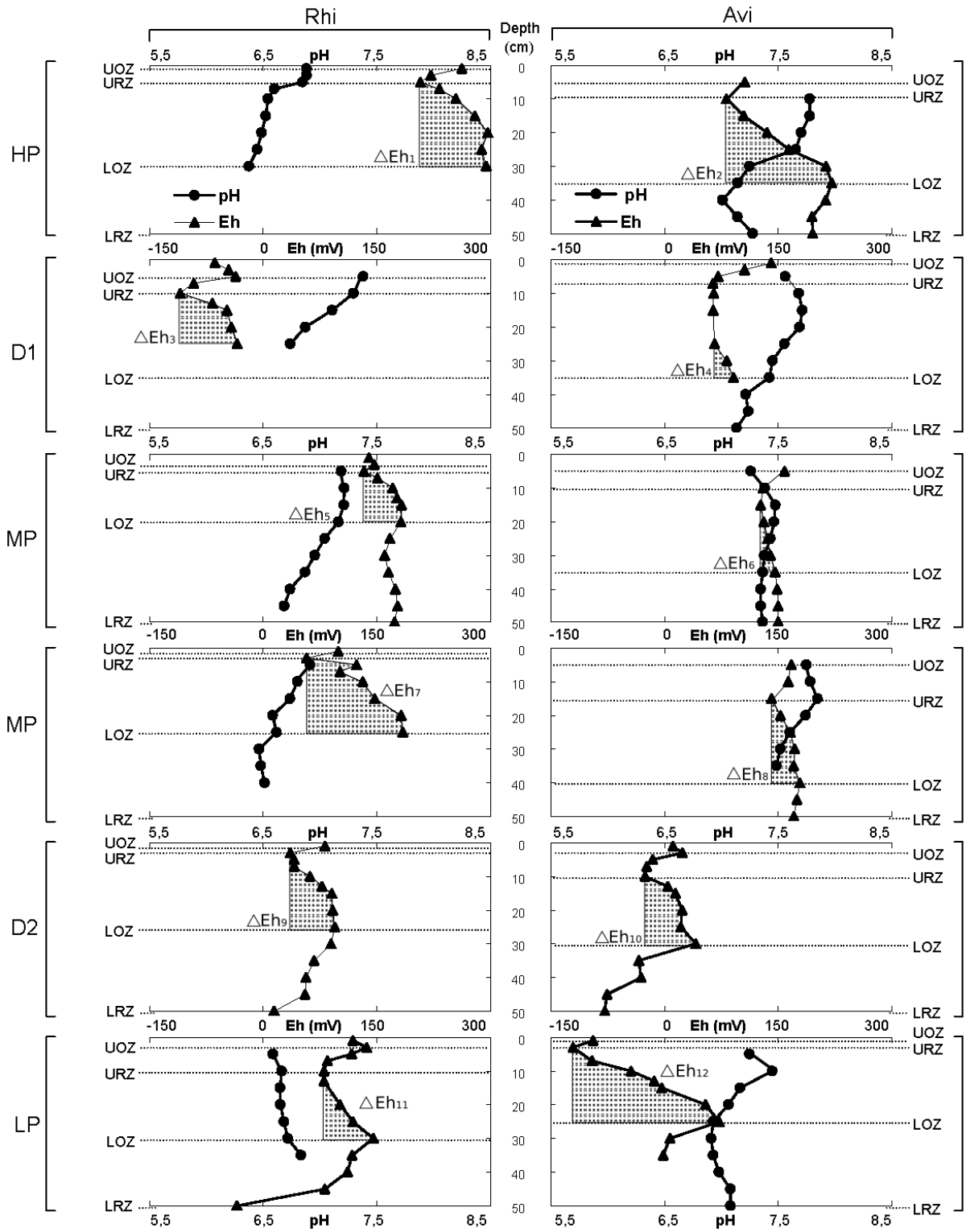

Figure 14: Vertical distribution of redox potential (mV) and pH below *A. germinans* and *R. mangle*. HP, high plain; MP, middle plain; D, depressions; LP, low plain. The figures share the same axis.

6.1.5. Phosphorus fractionation in sediments (1 m)

The analyzed tot.-P was compared with that calculated from the sum of org.-P + P-Fe/Al + P-Ca + extr.-P. Similarly the analysed and calculated inorganic P (P-Fe/Al + P-Ca + extr.-P) were compared. The analyzed fractions were considered as 100 %. These comparisons indicated that the calculated P fractions were 76 % and 74 % lower than the analyzed tot.-P and inorg.-P, respectively **(Fig. 15)**. The relationship between the analysed and calculated parameters showed highly significant correlations for tot.-P ($r=0.90$, $n=93$, $p<0.005$) and inorg.-P ($r=0.88$, $n=93$, $p<0.005$). These results suggested non dissolution of other P compounds by each specific analytical methodology, summed to a low and systematic variation. These comparisons indicated the convenience of using the analysed tot.-P for the general results description and the calculated fractions only for describe the inorg.-P proportions.

Values of tot.-P and fractionation between 10 and 40 cm depth (LOZ) are summarized in **Table 3**. Along the transect, tot.-P levels in sediments decreased with increasing elevation. Even though tot.-P is not representative of the reactive fraction of P in sediments, it is usually the component that can be compared to existing data based on less detailed geochemical determinations.

The percentage of analysed inorg.-P contributed more than 80% to tot.-P. The concentrations of inorg.-P increased markedly from HP to LP (0.21-1.28 mg P g^{-1} DW), following the same trend as tot.-P. The concentrations of org.-P in HP and LP were in the same range (0.01-0.08 mg P g^{-1} DW), with exception by the increase at the depressions (0.03-0.12 mg P g^{-1} DW) resulting in a proportion for 12-17% of tot.-P.

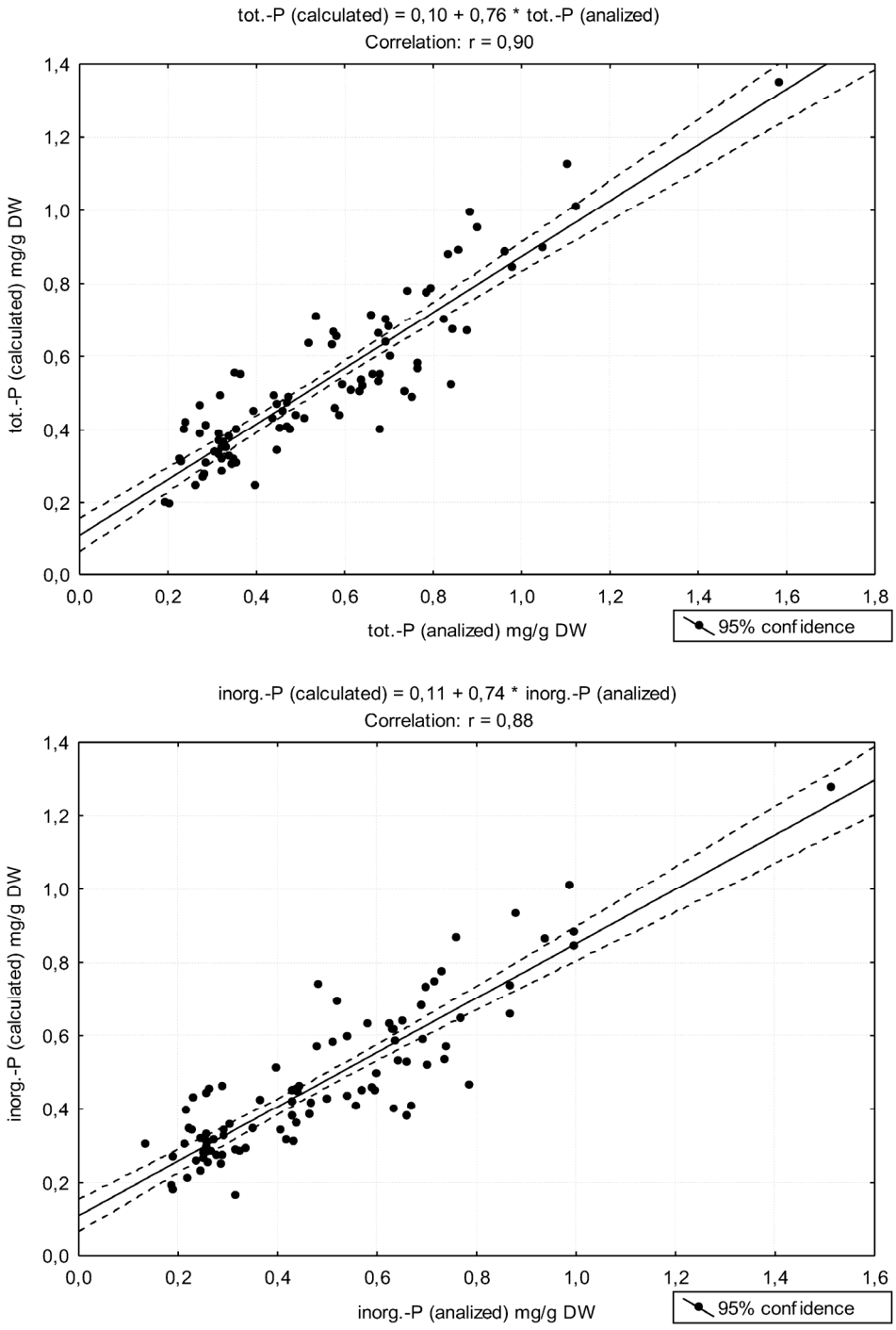

Figure 15: Comparison between analyzed and calculated phosphorus fractions of total P (tot.-P) and inorganic P (inorg.-P).

The dominant mineral fraction was the iron/aluminium bound phosphate (P-Fe/Al) ranging for 0.11-1.12 mg P g^{-1} DW. At LP, this fraction accounted for the higher proportion (81 %) of the calculated inorg.-P. At both depressions, the depletion of this pool (67-70 %) was coinciding with sediments most enriched with org.-P. The calcium bound phosphate (P-Ca), with a concentration range in one order of magnitude lower than those of P-Fe/Al (0.01-0.12 mg P g^{-1} DW), accounted for 6-12% of the calculated inorg.-P, showing the highest proportions at LP.

Along the transect, the levels of extr.-P varied for 0.02-0.19 mg P g^{-1} DW, with highest proportions (18-27 %) of the calculated inorg.-P at the depressions (**Tab. 3**). The extr.-P showed a high dependency with position along a tidal gradient (**Fig. 16**). The relation between extr.-P (25-30 cm) and inundation frequency was best described by a positive correlation ($r=0.81$, $n=29$, $p<0.005$).

Chemical analysis of surface sediments (5-10 cm) yielded means of 0.04 ± 0.03 extr.-P, 24 ± 1 react.-Fe, 13 ± 1 react.-Al and 0.19 ± 0.03 mg. g^{-1} DW react.-Ca (**Tab. 4**). The surficial layer was characterized by high Eh's (185-262 mV) in HP, contrasting to lower Eh's (-121 to 136 mV) in LP. In both forest a moderately acidic to basic pH values (6.5-7.5) was maintained. Marked differences in extr.-P and react.-Ca between aerobic (HP) and anaerobic (LP) sediments were observed. LP sediments have more extr.-P and react.-Ca in solution than HP sediments. The react.-Al was constant and the react.-Fe do not showed well-defined horizontal pattern. Concerning the minerals pools, LP accounted for the highest P-Fe/Al concentration (0.49 ± 0.10 mg. g^{-1} DW) opposite to HP (0.30 ± 0.05 mg. g^{-1} DW). Regarding P-Ca, the concentrations along the transect ranged 0.02-0.14 mg. g^{-1} DW, increasing (0.09 ± 0.03 mg. g^{-1} DW) in LP.

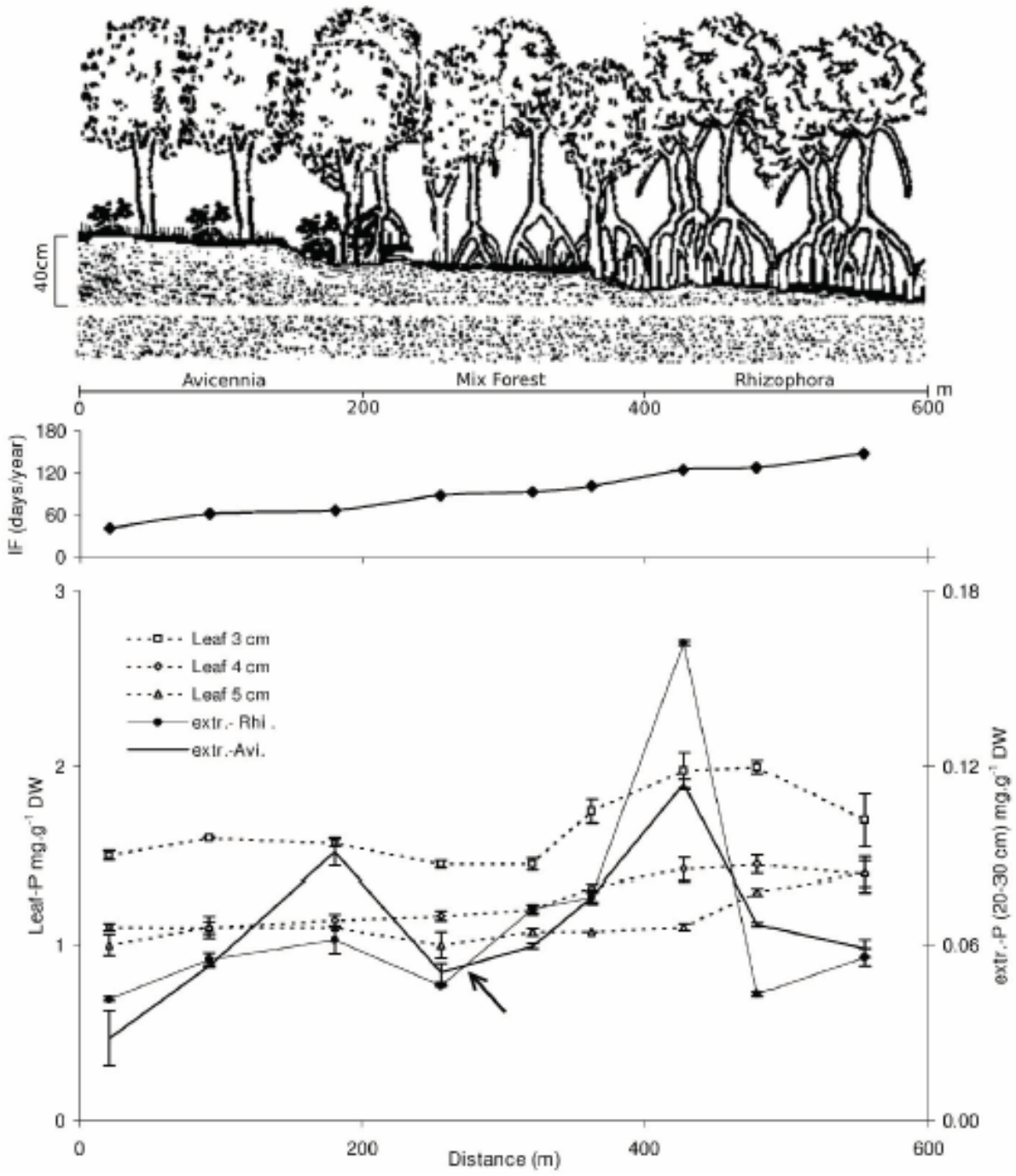

Figure 16: Horizontal distribution of inundation frequency (IF), extractable phosphorus (extr.-P) in sediments and leaf phosphorus (Leaf-P) (Cordeiro, Mendoza *et al*., 2003 reprinted with permission).

Table 4: Physical-chemical characteristics of surface sediments (0-10 cm), reactive fractions and phosphate molar ratios from transect. Mean values ($\bar{x}$), standard deviation (SD) and range.

Stations	Species	N	n	Eh (mV)	pH	exch.-P	react.-Fe	react.-Al	react.-Ca	Fe : P-Fe/Al	Al : P-Fe/Al	Ca : P-Ca
						mg.g^{-1} DW				mol/mol		
HP	*R. mangle*	3	6	223 ± 3	7.0 ± 0.5	0.03 ± 0.01	21 ± 1	13 ± 0.5	0.16 ± 0.01	105 ± 9	93 ± 2	11.8 ± 0.7
				220 - 226	6.5 - 7.5	0.02 - 0.03	20 - 22	12 - 13.5	0.15 - 0.17	99 - 115	91 - 93	11.0 - 12.4
	A. germinans	3	6	222 ± 29	7.2 ± 0.4	0.02 ± 0.005	25 ± 0.5	13 ± 0.5	0.19 ± 0.004	119 ± 2	122 ± 2	10.0 ± 1.0
				185 - 262	6.7 - 7.4	0.02 - 0.03	24 - 25	12 - 13.5	0.19 - 0.18	117 - 122	121 - 123	9.0 -11.3
LP	*R. mangle*	3	6	80 ± 33	6.8 ± 0.2	0.09 ± 0.04	23 ± 1	13 ± 0.5	0.19 ± 0.01	69 ± 7	56 ± 3	6.8 ± 1.3
				38 - 136	6.6 - 6.9	0.07 - 0.14	22 - 24	12 - 13.5	0.18 - 0.20	60 - 76	52 - 59	5.0 - 7.9
	A. germinans	3	6	7 ± 93	7.1 ± 0.3	0.04 ± 0.02	24 ± 1	14 ± 0.5	0.22 ± 0.01	84 ± 14	90 ± 5	6.2 ± 2.0
				-121 - 97	6.8 - 7.2	0.02 - 0.06	24 - 25	13 - 14.5	0.20 - 0.24	74 - 95	86 - 93	3.9 - 7.4

Abbreviations: N, number of stations; n, number of samples; HP, high plain; LP, low plain; Eh, redox potential; extr.-P, extractable P; react.-Fe, reactive iron; react.-Al, reactive aluminium; react.-Ca, reactive calcium; Fe : P-Fe/Al, reactive iron to iron/aluminium-bound P ratio; Al : P-Fe/Al, reactive aluminium to iron/aluminium-bound P ratio; Ca : P-Ca, reactive calcium to calcium-bound P ratio.

The react.-Fe : P-Fe/Al (Fe : P-Fe/Al), react.-Al : P-Fe/Al (Al : P-Fe/Al) and react.-Ca : P-Ca (Ca : P-Ca) ratios gave the highest values in HP (**Tab. 4**), reflecting in general the lower P-Fe/Al and P-Ca concentrations in HP. The only ratio that correlated significantly with extr.-P was Al : P-Fe/Al which was negatively related ($r= -0.74$, $n=23$, $p<0.05$). Sediment Fe : P-Fe/Al ratio showed r values of -0.63 ($n=24$, $p<0.05$), which were close to significant, while Ca : P-Ca ratio showed poor correlation with -0.49 ($n=24$, $p<0.05$).

6.1.6. Porewater and solid-phase elements interaction

The concentration of P compounds varied significantly among forest types and was affected by the physicochemical variability with sediment depth **(Fig. 17)**. Along the entire transect, P-Fe/Al showed the same variation pattern of tot.-P. In general, the extr.-P pattern varied as a function of dissolution and precipitation for P-Fe/Al and P-Ca pools (Saleque and Kirk, 1995; Wang *et al*., 1995). Due the low proportion of org.-P (<17 % of tot.-P) in relation to inorg.-P (> 83 % of tot.-P), the organic fraction did not seem to play a key role on the extr.-P, with exception of the depressions were more material accumulation occurred.

At HP the trend of tot.-P and P-Fe/Al was characterized by a short decline at URZ, followed by a smooth increase at LOZ and a substantial depletion at LRZ. Below *R. mangle* the P-Ca concentrations reflected a greater depletion with depth (0.08-0.03 mg P g^{-1} DW). Contrary, beneath *A. germinans*, occurred at LOZ a P-Ca increase (0.02-0.08 mg P g^{-1} DW) and at LRZ a decrease (0.08-0.03 mg P g^{-1} DW). In both species, the extr.-P (0.01-0.07 mg P g^{-1} DW) was controlled by the dissolution and precipitation for the minerals pools. The org-P concentration below *R. mangle* decreased sharply (0.08-0.01 mg P g^{-1} DW) and under *A. germinans* remained stable (~0.03 mg P g^{-1} DW).

In the intermediate plain (MP), the tot.-P increased at LOZ (0.35-0.58 mg P g^{-1} DW) and depleted at LRZ (0.58-0.17 mg P g^{-1} DW), the extr.-P follows the same pattern (data not showed). The lower tot.-P range may reflect the moderately and slightly oxidation intensity in *R. mangle* and *A. germinans*, respectively (**Fig. 14**). In both

species the org.-P sharp depleted with depth. This forest was lacking of P-Fe/Al and P-Ca data.

Contrasting to the intermediate plain, at the waterlogged areas, the extr.-P, P-Fe/Al and tot.-P showed two different features, linked to more anoxic or oxidized sediments (**Fig. 14**). The first trend, beneath *R. mangle* (D1) and *A. germinans* (D2), was linked to the redox stratification, reaching anoxic values in LRZ (**Fig. 14**). This trend was similar as the HP pattern, differing here by higher extr.-P, P-Fe/Al and tot.-P concentrations (**Fig. 17**). In the second feature, beneath *A. germinans* (D1) and *R. mangle* (D2), the extr.-P increased concomitant with P-Fe/Al dissolution and tot.-P pool depletion. Here beneath the dominant species of each forest side, the extr.-P accounted the maximal levels of all transect (0.20 mg P g^{-1} DW). Although the Fe/Al dissolution occurred in oxidized sediments, seem to be linked to the remarkably stable Eh values with depth (**Fig. 10**). In both cases the P-Ca remained stable and the org.-P content was higher than average (0.02-0.13 mg g^{-1} DW).

At low plain (LP), the features of P-Fe/Al, tot.-P and extr.-P were similar to D2, characterized below *R. mangle* by dissolution of Fe/Al-P (0.60-0.23 mg P g^{-1} DW) and tot.-P depletion (0.78-0.42 mg P g^{-1} DW); contrasting to higher P-Fe/Al (0.21-1.1 mg P g^{-1} DW) and tot.-P concentrations (0.32-1.6 mg P g^{-1} DW) beneath *A. germinans*. Here again the physicochemical parameters seem to play a key role in *R. mangle* by stable Eh influencing the P-Fe/Al dissolution and in *A. germinans* by a greater biological influence (i.e. oxidation by roots) affecting the P-Fe/Al precipitation (**Fig. 14**). Additionally, at the uppermost sediments (< 25 cm), the P-Ca pool accounted the highest concentrations of the entire transect in *R. mangle* (0.05-0.12 mg P g^{-1} DW) and *A. germinans* (0.03-0.10 mg P g^{-1} DW). In this plain the org.-P did not show any specific pattern.

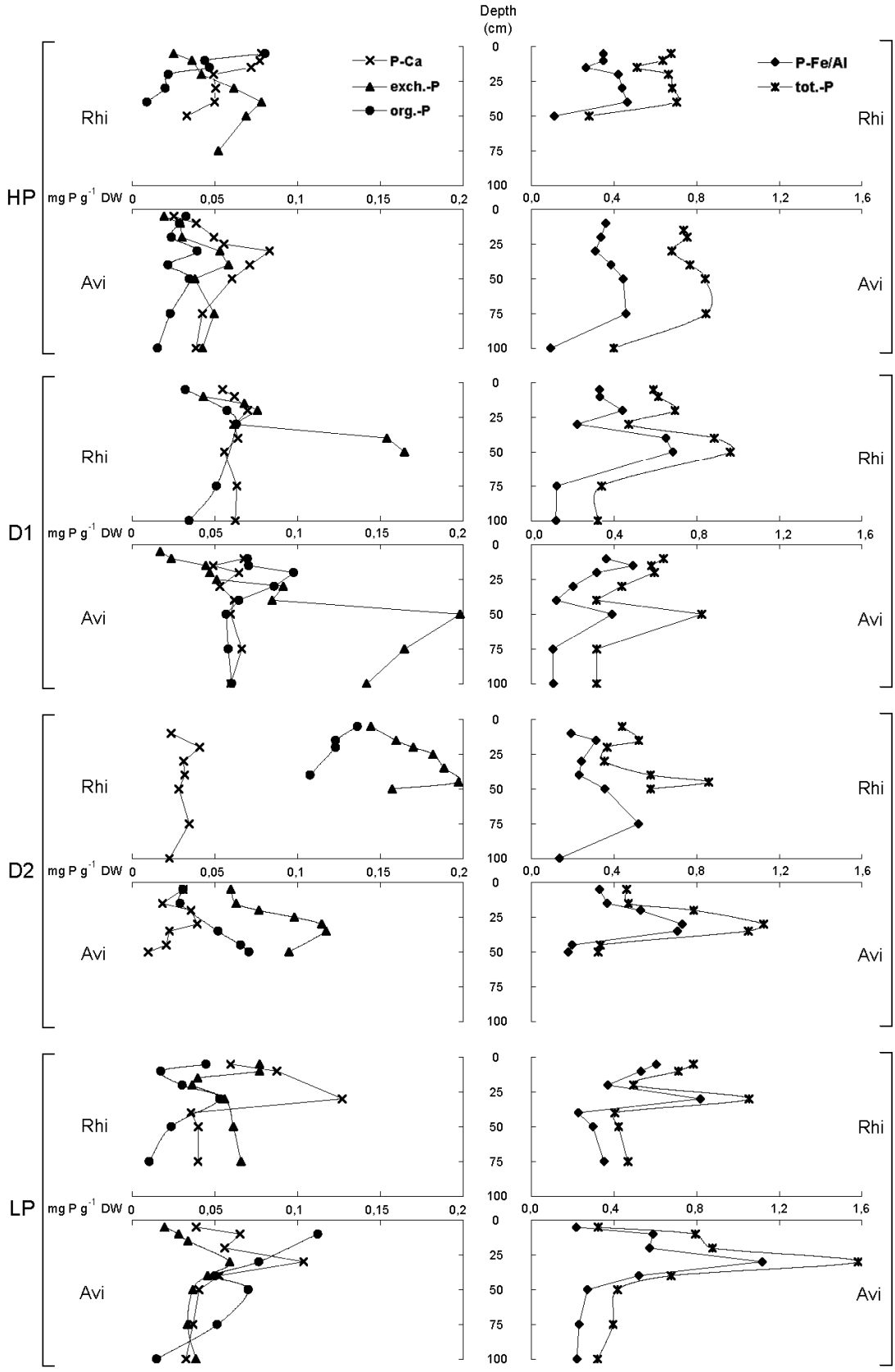

Figure 17: Vertical distribution of phosphorus compounds. The figures share the same axis. P-Ca, calcium-bound P; extr.-P, extractable P; org.-P, organic P; P-Fe/Al, iron/aluminium-bound P; tot.-P, total P; HP, high plain; MP, middle plain; D, depressions; LP, low plain.

6.2. Discussion

6.2.1. Effect of flooding conditions on P-exchange

In the 24- and 12 h-expeditions, during submergence the sediment changes in sulphide, Eh and pH shows a general pattern with rapid initial changes, followed by continuing more gradual changes, returning to stable values during non submergence (**Fig. 10, 11**).

In the 24 h-expedition, after a time-confined sulphide stability before the submergence, the sulphide rapid initial drop and gradual depletion (20-30 min.) in the early stage of the submergence could be apparently due to a) sulphide dilution by the floodwater, or b) the consumption of SO_4^{2-} during the degradation of the organic matter (**Fig. 10** (I) A, C). Unfortunately, the control of the salinity and Cl^-/ SO_4^{2-} molar ratio data in the sediments could not be evaluated, so the absence of these data not supported this hypothesis. This hypothesis can be supported by the mixing of freshly tidal water in the interstices of sediment surface (2 cm) with sea-water (Caetano *et al*., 1997). Meanwhile, the gradual sulphide depletion was similar to the theoretical H_2S decrease as the result of consumption of SO_4^{2-} (Postma and Jakobsen, 1996; Kehew, 2001). During submergence (**Fig. 10** (I) B, D), considering the tidal supply seawater as the source of SO_4^{2-} in these sediments, the sinusoidal sulphide increase over time, reflects the reduction of the electron acceptor SO_4^{2-} resulting in a gradual production of sulphide in the porewater (**Equation 9**, Tribovillard *et al*., 2006).

$$(CH_2O)_{106}(NH_3)_{16}(H_3PO_4) + 53SO_4^{2-} \rightarrow H_3PO_4 + 53S^{2-} + 16NH_3 + 106CO_2 +:106H_2O$$

Eq. 9

In the 12 h-expedition, the shift to anoxic conditions during sediment submergence reaching a minimum of -253 mV is consistent with recent studies in lowland rice fields in Philippines (Kirk, 2003) (**Fig. 11**, D). Meanwhile, our values are extreme reduced as compared to laboratory studies (240-60 mV) performed at 10 cm depth with 16 cm of water height above the sediment surface (Ellison and Farnsworth, 1997). In the Bragança sediments, the Eh minimum was reached in a shorter time (2.5

hrs) than in rice fields (few days), suggesting a difference on the "intensity" factor determined by the relative ease of the reduction (Kludze and DeLaune, 1995), caused probably due the water-saturated condition. Along the transect, at HP where the 12-h expedition was performed, the sediment humidity at 10 cm depth was lower (38 %) than at LP for the same depth (60 %). Thus, we expect that the "intensity" factor of the reduction in LP will be higher, due the high inundation frequency (146 ± 13 days/year) resulting in longer time of minimum Eh following each inundation.

In the same expedition, during the submergence the Eh decrease is consistent with the changes in pH attained a maximum of 13.3 units after 2.5 h (**Fig. 11** C, D). In fact, a pH of 13.3 not occurred in natural systems. In the next section is discussed the available information about this topic.

The Fe(III) and sulphate reduction consumes protons and is responsible for the increase in pH (**Equation 3 and 9**). This phenomenon is commonly observed in rice and normal acid sulphate soils after submergence (Konsten *et al.*, 1994; Ponnamperuma, 1972; Kirk, 2004). However, these experiments were conducted over prolonged submergence (several weeks), under such conditions an initially low pH will increase converging between 6.5 to 7 at steady state (Pavanasasivam and Axley, 1980). In the current study, the relation of 50 mV per 1 pH unit in sediment was maintained during submergence supporting the experimental data of Gotoh and Patrick (1974) and Gomez *et al*. (1999). The sharp Eh reduction and pH increase could be due the high concentrations of Fe/Al-P (0.35 ± 0.09 $mg.g^{-1}$) and SO_4^{2-} (17.7 ± 3.2 mM), summed to the organic matter (12.9 %, 0-10 cm) accumulation due the topographical high position of this station (HP).

Under anoxic conditions, Gotoh and Patrick (1974), and Gomez et al. (1999) proposed that the redox limit for the reduction of Fe(III) (hydr)oxides to Fe(II) change with pH: between 100 and -50 mV at pH 7, -100 mV at pH 8 and -150 mV at pH 9. Under this wide range of pH-redox potential conditions the reduction of Fe(III) apparently take place in a biologically active waterlogged soil. The interface between zones of Fe(III) (hydr)oxides and sulphate reduction is rather poorly defined. From a thermodynamic

point of view, iron reduction takes place at a higher Eh than sulphate reduction, the two reactions may proceed simultaneously over a wide range of environmental conditions. The dominant factors determining whether Fe(III) (hydr)oxides or sulphate reduction is energetically most favourable, are the stability of the Fe(III) (hydr)oxides and the pH, while the effect of the sulphate concentration is small (Postma and Jakobsen, 1996). An equilibrium reaction for the two couples can be written as (**Equation 10**, Appelo and Postma, 2005):

$$8Fe^{2+} + SO_4^{2-} + 20H_2O \leftrightarrow 8Fe(OH)_3 + HS^- + 15H^+ \qquad \textbf{Eq. 10}$$

During submergence the relations ~50 mV (sediments) and ~60 mV (water) per pH unit were maintained (**Fig. 11** C, D; **Fig. 12**). The first relation agreed with that proposed by Gotoh and Patrick (1974) and Gomez et al. (1999) for sediments of field rice and coastal lagoons, under oxic and anoxic conditions in a batch reactor, respectively. The overestimation of our results by the percolation of floodwater trough crabs burrows and bioturbation should be moderate, due to the local (HP) food limitation reflected in low crab density in the study area (Nordhaus *et al*., 2006). Clearly, the effect of flooding on these trends is irrefutable. Meanwhile, the presence of the electrode can amplify the intensity of the measurements.

6.2.2. Effect of the species on sediment properties

The comparison at equivalent elevations, of the root-induced oxidation capacity of *A. germinans* pneumatophores alone and in combination with the stilt roots of *R. mangle*, evidenced a greater oxidation effect on redox status of the sediments with one species (**Fig. 13**). A similar study performed by McKee et al. (1988) described spatial patterns of Eh contrary to these reported here, characterized by greater redox status on sediments with two species. The distance between species might explain the differential patterns, in McKee et al. (1988) was over short distances (≤ 1 m) and in the present study was over longer distances (5-22 m). These results indicated that the superposition of roots in our experimental design does not seem occurred. Nevertheless, the Eh values measured here were higher than those reported for McKee et al. (1988) and for Twin Cays in the Bahamas (Nickerson and Thibodeau, 1985) for

the same depth in mangrove substrates. The range of values obtained for sulphide concentrations (0.4-3.7 µM) were considerably lower. The reason for the lack of agreement between these studies with respect to S^{2-} is the different sulphide species analyzed, total soluble sulphide (H_2S, HS^-, S^{2-}) and H_2S values, respectively.

Across the topographically different plains, the finding beneath *Avicennia* forest stands (HP) of less reducing sediments, reflects well-drained sediments exposed to low IF, because the submergence results in a reduced state (Ponnamperuma, 1972) **(Fig. 14**). At the small-scale discontinuities in the topographic gradient (e.g. depressions), coincident with the transition between monoespecific stands, the hydrological effect was extremely evident due the increase of water residence time. Similarly to LP, where due to higher IF the water remains constant.

The present findings revealed for intense reduced sediments (LP) a significant greater root-induced oxidation capacity in *A. germinans* (ΔEh_{12}=193 mV) (**Fig. 14**). This result is in accordance with previous observations made by Nickerson and Thibodeau (1985), McKee et al. (1988), Andersen and Kristensen (1988) and Alongi et al. (2000). For low reduced sediments (HP) the species-specific oxidation was also higher in *Avicennia* (ΔEh_2= 139 mV) (**Fig. 14**). For instance, Kludze and DeLaune (1995) reported for rice field a high correlation between root radial oxidation loss (ROL) rates and sediment Eh intensity, where a higher ROL in reduced sediment occurred. The term ROL was proposed by Scholander et al. (1955) and defined by Colmer et al. (1998), Armstrong et al. (2000), and De Simone et al. (2002). Other studies in mangrove (Youssef and Saenger, 1996) and non-mangrove wetland species (Justin and Armstrong, 1987; Koncalová, 1990), observed a little effect of the degree of substrate aeration on root anatomy or aerenchyma development. In a seedling stage *Avicennia* roots are more porous than *Rhizophora*, this root porosity (POR) is related to the air space in the aerenchyma. The changes in POR and ROL in *A. germinans* can compensate for substrate changes associated with acid-sulphide sediments (Youssef and Saenger, 1996). However the lower but constant oxidation of *R. mangle* along the transect was only weakly affected by the different substrate conditions (**Fig. 14**),

consistent with data on this genus reported by McKee (1996), Youssef and Saenger (1996), and Ellison and Farnsworth (1997).

6.2.3. Redox stratification and pH pattern

Redox potential values of the vertical profiles agree with the stratification model described by Clark et al. (1998) (**Fig. 14**). The thickness of the UOZ, depend upon the balance between the rate of O_2 diffusion into the soil and the rate of O_2 consumption (Howeler and Bouldin, 1971). Soils with high OM content tend to have a high microbial respiration and consequently a thin UOZ (House, 2003). At the study area, the HP was characterized by an UOZ thickness of ~5 cm, as indicative of sediments with low biological heterotrophic activity. At MP and LP, the UOZ thickness depleted (1-3 cm), suggesting a greater biological heterotrophic activity, principally at D1 and D2 (~1 cm) coincident with the second vertical P trend (**Fig. 17**). Below UOZ, the URZ was restricted to a thin layer (≤ 10 cm depth). A deeper URZ (≤ 15 cm depth) was reported by Clark et al. (1998) also during rainy season. At Bragança, the LOZ merge for 10-35 cm depth, suggesting a maximum root activity and the outward diffusion of oxygen. This LOZ was lower than other mangrove below-ground root systems extended to 50 cm depth (Komiyama *et al*., 1987; Alongi *et al*., 2004).

The vertical pH distribution revealed two patterns, one varying as a function of the redox stratification model and a second displaying one monotonous smooth acid distribution centered around 6.7 (**Fig. 14**). In the first pattern, the tidal supply seawater of basic cations at UOZ and URZ contributes to an increase in pH (pH > 7.0). At LOZ the pH fall (pH = 7.0) exhibited a link with the redox increase. This pH depletion trend is probably the result of 1) H^+ generated by oxidation of Fe^{2+} (**Equation 1**, Beeg *et al*., 1994) and/or FeS_2 (**Equation 7a, 7b**, Kirk, 2004) by root released O_2, and/or 2) H^+ released from the roots to balance excess intake of cations over anions (Haynes, 1990). Concerning the second pattern, the acidic values seem to be derived from both organic decay and sulphur oxidation (Marchand *et al*., 2004). The pH values are in the range (4.5-7.5) reported by Schwendenmann (1998) for pore-water surface sediments at Furo do Chato creek, Bragança Peninsula. Additionally, previous studies of mangroves sediments indicated a seasonal shift with sediments

being more acidic in the wet season (Alongi *et al*., 1999; Marchand *et al*., 2004; Alongi *et al*., 2004).

6.2.4. Inundation frequency and availability of phosphorus

This study clearly documents that the phosphorus status at the sediments is directly correlated to the IF. Across the three floodplains, the decrease pattern of tot.-P with increasing topographic elevation (**Tab. 3**), was similar to the pattern found for the Australian mangroves studied by Boto and Wellington (1984). The tot.-P data, with exception of the depressions, are within the ranges previously reported for the upland and seaward sectors of the Bragança Peninsula (Medina *et al.*, 2001) and for the same study area (Reise, 2003). At the LP, our higher tot.-P value (1.58 mg P g^{-1} DW) is in the range of Sierra Leone (Hesse, 1961).

The effect of the IF on the dynamic behaviour of extr.-P was confirmed by a significant positive correlation. This pool fits very well with leaf-P for the same study area, showing also a significant positive correlation with the IF ($r = 0.86$, $n=33$, $p<0.005$) (Cordeiro *et al*., 2003) (**Fig. 16**). This effect was attributed to the solubility of P-Fe/Al brought by reducing conditions (Shapiro, 1958). The general low P status in sediments reported for the same species in Sierra Leone by Hesse (1961) and for the Australian mangrove by Boto and Wellington (1984), both used the similar phosphate extraction medium, reflecting the same dependency on the inundation gradient. Recent results for Micronesia reported also low P status (Gleason *et al*., 2003). Our high values, support the abundant plant-available P detected for sediments of tropical lowland evergreen rain forest and dry land forest (terra firme) of the Bragança Peninsula (Frizano *et al*., 2003).

Based on the fractionation analysis, the percentage of calculated inorg.-P accounts for the larger fraction dominated by P-Fe/Al (**Tab. 3**). These results are analogous for a low plain in Combu Island at the Amazon reported by Silva and Sampaio (1998) using the same methodology, but considerable higher as the values (*ca* 55 %) reported by Fabre et al. (1999) for French Guiana. The inorg.-P data suggests that P-Fe/Al is the main insoluble P compound present at the sediments in all parcels. These high results might be caused under tropical climate. The strong chemical weathering of the

lateritic source area supply oxidized particles (Fe(hydr)oxides), besides in water dissolved chemical components (aluminium complexes), that are transported and deposited partly as mangrove muddy sediment and/or transported to the ocean (Costa *et al*., 2004b).

6.2.5. Effect of flooding on P-exchange

Previous hydrological studies on a Caeté tidal creek, suggested that the inundation may influence the chemical reactions involved in the retention and release of P presumably pH-dependent (Cohen *et al*., 2004). At this creek, the basic pH range of the flooding water (7.2-7.9) registered by Cohen et al. (2004), can potentially precipitate P as Ca-phosphate minerals (Diaz *et al*., 1994; Dorozhkin, 2002). For the P-Ca crystallization in seawater, longer periods of time (8-20 month) will be needed (Gulbrandsen *et al*., 1984), and the presence of significant calcium (Ca^{2+}) and magnesium (Mg^{2+}) levels is determinant (Brown, 1981; Yadav *et al*., 1984), the latter masking the adsorption sites on apatite (Martens and Harriss, 1970; Wang *et al*., 1995). Additionally, effective P removal (60 %) from surface waters due to precipitation, requires Ca^{2+} concentration of >100 $mg.l^{-1}$ at pH >8 (Diaz *et al*., 1994). Previous works at Bragança Peninsula, reported pore-water levels of Mg^{2+} (1062-3124 $mg.l^{-1}$) in one order of magnitude than those of Ca^{2+} (269-1176 $mg.l^{-1}$) (Furtado da Costa, 2000), suggesting an inhibitory effect of Mg^{2+} on apatite.

At HP, the surface (5-10 cm) sediments with low react.-Ca content and slightly acidic to neutral pH (6.5-7.4) values, showed low precipitation of P-Ca reflected in higher Ca : P-Ca ratios (9-12) (**Tab. 4).** Any precipitate formed and settled on the sediment surface could also be rapidly solubilised, due the slightly acidic to neutral nature of this plain. These intermittently flooded sediments, shift to extreme basic conditions (13.3) during flooding periods, suggesting the formation of P-Ca (**Fig. 11**). However, by considering the relative duration of inundation (2-3.5 h), longer reactions periods may be needed to form more stable Ca-phosphate minerals. The calcium phosphates phases Amorphous Calcium Phosphate (ACP), Dicalcium Phosphate Dehydrate (DCPD) and occasionally Anhydrous Dicalcium Phosphate (DCPA), are the initial reaction products of P with $CaCO_3$ (Freeman and Rowell, 1981). Bell and Black

(1970) found that DCPD changed to Octacalcium Phosphate (OCP), thermodynamically more stable mineral, within 44 weeks in slightly acidic to alkaline (6.9-7.9) sediments. Murrmann and Peech (1969) reported sediment extracts to which a constant $Ca(OH)_2$ had been added, displaying a value about pH 8.5, nearly in equilibrium with OCP after 108 h. Thus, in LP higher P-Ca concentrations and thence lower Ca : P-Ca ratios (4-8) (**Tab. 4**), reflected longer time of maximum pH (>8) following each inundation, where freshly P-Ca are formed and these later reorder to more crystalline forms (Kirk, 2004).

At LP, Al and Fe phosphates, which are presumably the dominant forms of P minerals in high plains (Silva and Sampaio, 1998), increased concomitant with Eh depletion in moderately acidic to neutral pH (6.6-7.2) values, reflected by lower Fe : P-Fe/Al (60-95) and Al : P-Fe/Al (52-93) ratios (**Tab 4**). Besides, anoxic conditions provided a release of extr.-P associated with Fe and Al (hydro)oxides resulting in negative correlations with their ratios. These data support the early hypothesis of Patrick and Khalid (1974) and Khalid et al. (1977) that anaerobic sediments released more P to solution and sorbed more P from solution than did aerobic sediments. These authors suggested a greater surface area of the gel-like reduced ferrous compounds in anaerobic sediments resulting in more solubilisation and sorption. In intermittently flooded sediments, Huguenin-Elie et al. (2003) suggests that in reducing conditions following submergence the labile P in sediments increase, though with prolonged flooding the P became re-immobilized and in the sub-sequent drying the re-oxidation of reduced compounds immobilize P.

The higher significant negative correlation between extr.-P and Al : P-Fe/Al ratio, suggest that the aluminium phosphate fraction seems to be the most significant fraction in controlling the P concentration in sediments solution. Thus, this P control is reasonable to assume due 1) the terrigenous signature (laterites) of the source area (Aluminium complexes) (Costa *et al*., 2004b), and 2) the metal reactivity expressed as a decrease in logarithmic solubility potential (Ksp) in the order $Al(OH)_3$ (33.5) > $Fe(OH)_3$ (38.8) > $FeOOH(\alpha)$ (41.5) > $Fe_2O_3(\alpha)$ (42.7) > $Ca_5(PO_4)_3OH$ (55.6) at 25^oC and in ionic strength cero (Libes, 1992; Butler, 1998), the lack of Ksp data for marine

systems do not support this hypothesis. Concerning intermittently flooded sediments, Murrmann and Peech (1969) described the labile P increase with varying pH (4-10) involving the dissolution of Al (hydr)oxides containing occluded P. Inasmuch as P is adsorbed by Al (hydr)oxides, it is likely that P becomes distributed throughout the (hydr)oxides structure during the repeated dissolution re-precipitation process.

The solubility of Al and Fe phosphates decreases at lower pH, directly opposite to the solubility of calcium phosphates. Therefore, P is most available around pH 6.5 (Havlin *et al*., 1999) and pH 5-6 (Georgantas and Grigoropoulou, 2006). At lower pH levels, P retention is high due to P-Fe/Al precipitation, and at higher pH levels due to P-Ca minerals precipitation. On the other hand, aluminium is efficient in trapping P in a wider pH range (4-7) and when water pH is above 8 aluminium become soluble ($Al(OH)_4^-$) (Georgantas and Grigoropoulou, 2006). Across the transect, in surface sediments with a pH range for 6.5-7.5 we expect P availability to be relative high. Before submergence, neither sediment react.-Ca, Ca : P-Ca ratio nor P-Ca seemed to influence the release of extr.-P from sediment, supporting that adsorption of Ca^{2+} is of minor importance when Al(hydr)oxides and amorphous FeOOH is present (Golterman, 1988). As the pH increases during flooding periods, Al and Fe species in the soluble form being negatively charged cannot trapping P successfully, suggesting the formation of instable calcium phosphate phases due the limited inundation time.

6.2.6. Effect of redox stratification on P-exchange

The present study indicated that stands of *R. mangle* and *A. germinans* differs in their responses to low sediment Eh conditions and such differences may be partially explained by the distribution pattern along the transect and the species-specific oxidation ability.

In fact, the greater sensitivity of *A. germinans* to low Eh conditions was reflected on P compounds (**Fig. 17**). As above-mentioned, under anoxic conditions there is a flush of easily extr.-P attributed to solubility of P-Fe/Al brought by reduction (Shapiro, 1958). Below *A. germinans* (feature 1), the intense root-induced oxidation re-immobilized the extr.-P by increase of P-Fe/Al, tot.-P and acidification. At D2, this acidification

caused the dissolution of acid-soluble P (P-Ca). But countering this, the freshly precipitated ferric hydroxid formed by Fe^{2+} oxidation would have a large P sorbing capacity (Saleque and Kirk, 1995).

Beneath *R. mangle* (feature 2), occurred the diminution of the root-oxidation accompanied by the depletion of tot.-P and P-Fe/Al pools. The reduction of P-Fe/Al pool was reflected in an extreme increase of extr.-P. Concomitant with this extr.-P increase, the P-Ca was maintained stable or in some cases increased, probably due the basic pH caused by the reduction, suggesting the re-immobilization of P by the carbonates pool.

The diffuse supply of P to roots would therefore depend on the balance between increased sorption on ferric hydroxide and increased release from acid-soluble forms (Saleque *et al.*, 1995). The vertical profiles elucidated the extr.-P behavior in the horizontal profile (**Fig. 16**). Here, the inversion of the extr.-P curve at MP, suggest that the higher root-induced oxidation in *A. germinans* limited the availability of P and consequently their distribution. Thus, the adaptive response of *R. mangle* to nutrient uptake in water-logging could contribute to its dominance in low plain.

CHAPTER 7

DYNAMICS OF SULPHUR IN MANGROVE SEDIMENT

7.1. Results

7.1.1. Substrate characteristics: organic matter, salinity, granulometry, Eh and pH.

The sediments at the high plain (HP) were characterized by a silt and clay content of 96-98 %, this amount decreased along the transect to 90-97 % at the *Rhizophora*-forest in the low plain (LP), probably due to tidal effects on the sediments granulometry. HP was inundated on average 51 ± 13 days/year and remained continuously air-exposed during neap tides, whereas LP was inundated on average 146 ± 13 days/year, with the latter exposed to tidal currents. At the boundaries between both HP and LP, and the middle plain (MP), slightly depressions of 5-8 cm depth occurred, which appear to be remains of a paleo-channel identified as depression one (D1) and two (D2).

The salinities differed spatially among HP and LP, varying from 43.7 ± 16 $^{o}/_{oo}$ to 34.6 ± 10 $^{o}/_{oo}$ (n = 47), respectively (**Tab. 5**). Salinity data have been plotted in contour plots along the transect (**Fig. 21** (b)). In the surface layer, the iso-lines 20 $^{o}/_{oo}$ were discontinuous, due to the influence of sub-surface layers with higher salinity (30 $^{o}/_{oo}$). In the *Avicennia*-forest (HP), the salinity iso-lines distribution showed a strong gradient with depth, resulting in a profile with higher stratification. Conversely, at LP, being permanently under tidal influence, the salinity iso-lines 20-40 $^{o}/_{oo}$ sharply deepened into the *Rhizophora*-forest toward the estuary, characterized by sediments with low stratification.

The sedimentary organic matter (OM) ranged between 4 to 13 % with no systematic trend along the transect (**Tab. 5**). At HP, higher OM contents in the top 10-cm-thick layer (13 %) decreased (6 %) at 100 cm. At LP, the decrease was only moderate (4.1-3.8 %). At D1, the OM content was determined only below *R. mangle*, whereas at D2 below both species, characterized by an average of 3.5 ± 1.1 % (n=7) and 4.9 ± 0.8 % (n=11), respectively.

Redox potential (Eh) and pH iso-lines are presented in Figure 18, with the stations arranged with respect to an increasing inundation gradient. In this figure, the redox stratification model proposed by Clark et al. (1998) related to the oxidation and reduction zones, becomes not evidenced. The Eh pattern was higher (200 mV) in *Avicennia*-forest (HP) than in *Rhizophora*-forest (0-100 mV) (LP) (**Fig. 18** (a)). Examination of the depressions (D1, D2) revealed two oxic-anoxic interfaces: 1) Eh = 0-150 mV at HP; and 2) Eh = 0-50 mV at LP. These sectors agree both with the physical separation between the plains, the functional causes have to evaluated. Additionally, the pH range was 6.3-7.5, showing slightly basic values in HP and MP, and slightly acidic values in LP (**Fig. 18** (b)).

Table 5: Physical and chemical parameters in surface (10 cm), middle (15-35 cm) and deep (45-100 cm) sediment samples across a tidal gradient. C:N slope refers to the ratios calculated through the inclination (b=slope) of regression lines in Figure 20. Mean values ($\bar{x}$) and standard deviation (SD).[a]

Parameters	n	Depth (cm)	HP	D1	MP	D2	LP
IF (days/year)	1-4	-	41 - 62	67	80 - 101	124	128 - 162
Salinity ($^{o}/_{oo}$)	6-10	0-10	20 ± 2	27 ± 6	28 ± 11	26 ± 7	24 ± 7
	10-20	15-35	38 ± 9	37 ± 9	40 ± 9	34 ± 6	33 ± 8
	10-20	45-100	55 ± 16	53 ± 9	49 ± 8	38 ± 4	44 ± 7
OM (%)	6-10	0-10	12.9 ± 1.7	3.8 ± 1.8	6.9 ± 0.2	-	4.1 ± 1.3
	10-20	15-35	5.8 ± 2.7	3.7 ± 0.7	6.6 ± 0.8	6.1 ± 1.7	4.0 ± 0.8
	10-20	45-100	5.7 ± 1.7	3.0 ± 1.3	3.9 ± 1.5	4.8 ± 0.9	3.8 ± 1.1
C:N (mol/mol)	6-10	0-10	15 ± 1	17 ± 1	18 ± 2	16 ± 0	17 ± 3
	10-20	15-35	15 ± 3	15 ± 3	18 ± 2	16 ± 3	16 ± 3
	10-20	45-100	15 ± 2	16 ± 4	19 ± 3	17 ± 1	18 ± 2
C:N	9-12	5-15 Rhi	14	-	-	-	21
b = slope	9-13	5-15 Avi	15	-	-	-	25

[a] Abbreviations: n, number of samples; HP, high plain; D1, depression 1; MP, middle plain; D2, depression 2; LP, low plain; OM, organic matter; C:N, molar C:N ratio; Rhi, *R. mangle*; Avi, *A. germinans*.

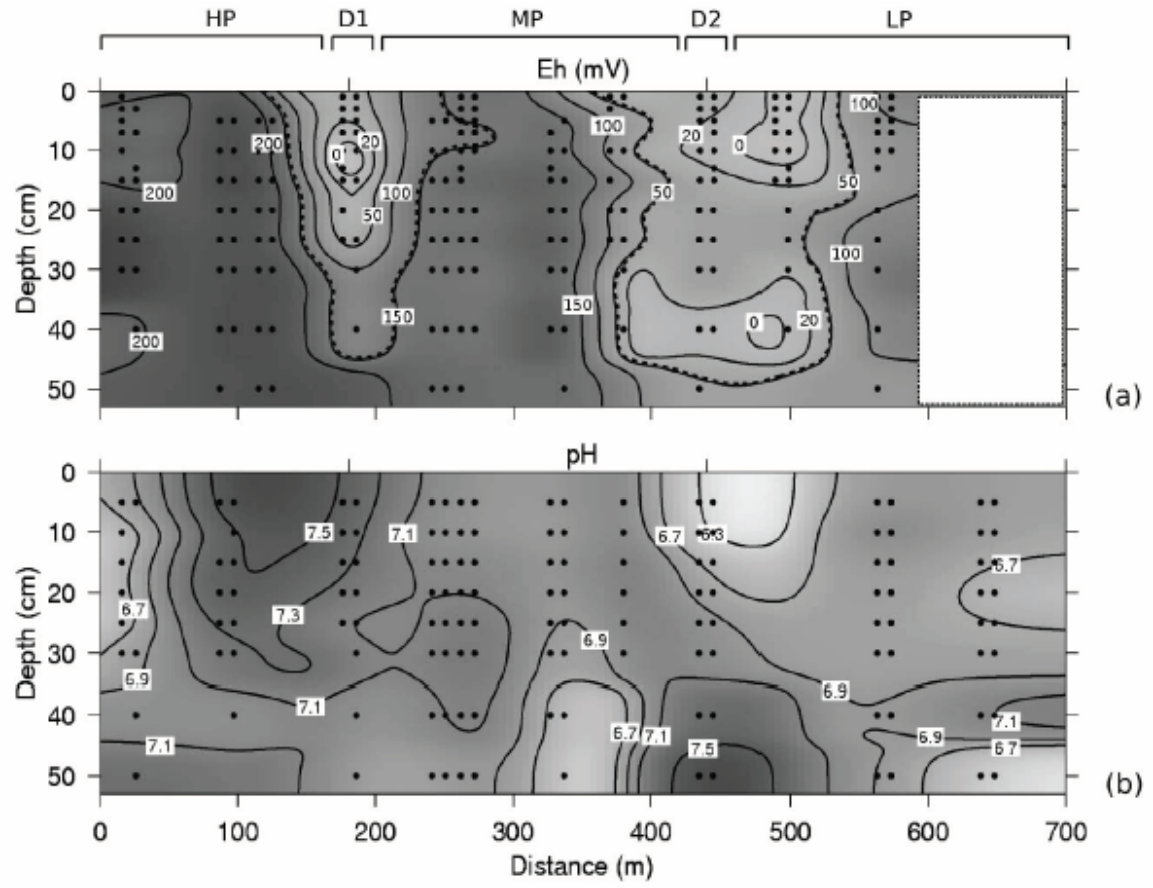

Figure 18: (**a**) Lateral view of Eh, (**b**) Lateral view of pH, both measured in sediments.

7.1.2. Elemental composition and ratios

The elemental composition considered the sediment below each species separately, due to their chemical differences. The organic carbon (org.-C) and total nitrogen (tot.-N) exhibited a wide range between 0.82-3.24 wt % and 0.09-0.22 wt %, respectively. The down core distribution of org.-C and tot.-N below *R. mangle* and *A. germinans* was examined in detail (**Fig. 19**). At HP, for both species, org.-C decrease from the surface to 50 cm depth increasing in deeper substrate (100 cm),whereas tot.-N showed a decreasing trend from the surface to 100 cm deep (**Fig. 19**). At LP, the org.-C down core profile differed among species in the upper 10-cm-thick layer with highest concentrations below *R. mangle* in comparison to *A. germinans*. At the middle layers (15-50 cm), both species showed a pronounced org.-C increase. Conversely, tot.-N below *A. germinans* was maintained higher in the upper 15-cm-thick layer, in relation to *R. mangle*, which showed a smooth decrease with depth; below *R. mangle* a uniform feature with slightly increase with depth occurred.

The molar C:N ratios showed lower values in HP (15 ± 2, n=46) in comparison to LP (17 ± 3, n= 45), this difference was not significant (**Tab. 5**). At HP, the C:N ratio remained almost stable, whereas at LP increased with sediment depth. To confirm the C:N difference between both plains and to attenuate the effect of outliers, the C:N ratios for surface sediments (5-15 cm) were calculated on the basis of the inclination (e.g. slope) of the regression line **(Fig. 20** (a), **Tab. 5**). A significant correlation between org.-C and tot.-N in *A. germinans*- (HP, r=0.95; LP, r=0.94, n=9, $p<0.05$) and *R. mangle*-dominated sediments (HP, r=0.86; LP, r=0.88, n=11, $p<0.05$) occurred. The slopes of the regression lines confirmed lower values in HP in comparison to LP and also showed lower C:N values below *R. magle* in relation to *A. germinans* (**Tab. 5**). Additionally, at intermediary layers (25-50 cm) the molar C:N ratio correlated significantly with Eh which was negatively related (HP, r=-0.74; LP, r= -0.74, n=11-19, $p<0.05$), showing that in intermediary layers the reducing environments are those with highest C:N values, whereas the environments with positive Eh record the lowest C:N values (**Fig. 20** (b)).

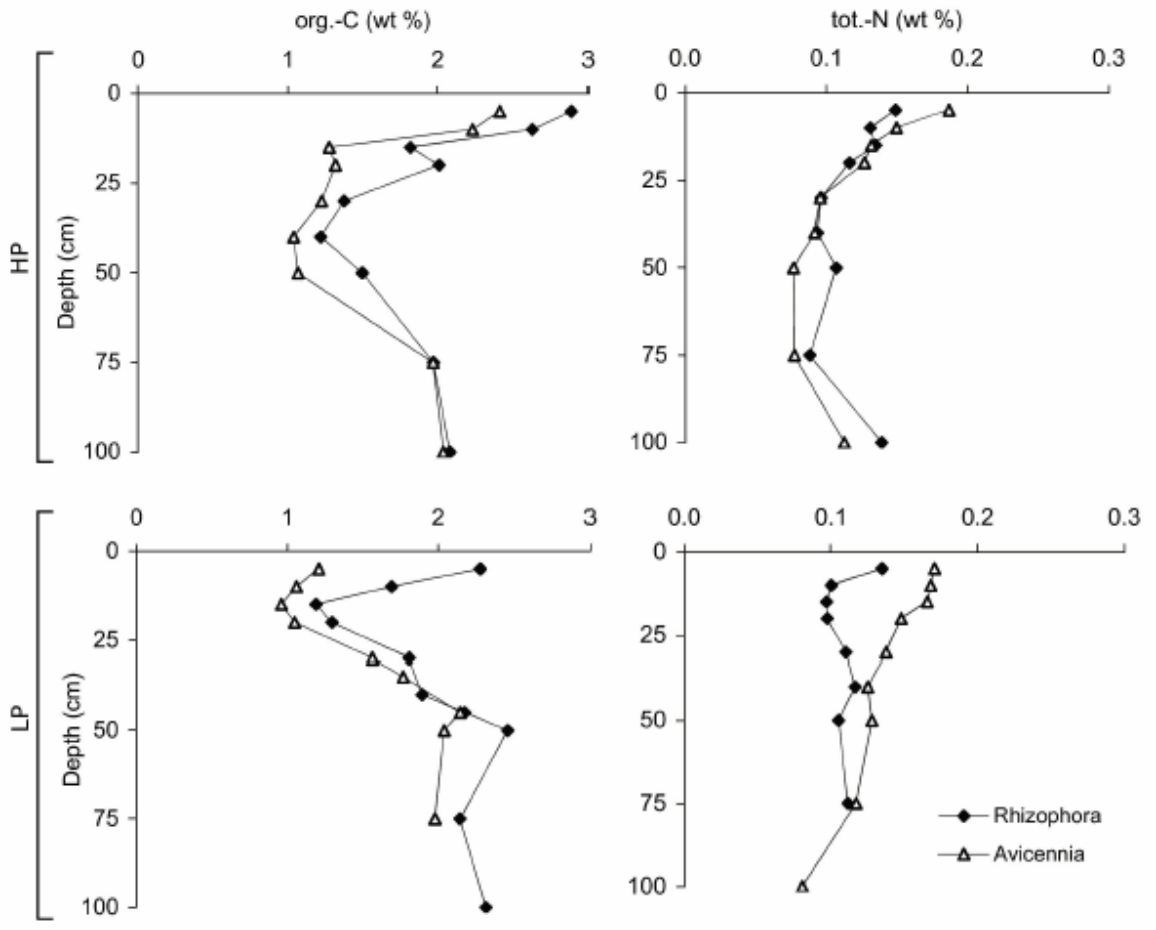

Figure 19: Concentration (wt%) versus depth profiles of organic carbon (org.-C) and total nitrogen (tot.-N) below *R. mangle* and *A. germinans* at high- (HP) and low-plain (LP).

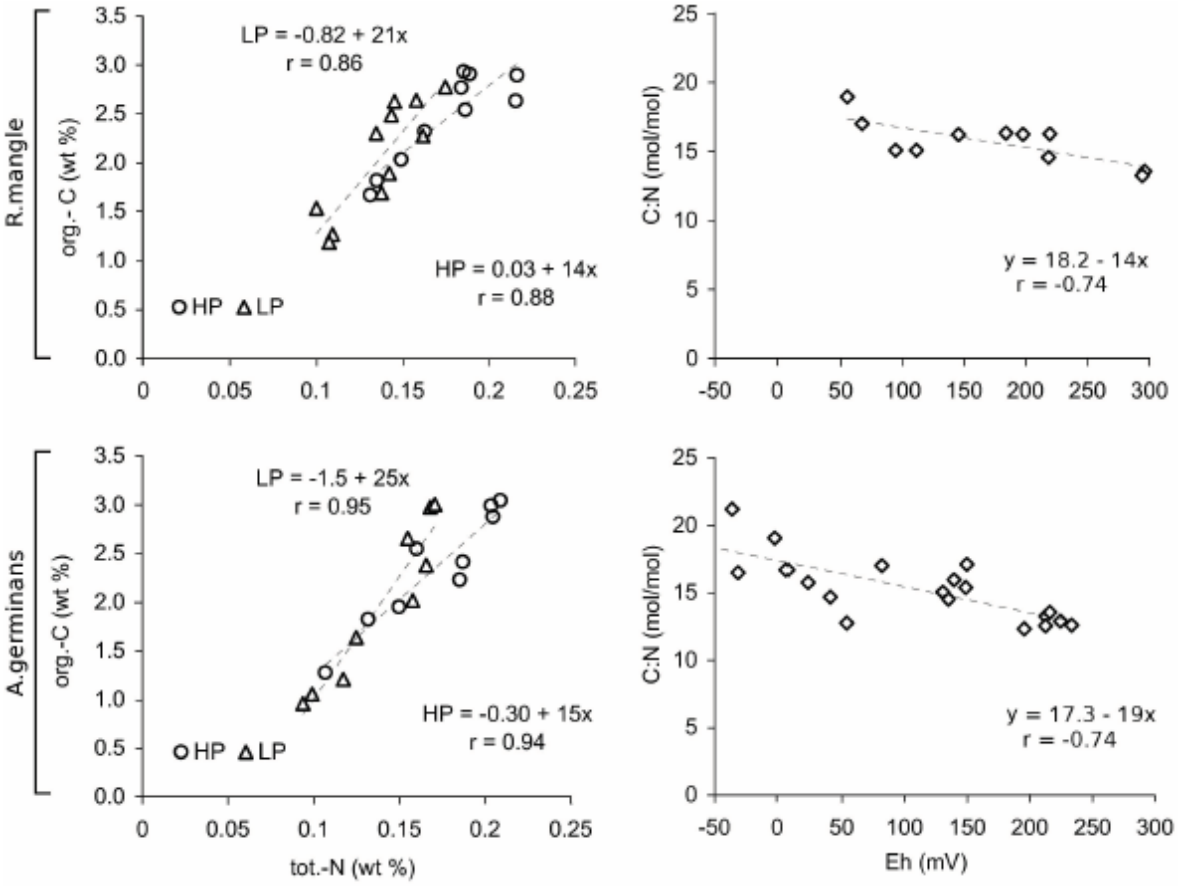

Figure 20: Relation between the organic carbon (wt %) and nitrogen contents (wt %) of Bragança sediments. The line represents a least-square with a slope corresponding with a molar C:N of 15.7 ± 2.3 and 17.2 ± 2.8 below *R. mangle* and *A. germinans*, respectively. C:N molar ratio vs. redox potential (Eh). HP, high plain; LP, low plain; D1, depression 1.

7.1.3. Sulphur pools

The horizontal profile of sulphide concentrations (20-25 cm), and the iso-lines for salinity, sulphate (SO_4^{2-}) and the percentage of expected concentration (PEC) of SO_4^{2-} are presented in Figure 21. In this figure the stations are arranged with respect to an increasing inundation gradient.

At D1 and MP, sediments have higher sulphide concentrations (10-47 μM) than those for HP and LP below the detection limit (<1 μM) (**Fig. 21** (a)). At MP, below *A. germinans*, sulphide reached higher concentrations (34-47 μM), compared to the extreme lower concentrations (<4 μM) below *R. mangle*. Here, the sulphide increase was concomitant with the lowest SO_4^{2-} concentrations (5 mM) and PEC (30 %) values of the transect (**Fig. 21** (c)(d)).

In general, SO_4^{2-} concentrations reflected the changes in salinity (i.e. source) across the transect (**Fig. 21** (b)(c)). At HP, a sharp SO_4^{2-} gradient with depth was coincident with high salinity stratification, whereas at LP, the SO_4^{2-} iso-lines 10-15 mM enters deeper into the more inundated a rea, similar as the salinity for the same plain. If exist a conservative behaviour it will be expected a high significant correlation between salinity and SO_4^{2-}, although a close to significant correlation ($r=0.70$, $n=143$, $p<0.05$), several deviations occurred. An evident deviation is found for MP, where the low SO_4^{2-} iso-lines 5-15 mM enter into deeper layers, differing for the salinity iso-lines pattern.

Salinity, considered as a conservative parameter (biologically and chemically non-reactive), was used as a tracer to determine whether decrease in SO_4^{2-} concentrations were due to either hydrological or biological and chemical processes (Madureira *et al*., 1997; Sherman *et al*., 1998; Cohen *et al*., 1999). In the present study, the percentage of expected concentration (PEC) of SO_4^{2-} showed most values below 100 % indicating that the sediment contains a lower amount of SO_4^{2-} as would be expected for a given salinity, suggesting biological uptake, reduction, sorption and/or precipitation processes (**Fig. 21** (d)). The absence of PEC values above 100 % indicate the lack of SO_4^{2-} input from other sources beyond seawater or net re-

oxidation processes. At MP, the PEC decreased sharply, indicating a loss (65-70 %) in SO_4^{2-} relative to salinity across the 30 to 60-cm thick layer. In contrast, at LP, the PEC increased attesting a lower SO_4^{2-} loss (35-40 %) in 30 to 80-cm thick layer.

To elucidate if the difference in the sulphur pools in sediment status among the forest types is a function of tree species or differences in tidal elevation, the down core distribution of the sulphur pools and associated parameters for two intermediate stations at HP and LP were examined. At HP (**Fig. 22** (a)), a different picture was obtained for water content between the species, where *A. germinans* displayed a subsurface (5-15 cm) water content maximum in relation to *R. mangle*. The salinity and SO_4^{2-} distribution, similarly as the humidity, increased with depth. Below *A. germinans*, at 5 to 15 cm thick layer, the PEC depletion (50-36 %) point out lower SO_4^{2-} values in relation to salinity. In addition, below *A. germinans*, the reactive iron (react.-Fe) profile was characterized by a subsurface depletion at 5-15 cm depth concomitant with a DOP increase (45-52 %), which indicated the iron sulphide formation trough the reaction of sulphide with react.-Fe. At LP (**Fig. 22** (b)), below *A. germinans* the water content displayed a deep (50 cm) maximum, in comparison to the subsurface maximum at HP for the same species. Here, PEC values (100 %) below *A. germinans* evidenced the maximum SO_4^{2-} value in relation to salinity, suggesting a continuous supply of SO_4^{2}. The highest DOP values in the lower part of the profile (50-100 cm), coincided with the react.-Fe depletion, indicating reduction processes.

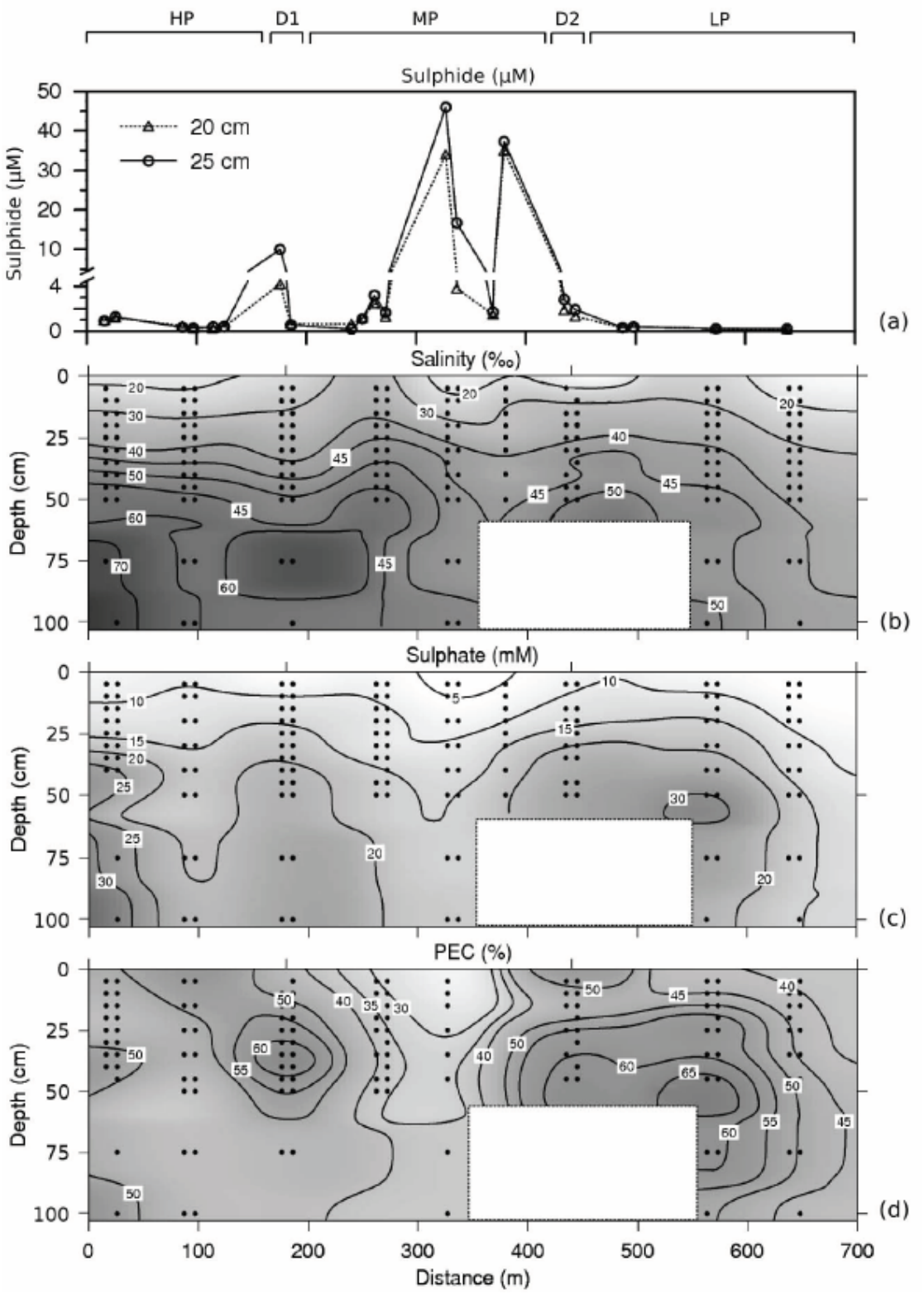

Figure 21: (**a**) Horizontal sediment profile of sulphide at 20-25 cm depth. Lateral transects of iso-lines for sediment pore-water data of (**b**) salinity (**c**) sulphate and (**d**) percentage of expected concentration (PEC). HP, high plain; D1; MP, middle plain; LP, low plain; depressions (D1, D2).

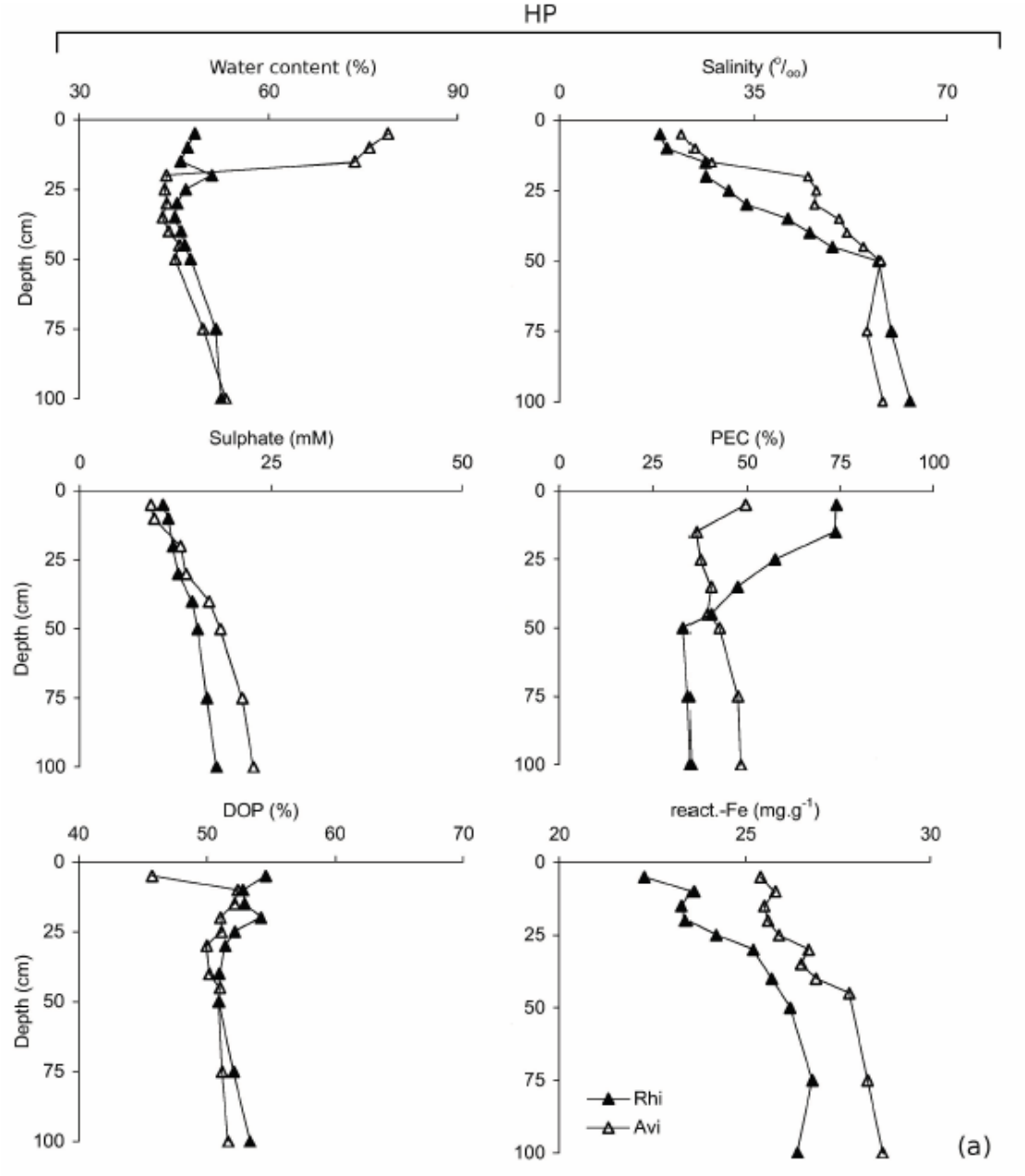

Figure 22: Vertical profiles of sediment water content, salinity, sulphate, percentage of expected concentration (PEC), degree of pyritization (DOP) and reactive iron (react.-Fe). (**a**) HP, high plain, (**b**) LP, low plain.

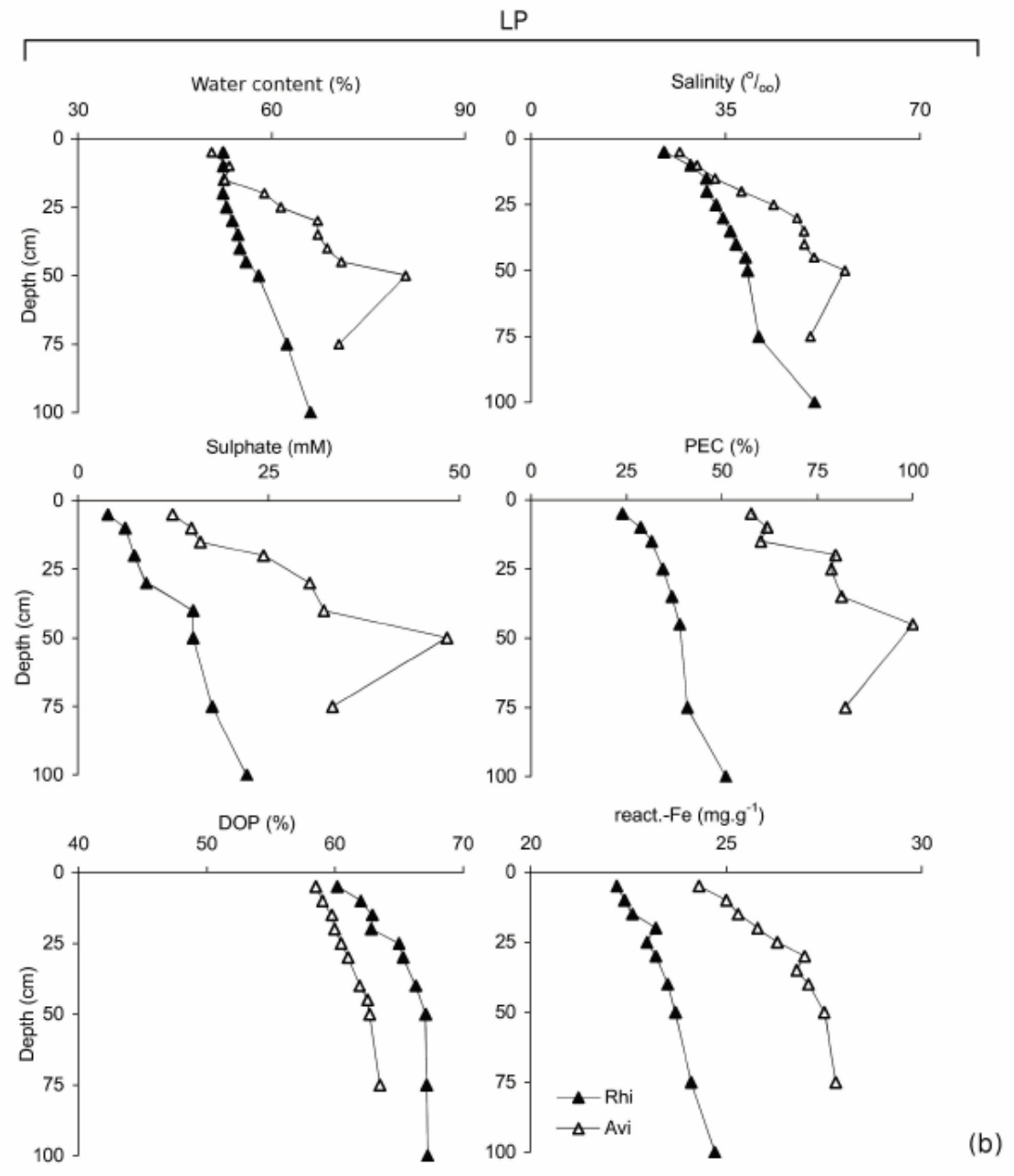

Continuation Figure 22

7.1.4. Iron pool and pyrite morphologies

The react.-Fe was characterized by minimum and maximum concentrations occurring at the surface and deep sediments, respectively (**Fig 23** (a)). At surface layers (D2, LP), the react.-Fe decreased (22.5 $mg.g^{-1}$) concomitant with an oxic-anoxic interface at redox potential Eh of 0 mV (**Fig 23** (a), **Fig. 18** (a)). At deep layers, react.-Fe decreased from 35 $mg.g^{-1}$ (MP) to 25 $mg.g^{-1}$ at the inland (HP).

Measuring react.-Fe and pyrite iron (Pyr.-Fe), the degree of pyritization (DOP) was used to determine whether Fe availability limited pyrite formation (Berner, 1970). DOP is a measure of completeness of the reaction of this react.-Fe (Fe III) with aqueous sulphide (Lenventhal and Taylor, 1990). Over the first 100 m of the transect (HP), the DOP was 52 ± 2 % indicating that less than half (48 %) of the remaining react.-Fe could be potentially sulphidized (**Fig. 23** (b)). At D1, the DOP increased to 55 ± 1 %, than decreased to 51 ± 3 % at MP. At LP, a pronounced increase for 61 ± 3 % occurred, which indicates that about 38 % of the total iron pool was still available potentially for pyrite formation.

The pyrite presence was confirmed through scanning electron microscope analyses (SEM-EDX). Pyrite grains were hard to locate below the interface sediment-water (<5 cm); they were restricted to the medium (10-25 cm) and deep (40-100 cm) layers in the vertical profiles. The single pyrite grains in the mangrove sediments average a mean diameter of 1.2 µm. Two range of pyrite grains were identified: 1) 0.6-2.3 µm-size at medium layers (**Fig. 24** (a)(b)), and 2) 0.8-4.1 µm-size at deep layers. Framboids morphology ranging in size from 2.7 to 21.5 µm-size with a mean diameter 7.4 µm, dominated in the reducing sediments at greater depths (40-100 cm). At LP, below *R. mangle* (100 cm), the framboids clustered in a diatom (45 µm-size) (**Fig. 24** (c)) and an octahedral crystal (5.2 µm-size) were observed (**Fig. 24** (d)). The latter textures were concomitant with the highest DOP value (67 %) at 100 cm depth (**Fig. 22** (b)).

In order to asses the reducing conditions with respect to pyrite framboid formation (Wilkin *et al*., 1996), a survey on the number of microcrystals (Nm) in framboids

along a topographic gradient was made (**Fig. 25**). Because the sample mounts represent a random cut of the sediment sample, the measured distributions are only an approximation of the true distribution. Individual framboids from sediments of the Bragança Peninsula contain less than 100 microcrystals arranged in a decreased gradient from LP to the inland (HP), indicating that the factors controlling framboid growth are different in the plains.

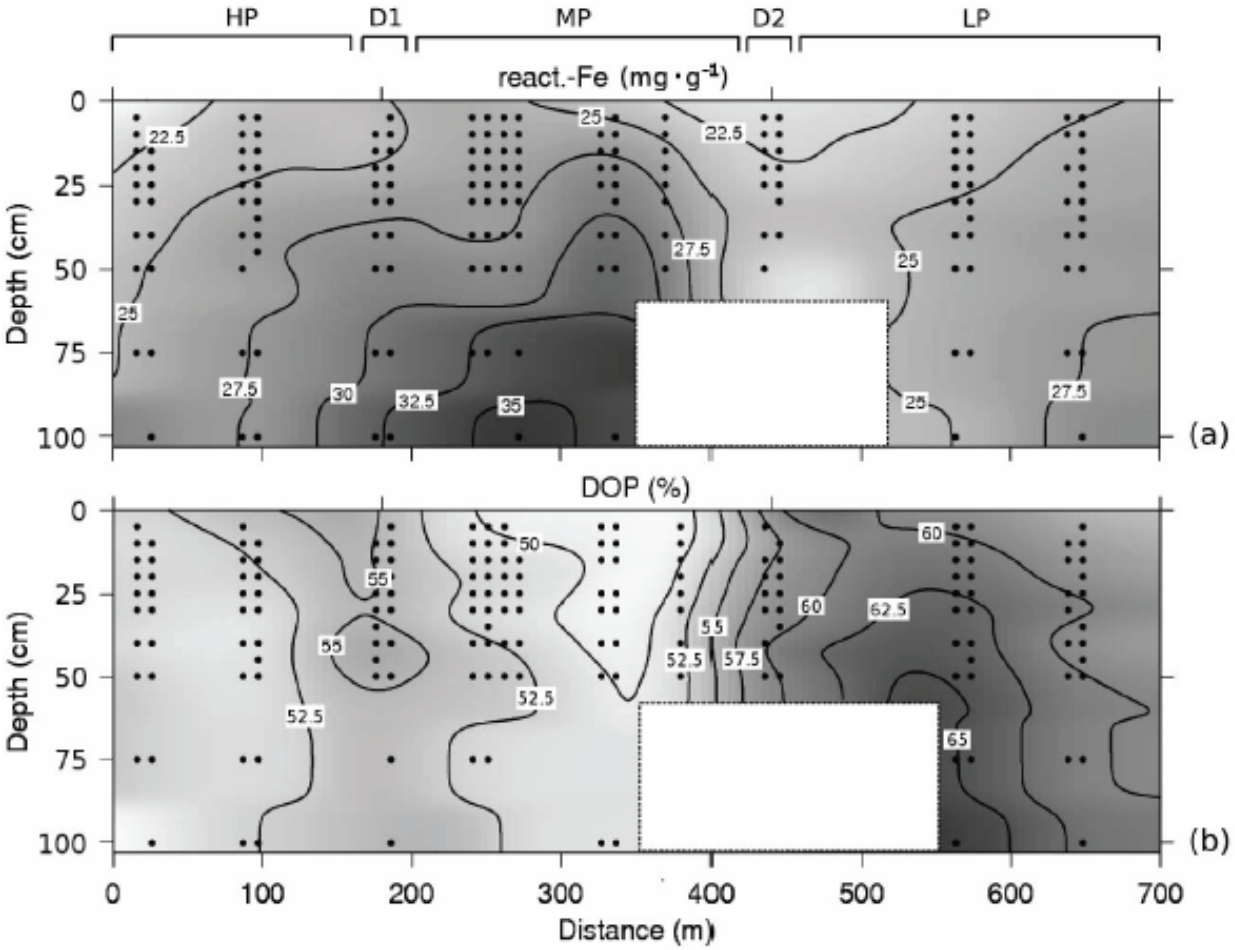

Figure 23: Lateral transect of iso-lines sediment data for (**a**) reactive iron (react.-Fe) and (**b**) degree of pyritization (DOP). HP, high plain; D1; MP, middle plain; LP, low plain; depressions (D1, D2).

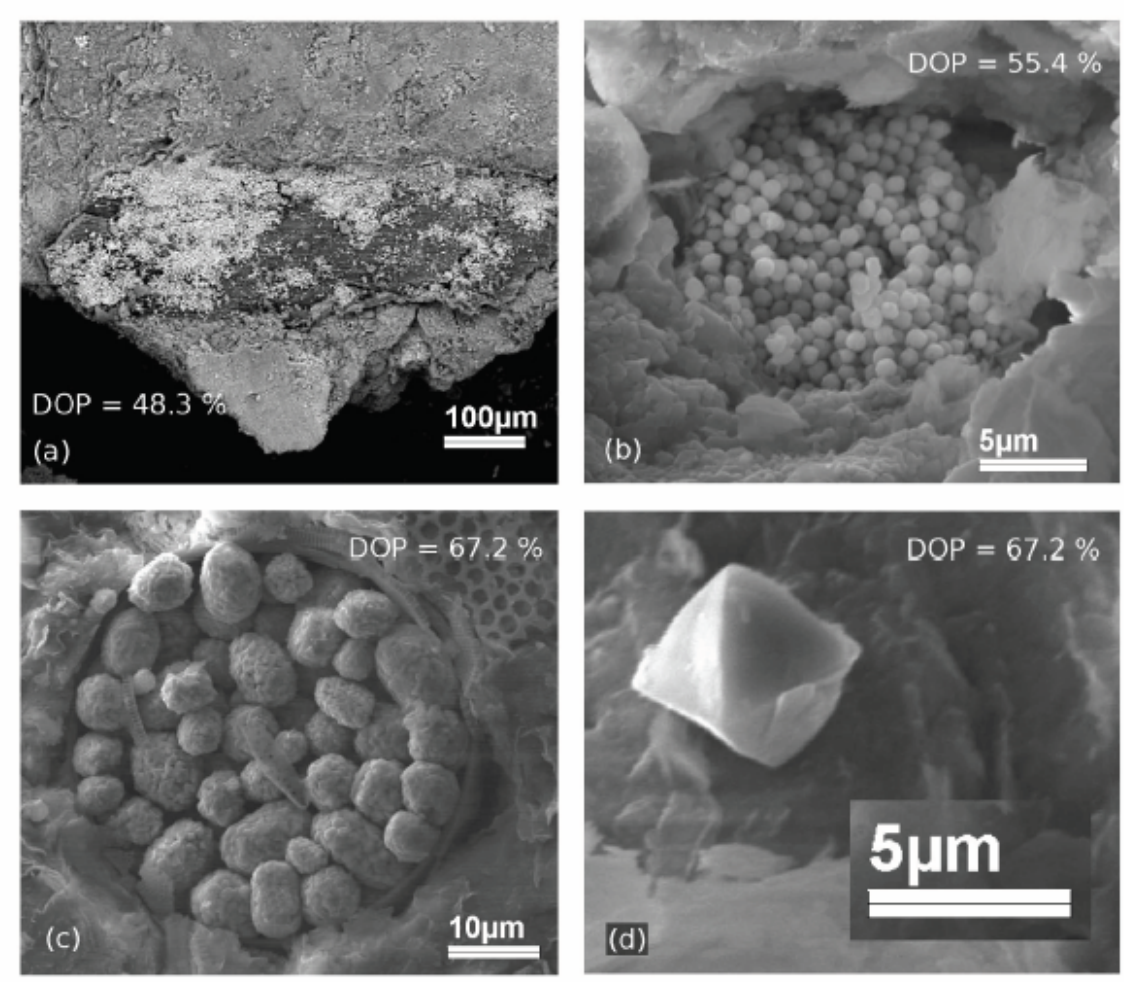

Figure 24: MEV microphotographs showing various pyrite textures observed at the Bragança mangrove sediments: (**a**) poorly developed minute pyrite covering a mangrove root, (**b**) group of pyrite crystals in a loci (**c**), cluster of framboids into a diatom, and (**d**) well developed octahedral crystal.

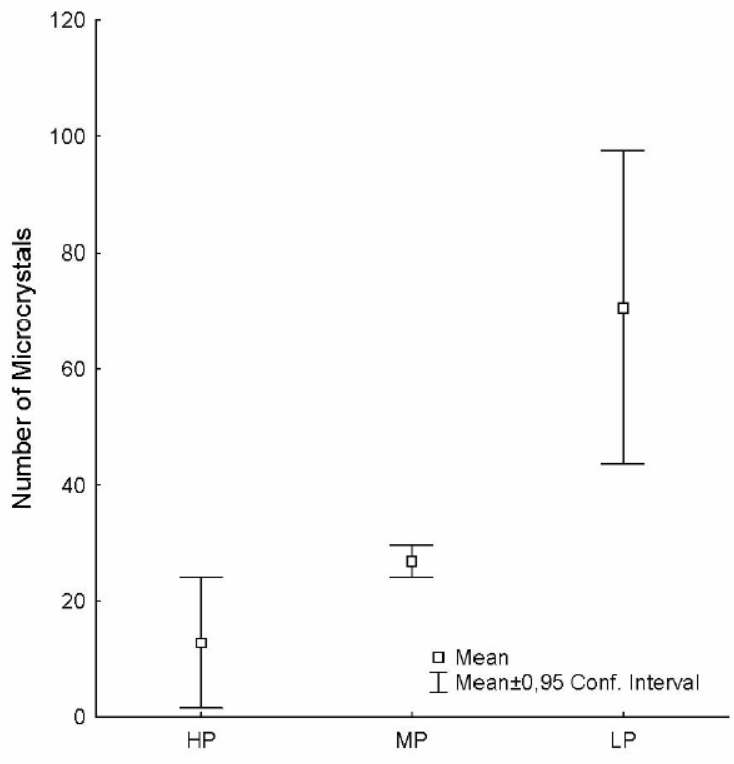

Figure 25: Distribution of the number of microcrystals (Nm) in framboids along a topographic gradient. HP, high plain; MP, middle plain; LP, low plain.

7.2. Discussion

7.2.1. Elemental source characterization

Sediment organic matter (OM) serves as nutritive substrate for micro-organisms and influences biologically mediated processes such as reduction-oxidation and the cycling of nutrients. The suitability of OM as a carbon or energy source can vary depending on the source of vegetal tissue (Anderson and Coleman, 1985). Therefore, it is important to consider the litter and root production, the retention and decomposition of these tissues within the mangroves when evaluating the effects of individual species.

Concerning HP, which was flooded only at spring tide, a high OM occurred; this contrasted with LP, which being highly flooded, obtained low OM (**Tab. 5**). These results act as supporting evidence with respect to tidal hydrology, which predicts that riverine and fringe forests have high rates of litter export due to higher tidal flushing (Lugo and Snedaker, 1974). The OM data do not clearly behaves with respect to decomposition, where the presence of more degradable OM in sediments below *A. germinans* can sustain a higher rate of microbial activity than sediments below *R. mangle*, and as a consequence, more decomposition of OM occurs (Lacerda *et al.*, 1995). Decomposition in the mangrove forest can be regulated by the quality of the organic substrate (Sherman *et al*., 1998). Decomposition studies have consistently demonstrated that *Rhizophora* leaves decompose more slowly than *Avicennia* leaves, as a result of lower N concentrations and higher tannin content. The tannin produced a decrease in the activity of benthic and microbial organisms, and as a consequence, a higher OM accumulation in sediments occurred (Cundell *et al.*, 1979; Boto *et al*., 1989; Robertson *et al*., 1992; Lacerda *et al*., 1995). Previous studies in Bragança showed that the leaves were the most important litter component, where as HP produced yearly the lowest amount of litter (7.2 $t.ha^{-1}.y^{-1}$) compared to LP (10.0 $t.ha^{-1}.y^{-1}$) (Menezes, 2006). Our OM data contrast with these results probably because of the fixation of the litter traps which not necessarily capture what falls from the tree (i.e. production). In the present study, OM values reflect remaining material in sediment after flooding during the rainy season (February) which is characterized by the minimum litter production of the year (Reise, 2003).

The org.-C and tot.-N dynamics in the surface sediments were most likely linked to the decomposition and export of the litter produced by both species (**Fig. 19**). The range in org.-C contents in sediments of Bragança (0.82-3.24 wt %) was higher than at other mangrove sediments (0.4-2.2 wt %) (Alongi *et al*., 1993; Kristensen *et al*., 1994). At HP and LP, although both org.-C and tot.-N are released during mineralization, the sub-surface (10 cm) clearly marked org.-C concentrations below *R. mangle* reflected a different control as mineralization was probably linked to 1) root exudation or degradation of fine roots (Boto *et al*., 1989; Holmer *et al*., 1999), and/or 2) higher necromass-root biomass for *R. mangle*, in comparison to the higher

live-root biomass for *A. germinans*, reported for the same study area (Reise, 2003). Here, high org.-C concentrations in deep sediments (50-100 cm) are consistent with previous studies of dissolved organic carbon (DOC) in groundwater made for Bragança Peninsula during the rainy season (Schwendenmann, 1998). Higher DOC concentrations in mangrove sediments indicate a relatively higher degree of anaerobiosis and stagnation as well as more abundant bacterial population and detrital matter on the forest floor (Alongi, 1988; Boto *et al*., 1989). Ovalle et al. (1990) hypothesize that during flood tide, groundwater is recharged by infiltration of water and solutes, and at ebb tide, groundwater migrates (vertical fluxes) back to the creek, and acts decoupling vegetation pattern from below-ground processes. The deeper zones being permanently under the influence of the pore water and submitted to permanently anoxic conditions would be favourable for the preservation of the org.-C content (Lallier-Verges *et al*., 1998).

The sedimentary C:N ratios range of 15 to 18 (**Tab. 5**), implies that the organic input does not comes completely from marine sources (i.e. algae and phytoplankton) that is characterized by a ratio about 7 (Meyers, 1994), although the microscopic study revealed algal-derived MO (**Fig. 24** (c)). During senescence of the mangrove leaves (i.e. before litterfall), about 64 % of the N is reabsorbed by the mangroves (Rao *et al*., 1994). Consequently, the sediments receive mangrove material that is depleted in N (Middelburg *et al.*, 1996), resulting in C:N ratios higher than the overlying vegetation. In contrast, our data indicated that sedimentary C:N ratios are rather low if compared to mangrove fresh leaves C:N ratios (22-32) from these species (Cordeiro and Mendoza, 2007). A similar observation about nitrogen excess with respect to carbon in sediments related to mangrove material, has been made in the East African mangrove (Middelburg *et al*., 1996). Previous studies in Bragança Pensinsula, suggested that low C:N ranges indicated that woody tissue did not contribute substantially to the sedimentary OM and, also, that this fact was indicative of a selective loss of carbon due to leaching or respiration (Dittmar and Lara, 2001c). At LP, the uniform and slightly rising down core distribution for tot.-N below *R. mangle* suggests that their immobilization (**Fig. 19**) relates to the high tannin content in *Rhizophora* leaves (Lacerda *et al*., 1995). Meanwhile, previous studies in the same

study area suggested that the tannins and other nitrogen compounds can not account for the uniform distribution of tot.-N values with depth (Schmitt, 2006). In fact, at the *Rhizophora*-dominated plain (LP), the molar C:N ratio rising at surface and deep layers (**Tab. 5**), reflected a proportionally higher increase in org.-C than in tot.-N values (**Fig. 19**). At middle layers (25-50 cm), the highest C:N ratios associated with more reducing environments (LP) and the lowest C:N ratios with positive Eh (HP) (**Fig. 20** (b)), support the studies of Lallier-Verges et al. (1998), suggesting that the oxidative conditions allow a more rapid formation of nitrogen compounds. For the same transect, the degradation of proteins and the partial loss of the corresponding nitrogen only drop from HP to LP during rainy season (Schmitt, 2006), confirms the results of the present study.

7.2.2. The sulphur-iron pools and some thermodynamic consideration

In Bragança, *A. germinans* and *R. mangle* grow under a wide range of salinities (18-68 $^{o}/_{oo}$) (**Tab. 5, Fig. 21** (b)). This range was higher as compared with seawater diluted by freshwater from the Caeté River during tidal inundation (8-32 $^{o}/_{oo}$), estimated in a contiguous creek during rainy season (Cohen *et al*., 1999). Surface salinity (20 $^{o}/_{oo}$) varied, responding to tidal inundation, intensity of the rain and evaporation. The inundation gradient controlled the surface salinity influencing the stability of the different forest stands. The elevated plain (HP) is flooded during spring tide only and in between evapotranspiration causes a salinity increase of the remaining water. Here, the higher salinity stratification reaching hyper saline conditions (70 $^{o}/_{oo}$) in deep (50 cm) sediments, suggests the lixiviation from the upper layers to the deeper layers during flooding. These results, were consistent with studies in Bragança, which reported higher salinity (60 ± 7 $^{o}/_{oo}$) for 50 cm in deep than for the surface (35 $^{o}/_{oo}$) (Furtado da Costa, 2000). At LP, the low salinity stratification reaching 50 $^{o}/_{oo}$ indicated that *R. mangle* requires an occasional fresh inundation, consistent with Marchand et al. (2004) in French Guiana.

On a whole-forest scale, the sediments had a high redox potentials (0-200 mV), indicating that the sulphate reduction is a less important diagenetic pathway in Bragança or that the reoxidation of hydrogen sulphide due to the high abundance of

iron keeps accumulating pore water sulphide concentrations low (Moeslund *et al.*, 1994) (**Fig. 18**). In addition, very low sulphide pool was found at HP and LP sites consistent with a low sulphate reduction, a large degree of aeration during low tide (HP) and probably due to enhanced sulphide reoxidation due to intense bioturbation by benthic fauna (LP) and reaction with oxides (**Fig. 21** (a)). Alongi et al. (1998b) estimated that sulphate reduction represented a considerably smaller proportion (42 %) of total organic matter oxidation and Holmer et al. (1999) reported similar results (<2 to 44 %) at a 2-years forest, in a Malaysian and Thailand mangrove forests, respectively. Other studies conducted in Thailand (Kristensen *et al*., 1991) and in Jamaica (Nedwell *et al*., 1994) suggest that aerobic respiration and sulphate reduction are the major pathways of OM diagenesis in mangrove sediments. The low SO_4^{2-} iso-lines (5-10 mM) in the surface layer (5-10 cm) during wet season (**Fig. 21** (c)), probably occur due to 1) the association to salinity gradients as suggested by the salinity variation (**Fig. 21** (b)), 2) an intensive bacterial dissimilatory sulphate reduction to the rapid mineralization of OM, and/or 3) diffusion of sulphate from the overlying water and from the underlying sediments to deep layers. Holmer et al. (1999) have similarly observed low sulphate values (11 mM) in the top sediment layers.

In spite of the oxic-anoxic interfaces (Eh = 0 mV) due to the rough surface topography at the depressions (D1, D2), the thickness (~1 cm) of the upper oxidation zone (UOZ) suggests a greater biological heterotrophic activity (**Fig. 14, Fig. 18**). At MP, the SO_4^{2-} loss (5 mM) and minimum PEC (30 %) iso-lines, suggest that biological and/or chemical processes controlled SO_4^{2-} concentrations in this plain (**Fig. 21** (c)(d)). As result of sulphate reduction, higher free sulphide concentrations (10-47 μM) were observed in the pore water below *A. germinans* (**Fig. 21** (a)). The decrease of sulphide concentrations below *R. mangle* was probably due to 1) higher oxidation capacity by iron (hydr)oxides related to *A. germinans* (**Fig. 14**), and/or 2) to the corresponding formation of metal sulphides. Apparently the amount of oxidants released from the living roots is sufficient to avoid the sulphate reduction (Hinnes *et al*., 1989). At our study area, the higher necromass-root biomass for *R. mangle* in relation to *A. germinans* (Reise, 2003), can be places for pyrite formation and trace

metal precipitation due to enhanced concentration of metals in dead roots (Alongi *et al*., 2005).

Within tree-scale, the down core distribution of sulphur and related parameters (water content, salinity and PEC) was consistent among the stations (**Fig. 22** (a)(b)). Regardless of whether the species-specific differences were caused by the species themselves or by existing microsite differences, a closer look on sediment conditions for the establishment, growth and survival of mangroves is necessary. In the present study, the down core distribution of SO_4^{2-} below *A. germinans* significantly correlates with salinity (r= 0.90, n= 8) (**Fig. 22** (b)) and the maximum PEC values (100 %) at 50 cm depth suggests SO_4^{2-} diffusion from the overlying layers, both intensified by the hydrological processes in LP and probably the presence of crabs burrows. Here, the bioturbation trough the presence of deep deposit-feeders, inhabiting burrows penetrating to a depth of 164 ± 52 cm with a living cave lying at the burrow end containing about 500 ml of water (Rademaker, 1998) facilitate oxygen transport and oxic decomposition (Alongi *et al*., 2001) in deep layers. Two points are clarified in relation to salinity as SO_4^{2-} source: 1) the presence of surface (HP) and deep (LP) humid layers resulting in saline intrusion, and 2) within tree-scale differences the water content can be greater than within forest-scale differences, these tree-scale differences tend to attenuate or to increase the average salinity in a forest-scale.

Because pyrite precipitation and iron solubility are partially dependent upon sulphate reduction, a sediment shift from oxic to anoxic conditions (Eh = 0 mV) was chosen to indicate conditions below which significant sulphate reduction occur, consistent with Schulz (2000) and Gleason et al. (2003). In a first scenario, at the surface (D2, LP), the react.-Fe depletion concomitant with an oxic-anoxic interface (Eh=0-50 mV) corresponds with observation of Luther et al. (1992), which demonstrate that the react.-Fe depletion occur under anoxic conditions (Eh<0 mV) and produce molecules with reactive functional groups such as hydroxyl- and carboxyl-groups (**Fig. 23** (a), **Fig. 18** (a)). Meanwhile, in a second scenario (D1), the depletion of react.-Fe concomitant with an oxic-anoxic interface (Eh=0-150 mV) do not occur. For both scenarios (D1, D2), the predominant alkaline range (7.1-7.5) in deep sediments (**Fig.**

18 (b)) support the sulphate reduction. The dissolution of Fe(III) minerals in the first scenario could be explained by 1) organic ligands produced by exudation of algae and plants (Stumm and Sulzberger, 1992), and 2) a higher primary productivity (Luther *et al*., 1992), as indicates the robust marine influence and the higher mean stand age of *R. mangle* (26 years), related to *A. germinans* stand (22 years) (Menezes, 2006). The implication for a functional cause of these oxic-anoxic interfaces can point out the limitation of the temporal equilibrium of the co-ocurrence of both species. In principle an oxic-anoxic interface (Eh = 0 mV) is favourable for pyrite formation via polysulphide pathway (Wilkin *et al*., 1996; Rickard and Morse, 2005), this exclude the possibility of a species-specific effect for sediment redox potential at the depressions.

7.2.3. Degree of pyritization and pyrite texture

The degree of pyritization (DOP) across the transect (**Fig. 23** (b)), fall between 50 and 60 % which is between the range of values (DOP = 40-70 %) typically reported for modern saltmarshes sediments (Giblin, 1988; Raiswell *et al*., 1988; Sherman *et al*., 1998). The DOP values obtained here are indicative for sulphide-limiting suboxic conditions (also called dysoxic or dysaerobic - very low to no O_2, but no H_2S) (Raiswell *et al*., 1988), in agreement with the measured low sulphide concentrations in the sediments (**Fig. 21** (a)).

The DOP values across the transect are largely controlled by tidal flushing and sulphate reduction (**Fig. 21** (c)), and to a lesser extent by root oxidation and bioturbation (**Fig. 22** (b)). Although Berner (1970) argued that Fe may control pyrite formation at DOP values above 50 %, our data do not showed a limitation of react.-Fe in LP, in relation to HP, where pyrite burial was greatest (**Fig. 23** (a)). The DOP approach seems do not provide a good accounting of iron availability during early diagenesis (Rickard and Morse, 2005). Thus, it appears that DOP values are reflective of the sediment sulphate reduction and pore-water redox conditions, supporting previous studies of Sherman et al. (1998) and Roychoudhury et al. (2003), respectively. Furthermore, the relative constant value of DOP with depth can be interpreted as pyritization being complete below the sediment-water interface (**Fig. 23**

(b)). Meanwhile, the pattern of pyrite formation can be regulated by 1) the rooting zone of the mangroves vegetation and their active radial oxidation loss (ROL), and 2) the iron concretions found on mangrove rhizospheres (Lacerda *et al*., 1993). At LP, the more efficient reduction and sulfidation of Fe, relative to the HP, increased the DOP (**Fig. 23** (b)) and consequently the number of microcrystals in framboids (**Fig. 25**).

At Bragança Peninsula pyrite morphologies occurs as minute dispersed grains, octahedral crystals, framboids and framboidal cluster (stoichiometry Fe_2S_2) (Wolthers *et al*., 2003) (**Fig. 24**). Diagenetic pyrite formation in the sediments significant contribute to the partially oxic to suboxic sediments sedimentary pyrite in Bragança, *syngenetic* pyrite in the water column was not evaluated. The scarce pyrite distribution in the 5 cm depth interval, pointed out the strong influence of the advective transport of pore water by tidal current and also the diffusive input of oxygen during non-submergence. Studies of Aragon et al. (1999) in mangroves of South-East Brazil, suggested that a smaller advective transport of pore water at the 10-25 cm depth interval in comparison to the 5 cm depth interval occurred. In our study area, the first range of pyrite grains (0.6-2.3 μm-size) predominated at medium layers of the vertical profiles (10-25 cm), providing evidence supporting their rapid formation (**Fig. 24** (a)(b)). The rapid formation of small (0.1-2 μm-size) euhedral pyrite particles have been observed previously in sediments of salt marsh by Howarth (1979) and Luther et al. (1982). It is reasonable that mangrove environments provide dynamic conditions for pyrite growth because the surface is exposed to the atmosphere and the rhizosphere of mangrove trees can oxidize deep sediments (10-35 cm) (Clark *et al*., 1998). The second range of pyrite grains (0.8-4.1 μm-size) at deep layers (40-100 cm) seems to be relative unaffected by the root oxidation and can further be interpreted as sufficient time to nucleation and growth, suggesting that pyrite was stable.

At the surface and middle layers (<35 cm), the lack of framboids accumulation suggested that the mangrove sediments are exposed to the active root systems controlling their formation. Although the rhizosphere environment of salt marsh may

provide places for the growing of framboids (Luther *et al*., 1982), this hypothesis is not consistent with field observations made in this study. In comparison, the abundance of framboids in deep layers (40-100 cm) pointed out the reduction of the transport processes and turnover ranges in these sediments (Wijsman *et al*., 2001). The increase from HP to LP of DOP (52.5-65 %) and the number of microcrystals (12.5-70), indicated the framboids formation in reducing mangrove sediments (**Fig. 23**, **Fig. 25**). The average mean framboid diameter (7.7 μm-size) is representative of an oxic and dysoxic environment (Wilkin *et al*., 1996). The approximate growth time of the larger framboid (21.5 μm-size) for Bragança sediments can be estimated comparing with the maximum 7 years for framboids of 25 μm-size (Wilkin *et al*., 1996). The maximum size of framboids formed in environment with typical concentration of dissolved Fe (<100 μm) in pore water would be 50 μm (Raiswell *et al*., 1993).

The close spatial association of a framboidal and euhedral grains was cited as very common in nature (Sawłowicz, 2005). The peculiar link between these two morphologies was studied by Love and Amstutz (1966), Sawłowicz (1993) and Wilkin and Barnes (1996). In the process of infilling "Sammelrekristallisation" (German term for fusion-recrystallisation), new pyrite fills the spaces between the microcrystals in the framboids (Love and Amstutz, 1966). Similar to the transformation from framboid to euhedral, the cluster framboid (FeS_{aq} cluster) may recrystallize to a massive grain (Sawłowicz, 1993; Butler and Rickard, 2000). At LP, below *R. mangle* (100 cm), the simultaneous presence of FeS_{aq} cluster and an octahedral grain corresponds with observations of Sawłowicz (1993) (**Fig. 24** (c)(d)). In this station (100 cm) (**Fig. 22** (b)), below *R. mangle*, the maximum DOP (67 %) and lower react.-Fe (24.7 $mg.g^{-1}$), in relation to *A. germinans*, suggests that the continuous supply of constituting material to the microenvironment of framboid formation occurred, this represents the simplest way of leading to a euhedral pyrite crystal, with framboidal pyrite as an intermediate stage (Sawłowicz, 1993). Additionally, apparently the poor development of octahedral grains of pyrite was related to slower rates of pyritization (Wilkin and Barnes, 1996). The FeS_{aq} cluster (**Fig. 24** (c)), seems to infill the free space in a fossil diatom, this may not always be

genetically related to fossilization, because the fossil serve only as available space in sediment (Sawłowicz, 2005).

CHAPTER 8 – CONCLUSIONS

During the short period of time (2-3.5 h) that the water flooded the HP of the mangrove area, there was a significant transient effect on surface sediment chemistry. During submergence, the sharp Eh reduction and pH increase could be due to the high Fe/Al-P and SO_4^{2-} concentrations, summed to the high mineralizable OM in HP. The sulphide rapid initial drop and gradual depletion was related to the SO_4^{2-}consumption during the OM degradation and/or sulphide dilution by the floodwater. The sulphide dilution supports the mixing of freshly tidal water in the interstices of sediment surface (2 cm) with sea-water. The re-establishment of non-submergence conditions may involve biological processes in the water column or simply oxidation and reduction inside the sediments (Caetano *et al*., 1997). Clearly, the effect of submergence on these trends is irrefutable. Meanwhile, the presence of the electrode can amplify the intensity of the measurements.

The interaction of different physicochemical characteristics between sediment pore water and flooding water, seems to control the concentration of P in the aqueous phase by the chemical equilibrium of several minerals for the lateritic source area. As the pH increases during submergence, Al and Fe species in the soluble form being negatively charged cannot trapping P successfully, suggesting the formation of instable Ca-phosphate phases due to the limited inundation time. The last hypothesis was confirmed by the ratios between reactive metals and phosphate minerals, and the negative correlations of theses ratios with extr.-P, the latter confirmed that Al-P was the most significant fraction controlling the P concentration in sediments. In addition, the positive correlation between extr.-P and inundation frequency, summed to the acidic pH at LP, supports the acidic range proposed for the highest P availability related to Fe/Al- and Ca-P minerals (Havlin *et al*., 1999; Georgantas and Grigoropoulou, 2006). The combined effects of flooding with the P dynamics appear to be a major factor responsible for the zonation of the investigated mangroves.

The redox model presented here, illustrated how several oxidation and reduction horizons can develop within the forest sediments. The “upper oxidation zone - UOZ”

is a result of atmospheric oxygen and their thickness depend upon the balance between the rate of O_2 diffusion into the sediment and the rate of O_2 consumption (Howeler and Bouldin, 1971). The "lower oxidation zone - LOZ" develops due the release of oxygen from mangrove roots (Armstrong *et al*., 2000). The resulting oxidation is accompanied by a reduction of pore water pH, as iron sulphides are converted to (hydr)oxides and sulphuric acid (Clark *et al.*, 1998). Both the "upper reduction zone - URZ" and the "lower reduction zone - LRZ" are characterized by decomposition of OM and sulphate reduction to produce potentially metal-binding sulphides. In this model, the pattern of pyrite formation and distribution was regulated by the active roots, resulting in minute dispersed grains at LOZ and framboidal texture at LRZ.

The redox model revealed for *A. germinans* a significant greater oxidation at LP, whereas for *R. mangle* the moderate but constant root-induced oxidation capacity was weakly affected by the different substrate conditions. The higher root-induced oxidation in *A. germinans* limited the availability of P and consequently their distribution; whereas the moderate root-oxidation in *R. mangle* enhancing the formation of extr.-P, and therefore can be considered as an adaptive response to nutrient uptake in water-logging that could contribute to its dominance in this plain. These findings indicated a species-specific differences in oxidise the rhizosphere that contribute to their differential flood tolerance and mangrove zonation.

Differences of sulphur speciation between *R. mangle* and *A. germinans* demonstrate that plant activity greatly influence sulphur cycling in Bragança mangroves. These chemical modifications are *in situ* processes resulting from root-sediment interactions. At LP, as result of a higher *A. germinans* root-oxidation capacity in comparison to *R. mangle*, a SO_4^{2-} increase in *A. germinans* occurred. Conversely, at MP, as result of a higher *R. mangle* root-oxidation activity related to *A. germinans*, sulphide concentrations were hardly detected below *R. mangle*. When low root-oxidation occurred, the formation of iron sulphides can prevent the re-supply of iron (hydr)oxides, enhancing the formation of extr.-P available for the vegetation. The low sedimentary OM at LP, supported evidence with respect to tidal hydrology, but do not

clearly behaves with respect to decomposition. At the more reduced *Rhizophora*-dominated plain (LP), the C:N ratio rising reflected the proportionally higher increase in org.-C than in tot.-N values.

In Bragança the SO_4^{2-} reduction is a less importance diagenetic pathway (Alongi *et al*. 1998b; Holmer *et al*., 1999) or the reoxidation of hydrogen sulphide due to the high abundance of iron keeps accumulating pore water sulphide concentrations low (Moeslund *et al.*, 1994). The SO_4^{2-} was largely controlled by the degree of aeration in sediments due to the intense root-oxidation and probably the ventilation by benthic fauna. The DOP values obtained here were also indicative for sulphide-limiting suboxic conditions (Raiswell *et al*., 1988). The DOP was largely controlled by tidal flushing and SO_4^{2-} reduction, and to a lesser extent by root oxidation and bioturbation. At the depressions, the sediment shift from oxic to anoxic conditions (Eh = 0 mV) was reflected in SO_4^{2-} and react.-Fe reduction. In principle an oxic-anoxic interface is favourable for pyrite formation via polysulphide pathway (Wilkin *et al*., 1996; Rickard and Morse, 2005). On a whole-forest scale, the presence of two oxic-anoxic interfaces apparently excluded the possibility of a species-specific effect on sediment sulphur and iron pools. Therefore these pools patterns depend on physical settings in the first place. On the basis of pyrite observations and the physicochemical parameters within the mangrove sediment, it was confirmed that oxidative processes and reactant availability, all control the observed resultant pyrite morphologies. The wide variation in pyrite texture and distribution of number of microcrystal's in framboids suggest that caution is needed in using pyrite as redox proxy to identify depositional environments.

CHAPTER 9– BIBLIOGRAPHY

Ajukai, T., Miller, D., Wolanski, E., and Spagnol, S. 1998. Fluxes of nutrients and dissolved and particulate organic matter in two mangrove creeks in Northeastern Australia. *Mangroves Salt Marshes.* **2**, 223-230.

Almeida, S. 1996. Estrutura e florística em areas de manguezais paraenses: evidências da influência do estuário amazônico. *Boletim Museu Paraense Emílio Goeldi, Série Ciências da Terra.* **8**, 93-100.

Alongi, D.M. 1988. Bacterial productivity and microbial biomass in tropical mangrove sediments. *Microbial Ecology*. **15**, 59-79.

Alongi, D.M., Boto, K.G. and Tirendi, F. 1989. Effect of exported mangrove litter on bacterial productivity and dissolved organic carbon fluxes in adjacent tropical nearshore sediments. *Marine Ecology Progress Series*. **56**, 133-144.

Alongi, D.M., Boto, K.G. and Robertson, A.I. 1992. Nitrogen and phosphorus cycles. *In*: Robertson, A.I. and Alongi, D.M. (Eds.) Tropical marine ecosystems. American Geophysical Union: Washington, DC. pp. 251-292.

Alongi, D.M., Christoffersen, P. and Tirendi, F. 1993. The influence of forest type on microbial nutrient relationships in tropical mangrove sediments. *Journal of Experimental Marine Biology and Ecology*. **171**, 201-223.

Alongi, D.M., Ayukai, T., Brunskill, G.J., Clough, B.F. and Wollanski, E. 1998a. Sources, sink and export of organic carbon through a tropical, semi-enclosed delta (Hinchinbrook Channel, Australia). *Mangroves and Salt Marshes.* **2**, 237-242.

Alongi, D. M., Sasekumar, A., Tirendi, F. And Dixon, P. 1998b. The influence of stand age on benthic decomposition and recycling of organic matter in managed mangrove forests of Malaysia. *Journal of Experimental Marine Biology and Ecology*. **225**, 197-218.

Alongi, D.M., Tirendi, F., Trott, L.A. and Brunskill, G.J. 1999. Mineralisation of organic matter in intertidal sediments of a tropical semi-enclosed delta. *Estuarine, Coastal and Shelf Science.* **48**, 451-467.

Alongi, D.M., Tirendi, F. and Clough, B.F. 2000. Below-ground decomposition of organic matter in forests of the mangroves *Rhizophora stylosa* and *Avicennia marina* along the arid coast of Western Australia. *Aquatic Botany*. **68**, 97-122.

Alongi, D.M., Wattayakorn, G., Pfitzner, J., Tirendi, F., Zagorski, I., Brunskill, G.J., Davidson, A. and Clough, B.F. 2001. Organic carbon accumulation and metabolic pathways in sediments of mangrove forests in southern Thailand. *Marine Geology*. **179**, 85-103.

Alongi, D.M., Wattayakorn, G., Boyle, S., Tirendi, F., Payn, C. and Dixon, P. 2004. Influence of roots and climate on mineral and trace elements storage and flux in tropical mangrove soils. *Biogeochemistry.* **69**, 105-123.

Alongi, D.M., Pfitzer, J., Trott, L.A., Tirendi, F., Dixon, P. and Klumpp, D.W. 2005. Rapid sediment accumulation and microbial mineralization in forests of the mangrove *Kandelia candel* in the Jiulongjiang Estuary, China. *Estuarine, Coastal and Shelf Science*. **63**, 605-618.

Allen, S.E. 1989. Analysis of vegetation and other organic materials. *In*: Allen, S.E. (Ed.) Chemical analysis of ecological materials. Blackwell Scientific Publications: Australia. pp. 46-60.

Aminot, A. and Kérouel, R. 1997. Reference material for nutrients for the QUASIMEME laboratory performance studies 1993-1996. *Marine Pollution Bulletin*. **35**(1-6), 78-83.

Andersen, F.O. and Kristensen, E. 1988. Oxygen microgradients in the rhizosphere of the mangrove *Avicennia marina*. *Marine Ecology Progress Series*. **44**, 201-204.

Anderson, D.W. and Coleman, D.C. 1985. The dynamics of organic matter in grassland soils. *Journal of Soil Water Conservation*. **40**, 211-216.

Appelo, C.A.J. and Postma, D. 2005. Geochemistry, groundwater and pollution. (2nd ed.) A.A. Balkema: Leiden. pp. 649.

Arai, M., Truckenbrodt, W., Nogueira, A.C.R., Goés, A.M. and Rossetti, D.F. 1994. Novos dados sobre estratigrafia e ambiente deposicional dos sedimentos Barreiras, NE do Pará. IV Simpósio de Geologia da Amazônia, Belém. Anais, Belém: SBG/NO. Boletim de Resumos Expandidos. pp. 185-187.

Aragon, G.T., Ovalle, A.R. and Carmouze, J-P. 1999. Porewater dynamics and the formation of iron sulfides in a mangrove ecosystem, Sepetiba Bay, Brazil. *Mangroves and Salt Marshes*. **3**, 85-93.

Armstrong, W., Cousins, D. Armstrong, J., Turner, D.W. and Beckett, P.M. 2000. Oxygen distribution in wetlands plant roots and permeability barriers to gas–exchange with the rhizosphere: a microelectrode and modelling study with *Phragmites australis*. *Annais of Botany.* **86**, 687-703.

Artemyev, V.E. 1996. Geochemistry of organic matter in river-sea systems. Kluwer Academic Publishers: Dordrecht. pp. 190 .

Bastos, R.C. A. 2002. Piritização de metais-traço na Baía de Sepetiba-RJ. PhD. Thesis. Departamento de Geoquímica. Universidade Federal Fluminense. Niterói, RJ, Brazil. pp. 187.

Begg, C.B.M, Kirk, G.J.D., Mackenzie, A.F. and Neue, H.-U. 1994. Root-induced iron oxidation and pH changes in the lowland rice rhizosphere. *New Phytology.* **128**, 469-477.

Behling, H., Cohen, M.C.L. and Lara, R.J. 2001. Studies on Holocene mangrove ecosystem dynamics of the Bragança Peninsula in Northeastern Pará, Brazil. *Palaeogeography, Palaeoclimatology, Palaeoecology.* **167**, 225-242.

Behling, H. and Costa, M.L. 2004. Mineralogy, geochemistry and palynology of modern and late Tertiary mangrove deposits in the Barreiras Formation of Mosqueiro Island, northeastern Pará state, eastern Amazonia. *Journal of South American Earth Sciences*. **17**, 285-295.

Bell, L.C. and Black, C.A. 1970. Transformation of dibasic calcium phosphate dehydrate and octacalcium phosphate in slightly acid and alkaline soils. *Soil Science Society of America Proceedings.* **34**, 583-587.

Benitez-Nelson, C.R. and Buesseler, K.O. 1999. Variability of inorganic and organic phosphorus turnover rates in the coastal ocean. *Nature.* **398**, 502-505.

Berrêdo, J.F. 2006. Geoquímica dos sedimentos de manguezais do Nordeste do Estado do Pará: o exemplo do estuário do Rio Marapanim. Ph.D. Thesis. Centro de Geociências, Universidade Federal do Pará. Belém do Pará, Brazil. pp. 185.

Berner, R.A. 1970. Sedimentary pyrite formation. *American Journal of Science*. **268**, 1-23.

Berner, R.A. 1984. Sedimentary pyrite formation: An update. *Geochimica et Cosmochimica Acta.* **48**, 605-615.

Bigarella, J.J. 1975. The Barreiras Group in the Northeastern Brazil. *Anais de Academia Brasileira de Ciências*. **47**, 365-393.

Billen, G., Lancelot, C. and Meybeck, M. 1991. N, P, and Si retention along the aquatic continuum from land to ocean. *In*: Mantoura, R.F.C, Martin, J.M. and Wollast, R. (Eds.) Ocean margin processes in global change. John Wiley and Sons: New York. pp. 19-44.

Blom, C.W., Voesenek, L.A., Banga, M., Engelaar, W.M., Rijnders, J.H., van de Steeg, H.M. and Visser, E.J. 1994. Physiological ecology of riverside species: adaptive responses of plants to submergence. *Annais of Botany*. **74**, 253-263.

Boesen, C. and Postma, D. 1988. Pyrite formation in anoxic environments of the Baltic. *American Journal of Science*. **288**, 575-603.

Boström, B., Andersen, J.M., Fleischer, S. and Jansson, M. 1988. Exchange of phosphorus across the sediment-water interface. *Hydrobiologia*. **170**, 229-244.

Boudreau, B.P. and Jørgensen, B.B. 2001. The benthic boundary layer: transport processes and biogeochemistry. Oxford Univ. Press: Oxford. pp. 404.

Bourman, R.P. and Ollier, C.D. 2002. A critic of the Schelmann definition and classification of "laterite". *Catena*. **47**, 117-131.

Boto, K.G. and Bunt, J.S. 1981. Tidal export of particulate organic matter from a Northern Australian mangrove system. *Estuarine, Coastal and Shelf Science.* **13**, 247-255.

Boto, K.G., Bunt, J.S. and Wellington, J.T. 1984. Variation in mangrove forest productivity in Northern Australia and Papua New Guinea. *Estuarine, Coastal and Shelf Science.* **19,** 321-329.

Boto, K.G. and Wellington, J.T. 1983. Phosphorus and nitrogen nutritional status of a Northern Australian mangrove forest. *Marine Ecology Progress Series.* **11**, 63-69.

Boto, K.G. and Wellington, J.T. 1984. Soil characteristics and nutrient status in a northern Australian mangrove forest. *Estuaries.* **7**, 61-69.

Boto, K.G. and Wellington, J.T. 1988. Seasonal variation in concentrations and fluxes of dissolved organic and inorganic materials in a tropical, tidally-dominated, mangrove waterway. *Marine Ecology Progress Series.* **50**, 151-160.

Boto, K.G., Alongi, D.M.M and Nott, A.L. 1989. Dissolved organic carbon and bacteria interactions at sediment-water interface in a tropical mangrove system. *Marine Ecology Progress Series.* **51**, 243-251.

Brandt, F. 1932. Ein neuer Typ von Eisentonerde-Phosphate-Vorkommen (Maranhão, Nordbrasilien). *Chemie der Erde*. **7**, 383-425.

Brown, J.L. 1981. Calcium phosphate precipitation: effects of common and foreign ions on hydroxyapatite crystal growth. *Soil Science Society of America.* **45**, 482-487.

Butler, J.N. 1998. Ionic Equilibrium: solubility and pH calculations. Wiley-Interscience Publication: Canada. pp. 543.

Butler, I.B. and Rickard, D. 2000. Framboidal pyrite formation via the oxidation of iron (II) monosulfide by hydrogen sulphide. *Geochimica et Cosmochimica Acta.* **64**, 2665-2672.

Caetano, M., Falcão, M., Vale, C. And Bebianno, M.J. 1997. Tidal flushing of ammonium, iron and manganese from inter-tidal sediment pore waters. *Marine Chemistry*. **58**, 203-211.

Canfield, D.E. and Berner, R.A. 1987. Dissolution and pyritization of magnetite in anoxic marine sediments. *Geochimica et Cosmochimica Acta*. **51**, 645-659.

Canfield, D.E. 1989. Reactive iron in marine sediments. *Geochimica et Cosmochimica Acta.* **53**, 619-632.

Cappellen, P.van and Berner, R.A. 1991. Fluorapatite crystal growth from modified seawater solutions. *Geochimica et Cosmochimica Acta.* **55**, 1219-1234.

Caraco, N.F., Cole, J.J. and Likens, G.E. 1989. Evidence for sulphate-controlled phosphorus release from sediments of aquatic systems. *Nature.* **341**, 316-318.

Clark, M.W., McConchie, D., Lewis, D.W. and Saenger, P. 1998. Redox stratification and heavy metal partitioning in Avicennia-dominated mangrove sediments: a geochemical model. *Chemical Geology.* **149**, 147-171.

Chang, S.C. and Jackson, M.L. 1957. Fractionation of soil phosphorus. *Soil Science.* **84**, 133-144.

Cheng, K.L. and Da-Ming, Z. 2005. On calibration of pH meters. *Sensors.* **5**, 209-219.

Chesnin, L. and Yien, C.H. 1950. Turbidimetric determination of available sulfates. *Soil Science American Society Proceedings.* **15**, 149-151.

Christoffersen, J., Christoffersen, M.R., Kibalczyc, W. and Andersen, F.A. 1989. A contribution to the understanding of the formation of calcium phosphates. *Journal of Crystals Growth.* **94**, 767-777.

Christoffersen, J. and Christoffersen, M.R. 1982. Kinetics of dissolution of calcium hydroxyapatite: V. The acidity constant for the hydrogen phosphate surface complex. *Journal of Crystal Growth*. **57**, 21-26.

Clark, M.W., Mc Conchie, D., Lewis, D.W. and Saenger, P. 1998. Redox stratification and heavy metal partitioning in Avicennia-dominated mangrove sediments: a geochemical model. *Chemical Geology.* **149**, 147-171.

Cline, J.D. 1969. Spectrophotometric determination of hydrogen sulfide in natural waters. *Limnology and Oceanography.* **14**, 454-458.

Clough, B. 1988. Mangrove forests productivity and biomass accumulation in Hinchinbrook Channel, Australia. *Mangrove Salt Marsh*. **2**, 191-198.

Cohen, M.C.L, Lara, R.J, Ramos, J.F.F and Dittmar, T. 1999. Factors influencing the variability of magnesium, calcium and potassium in waters of a mangrove creek in Bragança, North Brazil. *Mangroves and Salt Marshes*. **3**, 9-15.

Cohen, MC.L., Lara, R.J., Szlafsztein, C.F. and Dittmar, T. 2001. Digital elevation model applied to mangrove coast analysis, Amazon region, Brazil. *Journal of International Environment Creation.* **4**, 1-8.

Cohen, M.C.L., Lara, R.J., Szlafsztein, C. and Dittmar, T. 2004. Mangrove inundation and nutrient dynamics from a GIS perspective. *Wetlands Ecology and Management*. **12**, 81-86.

Colmer, T.D., Gibberd, M.R., Wiengweera, A. and Tinh, T.K. 1998. The barrier to radial oxygen loss from roots of rice (*Oryza sativa* L.) is induced by growth in stagnant solution. *Journal of Experimental Botany*. **49**, 1431-1436.

Cordeiro, C.daC., Mendoza, U.N. and Lara, R.J. 2003. Mangrove zonation and phosphorus distribution in sediment along an inundation gradient in Bragança, North Brazil. X COLACMAR. Décimo Congreso Latinoamericano de Ciencias del Mar. 22-26 Setiembre. San José de Costa Rica. pp. 376.

Cordeiro, C. daC. and Mendoza, U. 2007. Relações C/N, C/P e N/P indicando fonte e mineralização da matéria orgânica no manguezal de Bragança, Norte do Brasil. XI COLACMAR. Onceavo Congreso Latinoamericano de Ciencias del Mar. 15-20, Abril. Florianópolis, SC, Brasil. pp 489.

Costa, M.L. 1991. Aspectos geológicos dos lateritos da Amazônia. *Revista Brasileira de Geociências.* **21**(2), 146-160.

Costa, M.L. and Araújo, E.S. 1996. Application of multi-elements in Au-phosphate-bearing lateritic crusts for identification of their parent rocks. *Journal of Geochemical Exploration.* **57**, 257-272.

Costa, M.L., Fernández, O.C., Toledo, M.C.M., Passos, C.M. and Pereira, P.F. 2004a. A turquesa de Itacupim, Pará. *Revista da Escola de Minas*. **57**(4), 261-266.

Costa, M.L., Behling, H., Berrêdo, J.F., do Carmo, M.S. and Siqueira, N.V.M. 2004b. Mineralogical, geochemical and palynological studies of late holocene mangrove sediments from Northeastern Pará State, Brazil. *Revista Brasileira de Geociências*. **34**(4), 479-488.

Cottam, G. and Curtis, J.T. 1956. The use of distance measures in phytosociological sampling. *Ecology*. **37**, 451-460.

Cundell, A.M., Brown, M.S., Standford, R. and Mitchell, R. 1979. Microbial degradation of *Rhizophora mangle* leaves immersed in the sea. *Estuarine and Coastal Marine Science*. **9**, 281-286.

Dagg, M., Benner, R., Lohrenz, S. and Lawrence, D. 2004. Transformation of dissolved and particulate materials on continental shelves influenced by large rivers: plume processes. *Continental Shelf Research*. **24**, 833-858.

Davies, D.D. 1986. The fine control of cytosolic pH. *Physiology of Plant*s. **67**, 702-706.

Deutsche Institut für Normung-DIN 38405-D26. 1993. Deutsche Einheitsverfahren zur Wasser-, Abwasser- und Schlamm-Untersuchung: Physikalische, chemische, biologische und bakteriologische Verfahren. Photometrische Bestimmung des gelösten Sulfids. **2**, 2-10.

Deutsche Institut für Normung-DIN 38414-S2. 1993. Deutsche Einheitsverfahren zur Wasser-, Abwasser- und Schlamm-Untersuchung: Physikalische, chemische, biologische und bakteriologische Verfahren. Bestimmung des Wassergehaltes und des Trockenrückstandes bzw. der Trockensubstanz. **4**, 2-7.

Deutsche Institut für Normung-DIN 38414-S3. 1993. Deutsche Einheitsverfahren zur Wasser-, Abwasser- und Schlamm-Untersuchung: Physikalische, chemische, biologische und bakteriologische Verfahren. Bestimmung des Glührückstandes und des Glühverlustes des Trockenmasse eines Schlammes. **4**, 2-5.

De Simone, O., Haase, K., Müller, E., Junk, W.J., Gonsior, G. and Schmidt, W. 2002. Impact of root morphology on metabolism and oxygen distribution in roots and rhizosphere from two Central Amazon floodplain tree species. *Functional Plant Biology.* **29**, 1025-1035.

Diaz, O.A., Reddy, K.R. and Moore Jr, P.A. 1994. Solubility of inorganic phosphorus in stream water as influenced by pH and calcium concentration. *Water Research*. **28**(8), 1755-1763.

Dittmar, T. 1999. Outwelling of organic matter and nutrients from mangrove in North Brazil: evidence from organic tracers and fluxes measurements. Ph.D. Thesis. Zentrum für Marine Tropenökologie. Bremen Universität. Bremen, Germany. pp. 206.

Dittmar, T., Lara, R.J. and Kattner, G. 2001. River or mangrove? Tracing major organic matter sources in tropical Brazilian coastal waters. *Marine Chemistry.* **73**, 253-271.

Dittmar, T. and Lara, R.J. 2001a. Driving forces behind nutrient and organic matter dynamics in a mangrove tidal creek in North Brazil. *Estuarine, Coastal and Shelf Science.* **52**, 249-259.

Dittmar, T. and Lara, R.J. 2001b. Do mangroves rather than rivers provide nutrients to coastal environments South of the Amazonas River? Evidence from long-term flux measurements. *Marine Ecology Progress Series.* **213**, 67-77.

Dittmar, T. and Lara, R. 2001c. Molecular evidence for lignin degradation in sulfate-reducing mangrove sediments (Amazônia, Brazil). *Geochimica et Cosmochimica Acta.* **65**, 1417-1428.

Dorozhkin, S.V. 2002. A review on the dissolution models of calcium apatites. *Progress in Crystal Growth and Characterization of Materials*. **44**, 45-61.

Edmond, J.M., Boyle, E.A., Grant, B. and Stallard, R.F. 1981. The chemical mass balance in the Amazon plume I: The nutrients. *Deep Sea Research.* **11**(28A), 1339-1374.

Ellison, A.M. and Farnsworth, E.J. 1997. Simulated sea level change alters anatomy, physiology, growth, and reproduction of red mangrove (*Rhizophora mangle* L.) *Oecologia.* **112**, 435-446.

Ensminger, I. 1996. Hydrologische Veränderungen am Canal Clarín und ihre Bedeutung für die Regeneration salzgeschädigter Mangrove. Diplomarbeit. Justus-Liebig-Universität Gießen, Gießen. Germany. pp. 63.

Environmetal Protection Agency – EPA 365.5. 1997. Determination of orthophosphate in estuarine and coastal waters by automated colorimetric analysis. Arar, E.J. (Ed.) National Exposure Research Laboratory: Ohio. pp. 1-9.

Epstein, M. 1975. Nutrição mineral das plantas: princípios e perspectiva. Universidade de São Paulo: São Paulo. pp. 87.

Etcheber, H., Bourg, A.C.M. and Donard. O. 1983. Critical aspects of selective extractions of trace metals from estuarine suspended matter. Fe and Mn hydroxides and organic matter interactions. Poc. Int. Conf. Heavy Metals in the Environment, Heidelberg, CEP Consultants (Eds.): Edinburgh. pp. 1200-1203.

Fabre, A.C. 1992. Inorganic phosphate in exposed sediments of the river Garonne. *Hydrobiologia*. **228**, 37-42.

Fabre, A., Fromard, Fr. and Trichon, V. 1999. Fractionation of phosphate in sediments of four representative mangrove stages (French Guiana). *Hydrobiologia*. **392**, 13-19.

Folk, R.L. 1974. Petrology of sedimentary rocks. Hemphill Pub. Co.: Austin Tex. pp.182.

Freeman, J.S. and Rowell, D.L. 1981. The adsorption and precipitation of phosphate onto calcite. *Journal of Soil Science.* **32**, 75-84.

Frizano, J., Vann, D.R., Johnson, A.H. and Johnson, C.M. 2003. Labile phosphorus in soils of forest fallows and primary forest in the Bragantina region, Brazil. *Biotropica*. **35**, 2-11.

Furtado da Costa, M. 2000. Estudo dos cátions cálcio, magnésio, sódio, potássio e da salinidade na água intersticial do sedimento do manguezal de Bragança - NE do Pará. Master Thesis. Centro de Geociências. Universidade Federal de Pará. Belém do Pará. Brazil. pp. 87.

Furtado da Costa, M. 2000. Estudo dos cátions cálcio, magnésio, sódio, potássio e da salinidade na água intersticial do sedimento do manguezal de Bragança - NE do Pará.

Master Thesis. Centro de Geociências. Universidade Federal de Pará. Belém do Pará. Brazil. pp. 87.

Georgantas, D.A. and Grigoropoulou, H.P. 2006. Phosphorus and organic matter removal from synthetic wastewater using alum and aluminum hydroxide. *Global NEST Journal*. **10**(10), 1-9.

Gibbs, R.J. 1967. The geochemistry of the Amazon River system: the factors that control the salinity, composition and concentration of the suspended solids. *Bulletin of Geological Society of America.* **78**, 1203-1232.

Gibbs, R.J. 1970. Circulation in the Amazon River estuary and adjacent Atlantic Ocean. *Journal of Marine Research.* **28**, 113-123.

Giblin, A.E. 1988. Pyrite formation in marshes during early diagenesis. *Journal of Geomicrobiology*. **6**, 77-97.

Gill, A.M. and Tomlinson, P.B. 1977. Studies on the red mangrove (*Rhizophora mangle* L.). The adult root system. *Biotropica.* **9**, 145-155.

Gleason, S.M., Ewel, K.C. and Hue, N. 2003. Soil redox conditions and plant-soil relationships in a Micronesian mangrove forest. *Estuarine Costal and Shelf Science.* **56**, 1065-1074.

Goés, A.M., Rosetti, D.F., Nogueira, A.C.R and Toledo, P.M. 1990. Modelo deposicional preliminar da formação Pirabas no Nordeste do Estado do Pará. *Boletim do Museu Paraense Emílio Goeldi*. **19**, 3-15

Goldstein, J.I., Newbury, D.E., Joy, D.C., Lyman, C.E., Echlin, P., Lifshin, E., Sawyer, L. and Michael, J.R. 2003 Scanning electron microscopy and x-ray microanalysis. (Third Edition) Kluwer Academic/Plenum Publishers: New York. pp. 689.

Golterman, H.L. and Meyer, M.L. 1985. The geochemistry of two hard water rivers, the Rhine and the Rhone. Part 4: The determination of the solubility product of hydroxy-apatite. *Hydrobiologia*. **126**, 21-24.

Golterman, H.L. 1988. The calcium and iron bound phosphate phase diagram. *Hydrobiologia*. **159**, 149-151.

Gomez, E., Durillon, C., Rofes, G. and Picot, B. 1999. Phosphate adsorption and release from sediments of brackish lagoons: pH, O_2 and loading influence. *Water Research*. **33**, 2437-2447.

Goñi, M.A. and Hedges, J.I. 1995. Sources and reactivities of marine-derived organic matter in coastal sediments as determined by alkaline CuO oxidation. *Geochimica et Cosmochimica Acta.* **59**, 2956-2981.

Gotoh, S. and Patrick, J_R. W.H. 1974. Transformation of iron in a waterlogged soil as influenced by redox potential and pH. *Soil Science American Proceedings*. **38**, 66-70.

Goulden, P.D. and Anthony, D.H.J. 1978. Kinetics of uncatalyzed peroxydisulfate oxidation of organic material in fresh water. *Analytical Chemistry*. **50**, 953-958.

Grasshoff, K., Ehrhardt M. and Kremmling, K. 1983. Methods of seawater analysis. Verlag Chemie: Nürnberg. pp. 403.

Grimshaw, H.M., Allen, S.E. and Parkinson, J.A. 1989. Nutrient elements. *In*: Allen, S.E. (Ed.) Chemical analysis of ecological materials. Blackwell Scientific Publications: Australia. pp. 81-159.

Gulbrandsen, R.A., Roberson, C.E. and Neil, S.T. 1984. Time and the crystallization of apatite in seawater. *Geochimica et Cosmochimica Acta*. **48**, 213-218.

Gunnars, A., Blomqvist, S. and Martinsson, C. 2004. Inorganic formation of apatite in brackish seawater from the Baltic Sea: an experimental approach. *Marine Chemistry*. **91**, 15-26.

Haase, K., De Simone, O., Junk, W.J. and Schmidt, W. 2003. Internal oxygen transport in cuttings from flood-adapted várzea tree species. *Tree Physiology.* **23**, 1069-1076.

Havlin, J.L., Beaton, J.D., Tisdale, S.L. and Nelson, W.L. 1999. Soil fertility and fertilizers. 6th Edition. Prentice Hall : Upper Saddle River, NJ. pp. 499.

Haynes, R.J. 1990. Active ion uptake and maintenance of cation-anion balance: A critical examination of their role in regulating rhizosphere pH. *Plant and Soil.* **126**, 247-264.

Hedges, J.I. and Stern, J.H. 1984. Carbon and nitrogen determinations of carbonate-containings solids. *Limnology and Oceanography.* **29**, 657-663.

Hedges, J.I., Clark, W.A., Quay, P.D., Richey, J.E., Devol, A.H. and Santos, U.de M. 1986. Compositions and fluxes of particulate organic material in the Amazon River. *Limnology and Oceanography.* **31**, 717-738.

Hesse, P.R. 1957. The effect of colloidal organic matter on the precipitation of barium sulphate and a modified method for determining soluble sulphate in soils. *Analyst.* **82**, 710-712.

Hesse, P.R. 1961. Some differences between the soils of *Rhizophora* and *Avicennia* mangrove swamps in Sierra Leone. *Plant and Soil*. **14**, 335-346.

Hesse, P.R. 1971. A textbook of soil chemical analysis. Murray: London. 513 pp.

Hieltjes, A.H.M. and Lijklema, L. 1980. Fractionation of inorganic phosphate in calcareous sediments. *Journal of Environmental Quality.* **9**, 405-407.

Hinnes, M.E., Knollmeyer, S.L. and Tugel, J.B. 1989. Sulfate reduction and other sedimentary biogeochemistry in a northern New England salt marsh. *Limnology and Oceanography*. **34**, 578-590.

Hogarth, P.J. 1999. The biology of mangroves. Oxford University Press Inc: New York. pp. 228.

House, W.A. 2003. Factors influencing the extent and development of the oxic zone in sediments. *Biogeochemsitry*. **63**, 317-333.

Holmer, M., Andersen, F., Holmboe, N., Kristensen, E. and Thongtham, N. 1999. Transformation and exchange processes in the Brangrong mangrove forest-seagrass bed system, Thailand. Seasonal and spatial variations in benthic metabolism and sulfur biogeochemistry. *Aquatic Microbial Ecology*. **20**, 203-212.

Howarth, R.W. 1979. Pyrite: Its rapid formation in salt marsh and its importance in ecosystem metabolism. *Science*. **203**, 49-51.

Howeler, R.H. and Bouldin, D.R. 1971. The diffusion and consumption of oxygen in submerged soils. *Soil Science Society America Proceedings.* **35**, 202-208.

Huerta-Diaz, M.A. 1989. Geochemistry of trace metals associated with sedimentary pyrite from anoxic marine environments. Ph.D. Thesis. Texas University. Texas, USA. pp. 299.

Huguenin-Elie, O., Kirk, G.J.D. and Frossard, E. 2003. Phosphorus uptake in rice from soil that is flooded, drained or flooded then drained. *European Journal of Soil Science.* **54**, 77-90.

INMET, 1992. Normas climatológicas. Instituto Nacional de Meteorología, Brasília. DF. Brazil. pp. 56.

Jander, G. and Jahr, K.F. 1963. Mass Analyse: Theorie und Praxis der klasischen und der elektrochemischen Tirierverfahren. Gruyter: Berlin. pp. 359.

Jeroschewski, P., Steuckart, C. and Kühl, M. 1996 An amperometric microsensor for the determination of H_2S in aquatic environments. *Analytical Chemistry*. **68**, 4351-4357.

Jorgensen, B.B. 1977. The sulfur cycle of coastal marine sediments (Limfjorden, Denmark). *Limnology and Oceanography*. **5**, 814-832.

Justin, S.H.F. and Armstrong, W. 1987. The anatomical characteristics of roots and plant response to soil flooding. *New Phytologist*. **106**, 465-495.

Karl, D.M., Tien, G., Dore, J. and Winn, C.D. 1993. Total dissolved nitrogen and phosphorus concentrations at US-JGOFS Station ALOHA: Redfield reconciliation. *Marine Chemistry.* **41**, 203-208.

Karl, D.M. and Yanagi, K. 1997. Partial characterization of the dissolved organic phosphorus pool in the oligotrophic North Pacific. *Limnology and Oceanography.* **42**, 1398-1405.

Kattner, G. 1999. Storage of dissolved inorganic nutrients in seawater: Poisoning with mercuric chloride. *Marine Chemistry.* **67**, 61-66.

Khalid, R.A., Patrick, W.H, and DeLaune, R. D. 1977. Phosphorus sorption characteristics of flooded soils. *Soil Science Society of America*. **41**, 305-310.

Kehew, A.E. 2001. Applied Chemical Hydrogeology. Prentice Hall : Upper Saddle River, NJ. pp. 368.

Kirk, G.J.H. 1999. A model of phosphate solubilization by organic anion excretion from plant roots. *European Journal of Soil Science.* **50**, 369-378.

Kirk, G.J.D. 2003. Effects of flooding and redox conditions on solute diffusion in soil. *European Journal of Soil Science*. **54**, 617-624.

Kirk, G. 2004. The biogeochemistry of submerged soils. John Wiley and Sons: England. pp. 291.

Kjerfve, B. and Lacerda, L.D. 1993. Mangroves of Brazil. *In*: Lacerda, L.D. (Ed.), Mangrove Ecosystems Technical Reports. ITTO TS-13. pp. 245-272.

Kjerfve, B. and Macintosh, D. J. 1997. The impact of climatic change on mangrove ecosystems. *In*: Kjerfve B., Lacerda L.D. and Diop E. H.S. (Eds.) Mangrove ecosystem studies in Latin America and Africa. UNESCO: Paris. pp. 1-7.

Kjerfve, B., Lacerda, L.D. and Diop, E.H.S. 1997 Mangrove ecosystem studies in Latin America and Africa. UNESCO: Paris. pp. 349.

Kludze, H.K. and DeLaune, R.D. 1995. Straw application effects on methane and oxygen exchange and growth in rice. *Journal of Soil Science Society of America*. **59**, 824-830.

Kolowith L.C., Ingall E.D. and Benner R. 2001. Composition and cycling of marine organic phosphorus. *Limnology and Oceanography.* **46**, 309-320.

Komiyama, A., Ogino, S., Aksornkoae S. and Sabhasari, S. 1987. Root biomass of a mangrove forest in Southern Thailand. 1. Estimation by the trench method and the zonal structure of root biomass. *Journal of Tropical Ecology*. **3**, 97-108.

Koncalová, H. 1990. Anatomical adaptations to waterlogging in roots of wetland graminoids: limitation and drawbacks. *Aquatic Botany*. **38**, 127-134.

Konsten, C., Van Breemen, N., Suping, S., Aribawa, I. and Gronenberg, J. 1994. Effects of flooding on pH of rice-producing, acid sulfate soils in Indonesia. *Journal of Soil Science Society of America.* **58,** 871-883.

Koroleff, F. 1983. Determination of phophorus. *In*: Grasshoff, K., Ehrhardt, M. and Kremling, K. (Eds.) 2nd Edition. Methods of seawater analysis. Verlag Chemie: Weinheim. pp. 125-139.

Kostka, J. E. and Luther, G.W. 1994. Partitioning and speciation of solid phase iron in saltmarsh sediments. *Geochimica et Cosmochimica Acta.* **58**, 1701-1710.

Kozlowski, T.T. 1997. Responses of woody plants to flooding and salinity. *Tree Physiology* . **1**, 1-29.

Krause, G., Schories, D. and Diele, K. 2001. Spatial patterns of mangrove ecosystems: the Bragantinian mangrove of Northern Brazil (Bragança, Pará). *Ecotropica.* **7**, 93-107.

Krause, G. and Glaser, M. 2003. Co-evolving geomorphical and socio-economic dynamics in a coastal fishing village of the Bragança region (Pará, North Brazil). *Ocean and Coastal Management.* **46**, 859-874.

Kristensen, E., Holmer, M. and Bussarawit, N. 1991. Benthic metabolism and sulfate reduction in a southeast Asia mangrove swamp. *Marine Ecology Progress Series*. **73**, 93-103.

Kristensen, E., King, G.M., Holmer, M., Banta, G.T., Jensen, M.H., Hansen, K. and Bussarawit, N. 1994. Sulfate reduction, acetate and carbon metabolism in sediments of Ao Nam Bor mangrove, Phuket. Thailand. *Marine Ecology Progress Series*. **109**, 245-255.

Kurmies, B. 1972. Zur Fraktionierung der Bodenphosphate. *Phosphorsäure.* **29**, 118-149.

Kühl, M., Steuckart, C., Eickert, G. and Jeroschewski, P. 1998. A H_2S microsensor for profiling biofilms and sediments: application in an acidic lake sediment. *Aquatic Microbial Ecology.* **15**, 201-209.

Küster, F.W. and Thiel, A. 1982. Rechentafeln für die chemische Analitik. Berlin. pp. 102.

Lacerda, L.Dl., Carvalho, C.E.V., Tanizaki, K.F., Ovalle, A.R.C. and Rezende, C.E. 1993. The biogeochemistry and trace metal distribution of mangrove rhizospheres. *Biotropica*. **25**, 252-257.

Lacerda, L.D., Ittekot, V. and Patchineelam, S.R. 1995. Biogeochemistry of mangrove soil organic matter: a comparison between *Rhizophora* and *Avicennia* soils in South-eastern Brazil. *Estuarine, Coastal and Shelf Science*. **40**, 713-720.

Lallier-Verges, E., Perrussel, B.P., Disnar, J-R and Baltzer, F. 1998. Relationships between environmental conditions and the diagenetic evolution of organic matter derived from higher plants in a modern mangrove swamp system (Guadaloupe, French West Indies). *Organic Geochemistry*. **29**, 1663-1686.

Langner, C.L. and Hendrix, P.F. 1982. Evaluation of a persulfate digestion method for particulate nitrogen and phosphorus. *Deep Sea Research.* **16**, 1451-1454.

Lara, R.J. and Dittmar, T. 1999. Nutrient dynamics in a mangrove creek (North Brazil) during the dry season. *Mangrove and Salt Marshes.* **3**, 185-195.

Leeg, J.O. and Black, C.A. 1955. Determination of organic phosphorus in soils: II ignition method. *Soil Science Society Proceedings.* **19**, 139-143.

Leventhal, J.S. 1983. An interpretation of carbon and sulfur relationships in Black Sea sediments as indicators of deposition environments. *Geochimica et Cosmochimica Acta.* **47**, 133-138.

Leventhal, J. and Taylor, C. 1990. Comparison of the methods to determine degree of pyritization. *Geochimica et Cosmochimica Acta*. **54,** 2621-2625.

Libes, S.M. 1992. An introduction to marine biogeochemistry. John Wiley and Sons, Inc.: Canada. pp. 715.

Lindsay, W.L. 1979. Chemical equilibria in soils. John Wiley and Sons: New York, USA. pp. 449.

Lindsay, W.L., Vlek, P.L.G. and Chien, S.H. 1989. Phosphate minerals. *In*: Dixon, J.B. and Weed, S.B. (Eds.) 2nd edition. Minerals in Soil Environments. Soil Science Society of America: Madison, Wis. pp. 1089-1130.

Lord, C.J. 1982. A selective and precise method for pyrite determination in sedimentary materials. *Journal of Sedimentary Petrology*. **52**, 664-666.

Love, L.G. and Amstutz, G.C. 1966. Review of microscopic pyrite from the Devonian Chattanooga Shale and Rammelsberg Banderz. *Fortschrift Mineralogie*. **43**, 273-309.

Love, L.G. 1971. Early diagenetic polyframboidal pyrite, primary and redeposited from the Wenlockian Denbigh Grit Group, Conway, North Wales, UK. *Journal of Sedimentary Petrology*. **41**, 1038-1044.

Lugo, A.E. and Snedaker, S.C. 1974. The ecology of mangroves. *Annual Review of Ecology and Systematic.* **5**, 39-64.

Luther, G.W., Giblin, A., Howarth, R.W. and Ryans, R.A. 1982. Pyrite and oxidized iron mineral phases formed from pyrite oxidation in salt marsh and estuarine sediments. *Geochimica et Cosmochimica Acta*. **46**, 2665-2669.

Luther, G.W., Kotsky, J.E., Church, T.M., Sulzberger, B. and Stumm, W. 1992. Seasonal iron cycling in the salt-marsh sedimentary environment: the importance of ligand complexes with Fe(II) and Fe(III) in the dissolution of Fe(III) minerals and pyrite, respectively. *Marine Chemistry*. **40**, 81-103.

Madureira, M.J., Vale, C. and Gonçalves, S.M.L. 1997. Effect of plants on sulphur geochemistry in the Tagus salt-marshes sediments. *Marine Chemistry*. **58**, 27-37.

Marchand, C., Lallier-Vergès, E. and Baltzer, F. 2003. The composition of sedimentary organic matter in relation to dynamic features of a mangrove-fringed coast in French Guiana. *Estuarine, Coastal and Shelf Science*. **56**, 119-130.

Marchand, C., Baltzer, F., Lallier-Vergès, E and Albéric, P. 2004. Pore-water chemistry in mangrove sediments: relationship with species composition and developmental stages (French Guiana). *Marine Geology.* **208**, 361-381.

Marschner, H. 1995. Mineral nutrition of higher plants. Academic press: London. pp.889.

Martens, C.S. and Harriss, R.C. 1970. Inhibition of apatite precipitation in the marine environment by magnesium ions. *Geochimica et Cosmochimica Acta*. **34**, 621-625.

Martin, J. M., Nirel, P. and Thomas, A.J. 1987. Sequential extraction techniques: promises and problems. *Marine Chemistry.* **22**, 313-341.

Matthijs, S., Tack, J., van Speybroeck, D. and Koedam, N. 1999. Mangrove species zonation and soil redox state , sulphide concentration and salinity in Gazi Bay (Kenya), a preliminary study. *Mangroves and Salt Marshes.* **3**, 243-249.

Mayer, L.M., Keil, R.G. Macko, S.A., Joye, S.B., Ruttemberg, K.C. and Aller, R.C. 1998. Importance of suspended particulates in riverine delivery of bioavailable nitrogen to coastal zones. *Global Biogeochemical Cycles*. **12**, 573-579.

McKee, K.L., Mendelssohn, I.A. and Hester, M.W. 1988. Reexamination of pore water sulfide concentrations and redox potentials near the aerial roots of *Rhizophora mangle* and *Avicennia germinans*. *American Journal of Botany.* **75**, 1352-1359.

McKee, K.L. 1993. Soil physicochemical patterns and mangrove species distribution - reciprocal effects? *Journal of Ecology*. **81**, 477-487.

Medina, E., Giarrizzo, T., Menezes, M., Carvalho, LM., Carvalho, E.A., Peres, A., Silva, B., Vilhena, R., Reise, A. and Braga, F.C. 2001. Mangal communities of the "Salgado Paraense": Ecological heterogeneity along the Bragança Peninsula assessed through soil and leaf analyses. *Amazoniana.* **16** (3/4), 397-416.

Mendelssohn, I.A. and McKee, K.L. 1988. Spartina alterniflora die back in Lousiana: time-course investigation of soil waterlogging effects. *Journal of Ecology.* **76**, 509-521.

Menezes, M., Berger, U. and Worbes, M. 2003. Annual growth rings and long-term growth patterns of the mangrove trees from the Bragança Peninsula, North Brazil. *Wetlands Ecology and Management*. **11**, 233-242.

Menezes, M. 2006. Investigations of mangrove forest dynamics in Amazonia, North Brazil. Ph.D. Thesis. Zentrum für Marine Tropenökologie. Bremen Universität, Germany. pp.149.

Meyer, B., Ward. K., Koshalp, K. and Peter, L. 1983. Second dissociation constant of hydrogen sulfide. *Inorganic Chemistry*. **22**, 2345-2346.

Meyers, P.A. 1994. Preservation of elemental and isotopic source identification of sedimentary organic matter. *Chemical Geology*. **114**, 289-302.

Middelburg, J.J., Nieuwenhuize, J., Slim, F.J. and Ohowa, B. 1996. Sediment biogeochemistry in an East African mangrove forest (Gazi Bay, Kenya). *Biogeochemistry.* **34**, 133-155.

Millero, F.G., Plese, T. and Fernandez, M. 1988. The dissociation of hydrogen sulfide in seawater. *Limnology and Oceanography*. **33**, 269-274.

Milliman, J.D., Barreto, L., Amaral, C.A. and Francisconi, O. 1975. Upper continental margin sedimentation of Brazil: Northern Brazil. *Contribution of Sedimentology.* **4**, 11-43.

Moeslund, L., Thamdrup, B. and Jorgensen, B.B. 1994. Sulfur and iron cycling in a coastal sediment: radiotracer studies and seasonal dynamics. *Biogeochemistry*. 27, 129-172.

Morris, A.W., Bale, A.J., and Howland, R.J.M. 1981. Nutrient distribution in an estuary: evidence of chemical precipitation of dissolved silicate and phosphate. *Estuarine, Coastal and Shelf Science.* **12**, 205-216.

Morita, T. and Viegas, R.M.A. 1981. Manual de soluções, reagentes e solventes. Padronização, preparação e purificação. Edgard Blücher Ltda.: São Paulo. pp 592.

Murrmann, R.P. and Peech, M. 1969. Effect of pH on labile and soluble phosphate in soils. *Soil Science Society of America Proceedings.* **33**, 205-210.

Näser, von K-H. 1976. Physikalische Chemie für Techniker und Ingenieure. Dt. Verl. für Grundstoffindustrie: Leipzig. pp. 480.

Nedwell, D.B., Blackburn, T.H. and Wiebe, W.J. 1994. Dynamic nature of the turnover of organic carbon, nitrogen and sulphur in the sediments of a Jamaican mangrove forest. *Marine Ecology Progress Series*. **110**, 223-231.

Neumann, G., Massonneau, A., Langlade, N., Dinkelaker, B., Hengeler, C., Romheld, V. and Martinoia, E. 2000. Physiological aspects of cluster root and development in phosphorus-deficient white lupins. *Annais of Botany.* **85**, 909-919.

Nickerson, N.H. and Thibodeau, F.R. 1985. Association between pore water sulphide concentrations and the distribution of mangroves. *Biogeochemistry.* **1**, 183-192.

Nriagu, J.O. 1976. Phosphate - clay mineral relations in soils and sediments. *Canadian Journal of Earth Sciences.* **13**, 717-735.

Nordhaus, I., Wolff, M. and Diele, K. 2006. Litter processing and population food intake of the mangrove crab *Ucides cordatus* in a high intertidal forest in Northern Brazil. *Estuarine, Coastal and Shelf Science*. **67**, 239-250.

Nye, P.H. 1979. Diffusion of ions and uncharged solutes in soils and soil clays. *Advanced in Agronomy*. **31**, 225-272.

Olila, O.G., Reddy, K.R. and Stites, D.L. 1997. Influence of draining on soil phosphorus forms and distribution in a constructed wetland. *Ecological Engineering*. **9**, 157-169.

Oliveira, S. R. 1999. Ciclagem do fósforo em uma floresta de manguezal. Natal/RN. Msc. Thesis. Universidade Federal do Rio Grande do Norte. Bioecologia Aquática. Brazil. pp. 43.

Orion Research. 2003. Model 94-16 Ionplus. Silver/Sulphide Electrode Instruction. Thermo Electron Corporation: Boston. pp. 67.

Orrett, K. and Karl, D.M. 1987. Dissolved organic phosphorus production in surface seawater. *Limnology and Oceanography.* **32**, 383-395.

Ovalle, A.C.R., Rezende, C.E., Lacerda, L.D. and silva, C.A.R. 1990. Factors affecting the hydrochemistry of a mangrove tidal creek, Sepetiba Bay, Brazil. *Estuarine, Coastal and Shelf Science*. **31**, 639-650.

Patrick, W.H. and R.A. Khalid 1974. Phosphate release and sorption by soils and sediments: effect of aerobic and anaerobic conditions. *Science*. **186**, 53-55.

Pavanasasivam, V. and Axley, J,H. 1980. Influence of flooding on the availability of soil zinc. *Communication of Soil Science and Plant Analysis*. **11**, 163-174.

Pezeshki, S.R., Pan, S.Z., De Laune, R.D and Patrick, W.H. 1988. Sulfide-induced toxicity: Inhibition of carbon assimilation in *Spartina alterniflora*. *Photosynthetica.* **22(3),** 437-442.

Pizzaro, M.J., Hammerley, J., Maine, M.A. and Sune, N. 1992. Phosphate adsorption on bottom sediments of the Rio de la Plata. *Hydrobiologia*. **228**, 43-54.

Poulton, S.W. and Canfield, D.E. 2005. Development of a sequential extraction procedure for iron: implications for iron partitioning in continentally derived particulates. *Chemical Geology*. **214**, 209-221.

Ponnamperuma, F.N. 1972. The chemistry of submerged soils. *In*: Brady, N.C. (Ed.) Advances in agronomy. American Society of Agronomy: New York. pp. 29-88.

Postma, D. and Jakobsen, R. 1996. Redox zonation: Equilibrium constraints on the Fe(III)/SO_4-reduction interface. *Geochimica et Cosmochimica Acta*. **60**, 3169-3175.

Rademaker, V. 1998. Ernährungsökologie, Habitatbeschreibung und Populationsstruktur der Mangrovenkrabbe *Ucides Cordatus* (Linneaus, 1763) im Caeté-Mangrovenästuar, Nordostbrasilien. Msc. Thesis. Zentrum für Marine Tropenökologie. Bremen Universität. Bremen, Germany. pp. 94.

Raiswell, R. and Berner, R.A. 1985. Pyrite formation in euxinic and semi-euxinic sediments. *American Journal of Science.* **285**, 710-724.

Raiswell, R., Buckley, F., Berner, R.A. and Anderson, T.F. 1988. Degree of pyritization of iron as a paleoenvironmental indicator of bottom-water oxygenation. *Journal of Sedimentary Petrology.* **58**, 812-819.

Raiswell, R., Whaler, K., Dean, S., Coleman, M.L. and Briggs, D.E. 1993. A simple three-dimensional model of diffusion-with-precipitation applied to localised pyrite formation in framboids, fossils and detrital iron minerals. *Marine Geology*. **113**, 89-100.

Rao, R.G., Woitchik, A.F., Goeyens, L. Van Riet A., Kazungu, J. and Dehairs, F. 1994. Carbon, nitrogen contents and stable carbon isotope abundance in mangrove leaves from an east African coastal lagoon (Kenya). *Aquatic Botany*. **47**, 175-183.

Redfield, A.C. 1958. The biological control of chemical factors in the environment. *American Scientist*. **46**, 205-222.

Reise, A. 2003. Estimates of biomass and productivity in fringe mangroves of North-Brazil. Ph.D. Thesis. Zentrum für Marine Tropenökologie. Contribution 16. University of Bremen. Bremen, Germany. pp. 166.

Rickard, D.T. 1970. The origin of framboids. *Lithos.* **3**, 269-293.

Rickard, D. and Luther, G.W. 1997. Kinetics of pyrite formation by the H_2S oxidation of iron (II) monosulfide in aqueous solutions between 25 and 125^{o}C: the mechanism. *Geochimica et Cosmochimica Acta*. **61**, 135-147.

Rickard, D. and Morse, J.W. 2005. Acid volatile sulfide (AVS). *Marine Chemistry*. **97**, 141-197.

Robertson, A.I., Alongi, D.M and Boto, K.G. 1992. Food chain and carbon fluxes. *In*: Robertson, A.I. and Alongi, D.M (Eds.). Tropical Mangrove ecosystems - Coastal and Estuarine Series 41. American Geophysical Union: Washington. pp. 293-326.

Rossetti, D. F., Truckenbrodt, W. and Goés, A.M. 1989. Estudo paleoambiental e estratigráfico dos sedimentos Barreiras e Pós-Barreiras na Região Bragantina, Nordeste do Pará. *Boletim do Museu Paraense Emílio Goeldi*. **1**, 25-74.

Roychoudhury, A.N., Kostky, J.E. and van Cappellen, P. 2003. Pyritization: a paleoenvironmental and redox proxy reevaluated. *Estuarine Coastal and Shelf Science.* **57**, 1183-1193.

Ruttemberg, K.C. 1993. Development of a sequential extraction method for different forms of phosphorus in marine sediments. *Limnology and Oceanography.* **37**, 1460-1482.

Ruttemberg, K.C. and Goñi, M.A. 1997. Phosphorus distribution, C:N:P ratios, and δ^{13} C_{oc} in artic, temperate, and tropical coastal sediments: tools or characterizing bulk sedimentary organic matter. *Marine Geology.* **139**, 123-145.

Sahai, N. 2003. The effects of Mg^{2+} and H^{+} on apatite nucleation at silica surfaces. *Geochimica et Cosmochimica Acta.* **67**, 1017-1030.

Salcedo, I.H. and Medeiros, C. 1995. Phosphorus transfer from tropical terrestrial to aquatic systems - mangroves. *In*: Tiessen, H. (Ed.) Phosphorus in the global environment: transfer, cycles and management. SCOPE 54. John Wiley and Sons Ltd.: England. pp. 347-362.

Saleque, M.A. and Kirk, G.J.D. 1995. Root-induced solubilization of phosphate in the rhizosphere of lowland rice. *New Phytology.* **129**, 325-336.

Sawłowicz, Z. 1987. Framboidal pyrite from the metamorphic Radzimowice Schists of Stara Gora (Lower Silesia, Poland). *Mineralogy Polonica*. **18**, 57-67.

Sawłowicz, Z. 1993. Pyrite framboids and their development: a new conceptual mechanism. *Geologie Rundschau*. **82**, 148-156.

Sawłowicz, Z. 2005. Framboids: from their origin to application. *Mineralog. Trans*. **88**, 1-80.

Schaeffer-Novelli, Y., Cintrón, M.G., Rothleder, A.R. and Carmargo, T.M.D. 1990. Variability of mangrove ecosystems along the Brazilian coast. *Estuaries.* **13**(2), 204-218.

Schellmann, W. 1983. A new definition of laterite. *Natural Resources of Devonian*. **18**, 7-21.

Schellmann, W. 2003. Discussion of "a critique of the Schellmann definition and classification of laterite" by R.P. Bourman and C.D. Ollier (*Catena* 47, 117-131). *Catena.* **52**, 77-79.

Schmitt, B.B. 2006. Characterization of organic nitrogen compounds in sediment and leaves of a mangrove ecosystem in North Brazil. Ph.D. Thesis. Zentrum für Marine Tropenökologie. Bremen Universität. Bremen, Germany. pp. 186.

Scholander, P.F., Van Dam, L. and Scholander, S.I. 1955. Gas exchange in the roots of mangroves. *American Journal of Botany.* **42,** 92-98.

Schulz, H.D. 2000. Redox measurements in marine sediments. In: Schuring, J., Schulz, H.D., Fischer, W.R., Bottcher, J. and Duijnisveld, W.H.M. (eds.). Redox: Fundamentals, processes and applications. Springer: Berlin. pp. 81-93.

Schwendenmann, L. 1998. Tidal and seasonal variations of soil and water properties in a Brazilian mangrove ecosystem. Master Thesis, Ressources Engineering Programme. University of Karlsruhe. Karlsruhe, Germany. pp. 101.

Shapiro, R.E. 1958. Effect of flooding on availability of phosphorus and nitrogen. *Soil Science*. **85**, 190-197.

Shepard, F.P. 1932. Sediments of the continental shelves. *Bulletin of Geology of Society America.* **43**, 1017-1040.

Sherman, R.E., Fahey, T.J. and Howarth, R.W. (1998). Soil-plant interactions in a neotropical mangrove forest: iron, phosphorus and sulfur dynamics. *Oecologia.* **114**, 553-563.

Silva, C.A. 1992. Formas e taxas de ciclagem do fósforo no ecossistema manguezal de Itacurucá, Baía de Sepetiba, RJ. PhD Thesis. Ecologia e Recursos Naturais. Universidade Federal de São Carlos. São Paulo, Brazil. pp. 118.

Silva, C.A.R., Mozeto, A.A. and Ovalle, A.R.C. 1998. Distribution and fluxes of phosphorus in red mangroves, Sepetiba Bay, Brazil. *Mangroves and Salt Marshes.* **2**, 37-42.

Silva, C.A.R. and Sampaio, L.S. 1998. Speciation of phosphorus in a tidal floodplain forest in the Amazon estuary. *Mangroves and Salt Marshes.* **2**, 51-57.

Smith, F.W., Mudge, S.R., Rae, A.L. and Glassop, D. 2003. Phosphate transport in plants. *Plant and Soil.* **248**, 71-83.

Snedaker, S. C. 1982. Mangrove species zonation: why? *In*: Sen, D.N. and Rajpurohit, K.S. (Eds.) Contribution to the ecology of halophytes. Kluwer Academic: Netherlands. pp. 111-125.

Sombroek, W.G. 1984. Soils of the Amazon region. *In*: Sioli, H. (Ed.) The Amazon: limnology and landscape ecology of the mighty tropical river and its basin. Dr. Junk, W. Publishers: The Hague. pp. 234-271.

Souza Filho, P.W.M., Martins, E. and El-Robrini, M. 1997. Influência das variações do nível do mar na sedimentação da planície costeira Bragantina durante o holoceno - Nordeste do Pará, Brasil. *In*: Lima da Costa M. and Simões A.R. (Eds.) Contribuções à geologia da Amazônia. FINEP/SBG-NO: Belém. pp. 307-337.

Souza Filho, P.W.M. and El-Robrini, M. 1998. As variações do nível do mar e a estratigrafia de sequências da Planície Costeira Bragantina - Nordeste do Pará, Brasil. *Boletim Museu Paranaense Emílio Goeldi, Série Ciências da Terra.* **10**, 1-34.

Souza Filho, P.W.M. 2000. Tectonic control on the coastal zone geomorphology of the Northeastern Pará State. *Revista Brasileira de Geociências.* **30**, 523-526.

Spalding, M.D., Balsco, F. and Field, C.D. 1997. World mangrove atlas. International Society for Mangrove Ecosystems: Okinawa. pp. 178.

Staupendahl, K. 2001. Das flächebezogene Winkelmass Wf-Ein Index zur quantitativen Beschreibung der horizontalen Baumverteilung. *In*: Akca, A., *et al*., (Ed.) Waldinventur, Waldwachstum und Fortplannung - Moderne Technologien, Methoden und Verfahrenweisen. Zohab-Verl: Göttingen. pp. 101-115.

Strickland, J.D.H. and Parsons, T.R. 1972. A practical handbook of seawater analysis. 2nd. Ed. Fisheries Research Board of Canada: Otawa. pp. 167.

Stumm, W. and Morgan, J.J. 1981. Aquatic chemistry: An introduction emphasizing chemical equilibria in natural waters. John Wiley and Sons Inc.: New York. pp. 767.

Stumm, W. and Sulzberger, B. 1992. The cycling of iron in natural environments: Considerations based on laboratory studies of heterogeneous processes. *Geochimica et Cosmochimica Acta*. **56**, 3233-3257.

Suit, N.S. and Wilkin, R.T. 1998. Pyrite formation in the water column and sediments of a meromictic lake. *Geolog*y. **26**, 1099-1102.

Thibodeau, F.R. and Nickerson, N.H. 1986. Differential oxidation of mangrove substrate by *Avicennia germinans* and *Rhizophora mangle*. *American Journal of Botany*. **73**, 512-516.

Thüllen, N. and Berger, U. 2000. A comparative examination of environmental factors at patchy mangrove seedling stands on the peninsula of Bragança, Northern Brazil. *Ecotropica.* **6**, 1-12.

Tribovillard, N., Algeo, T.J., Lyons, T. and Riboulleau, A. 2006. Trace metals as paleoredox and paleoproductivity proxies: an update. *Chemical Geology*. **232**, 12-32.

Twilley, R.R. 1985. The exchange of organic carbon in basin mangrove forest in a Southwestern Florida estuary. *Estuarine, Coastal and Shelf Science.* **20**, 543-557.

Verardo, D.J., Froelich, P.N. and McIntyre, A. 1990. Determination of organic carbon and nitrogen in marine sediments using the Carlo Erba NA 1500 (2100) Analyzer. *Deep Sea Research*. **37**, 157-165.

Vamos, R. and Koves, E. 1972. Role of light on the prevention of the poisoning action of hydrogen sulphide in the rice plant. *Journal of Applied Ecology*. **9**, 519-525.

Wang, H.D., Harris, W.G., Reddy, K.R. and Flaig, E.G. 1995. Stability of phosphorus forms in dairy-impacted soils under simulated leaching. *Ecological Engineering.* **5**, 209-227.

Wattayakorn, G., Wolanski, E. and Kjerve, B. 1990. Mixing, trapping and outwelling in the Klong Ngao mangrove swamp, Thailand. *Estuarine, Coastal and Shelf Science.* **31**, 667-688.

Wijsman, J.W.M., Middelburg, J.J. Herman, P.M.J., Böttcher, M.E. and Heip, C.H.R. 2001. Sulfur and iron speciation in surface sediments along the northwestern margin of the Black Sea. *Marine Chemistry*. **74**, 261-278.

Williams, J.D.H., Systers, J.K. and Walker, T.W. 1967. Fractionation of soil inorganic phosphate by modification of Chang and Jackson´s procedure. *Soil Science Society American Proceedings.* **31**, 736-739.

Wilkin, R.T., Barnes, H.L. and Brantley, S.L. 1996. The size distribution of framboidal pyrite in modern sediments: An indicator of redox conditions. *Geochimica et Cosmochimica Acta.* **60**(20), 3897-3912.

Wilkin, R.T. and Barnes, H.L. 1996. Pyrite formation by reactions of iron monosulfides with dissolved inorganic and organic sulfur species. *Geochimica et Cosmochimica Acta*. **60**, 4167-4179.

Wilkin, R.T., Arthur, M.A. and Dean, W.E. 1997. History of water-column anoxia in the Black Sea indicated by pyrite. *Earth and Planetary Science Letters*. **148**, 517-525.

Wolanski, E., Mazda, Y. and Ridd, P. 1992. Mangrove Hydrodynamics. *In*: Robertson A.I. and Alongi D.M (Eds.). Tropical Mangrove ecosystems - Coastal and Estuarine Series 41. American Geophysical Union: Washington. pp. 43-62.

Wolthers, M. 2003. Geochemistry and environmental mineralogy of the iron-sulfur-arsenic system. *Geologica Ultraiectina*. **225**, 185-190.

Woodroffe, C.D. 1992. Geomorphology and development of mangrove swamps, Grand Cayman Island, West Indies. *Bulletin Marine Science*. **32**, 381-398.

WTW-Wissenschaftlich-Technische Werkstätten GmbH, 1997. Redox-Fibel. Grundlagen und Tips zur Redox-Messung. Firmenschrift: Weilheim. pp. 48.

Yadav, B.R., Paliwal, K.V. and Nimgade, N.M. 1984. Effect of magnesium-rich waters on phosphate adsorption by calcite. *Soil Science.* **138**, 153-157.

Youssef, T. and Saenger, P. 1996. Anatomical adaptive strategies to flooding and rhizosphere oxidation in mangrove seedlings. *Australian Journal of Botany*. **44**, 297-313.

Ziebis, W. Huettel, M. and Forster, S. 1996. Impact of biogenic sediments topography on oxygen fluxes in permeable seabeds. *Marine Ecology Progress Serie*. **140**, 227-237.